SOUTHWEST RESEARCH INSTITUTE
FINAL REPORT
VENUS DATA ANALYSIS PROGRAM
NASA GRANT NO. NAGW-3779
SwRI Project No. 15-6083

MHD MODELING OF THE INTERACTION OF THE SOLAR WIND WITH VENUS

Submitted by

Dr. R. S. Steinolfson
Principal Investigator

October 25, 1996

SUMMARY

The primary objective of this research program is to improve our understanding of the physical processes occurring in the interaction of the solar wind with Venus. This will be accomplished through the use of numerical solutions of the two- and three-dimensional magnetohydrodynamic (MHD) equations and through comparisons of the computed results with available observations. A large portion of this effort involves the study of processes due to the presence of the magnetic field and the effects of mass loading.

Data from the Pioneer Venus Orbiter (PVO), as well as data from Venera 9 and 10 and other sources, have contributed to a growing understanding of the interaction of the solar wind with an unmagnetized body such as Venus. The general picture derived from the available data is that, for typical solar wind conditions, an electrically conducting ionosphere deflects the supersonic solar wind around the planet. A bow shock forms upstream of the ionosphere and serves to slow, and also assists in deflecting, the solar wind. The boundary separating the chocked and magnetized solar wind plasma from the thermal ionosphere plasma is referred to as the ionopause, and the region between the bow shock and the ionopause is referred as the magnetosheath. The inner portion of the magnetosheath contains a region of enhanced magnetic pressure referred to as the magnetic barrier. It is the physical processes involved in these relatively large-scale interaction region as well as in the downstream magnetic tail that this work has application to.

The general approach that we use is to treat the planet as a solid, ideally conducting electrical sphere. Consequently, the plasma velocity and magnetic field are required to be parallel to the surface of the planet. The equations are solved in time and space in a spherical coordinate system centered on the planet. A particular simulation is obtained by maintaining predetermined, fixed solar wind conditions on the dayside of the outer boundary. For given initial conditions the computation is continued in time until the interaction of the specified solar wind with the planet has reached an equilibrium in time. The spatial distribution of the initial velocity and magnetic field are taken from the potential solutions for incompressible flow over a sphere.

1. Scope of the investigation

The four specific research topics that have been investigated in detail to date include (1) the study of bow shocks at unusually large distances from the planet, (2) the effect of the interplanetary magnetic field direction and strength on the interaction, (3) the effect of mass loading on the interaction for the special orientation of the interplanetary magnetic field perpendicular to the flow velocity, and (4) the effect of mass loading for other orientations relative to the flow velocity and for other values of the plasma beta. Each of the four studies carried out are described in more detail below. All of these results have been presented in international or national meetings and published in journals.

2. Venus bow shocks at unusually large distances from Venus

Recent analysis of data from the Pioneer Venus Orbiter (PVO) has shown that

the bow shock often travels to unusually large distances from the planet when the solar wind magnetosonic Mach number is near unity. We suggest that distant bow shocks can be explained as an integral part of the response of the global solar wind/Venus interaction to anomalous local solar wind conditions that existed during the time of these observations. The lower than normal plasma beta and magnetosonic Mach number are in a parameter regime for which the usual fast-mode bow shock close to the planet may not provide the necessary compression and deflection of the solar wind. The solar wind conditions in the vicinity of Venus become such that the usual fast MHD shock near the planet is no longer a stable solution. The fast MHD shock is replaced by a shock configuration containing an intermediate MHD shock over at least a portion of the shock front, and the resulting configuration propagates upstream.

The MHD equations without explicit dissipation are used in this study. The equations are solved numerically using the modified Lax-Wendroff scheme with a smoothing term. In our simulations the planet is replaced by a cylinder aligned along the z-axis in a cylindrical coordinate system. The z-axis is taken to be in the ecliptic plane perpendicular to the Sun-Venus plane, and the MHD equations are solved in the r-θ plane. The cylindrical approximation should retain the essential physics for this problem.

Using MHD simulations we show that, for these conditions, the usual fast shock is replaced by a bow shock consisting of an intermediate shock near the Sun-Venus line and a fast shock at large distances from the Sun-Venus line. This composite bow shock propagates upstream away from the planet at a low speed and appears to be approaching a new equilibrium stand-off location at a large distance from the planet. These results are published in the article entitled "Venus bow shocks at unusually large distances from the planet" in Geophysical Research Letter, Vol. 20, 755-758, 1993.

3. Three-dimensional MHD simulations of the interaction between Venus and the solar wind

We have developed a three-dimensional, single-fluid, MHD code which has successfully simulated the major qualitative features of the Venus-solar wind interaction. We model the Venus obstacle as a hard, conducting sphere and the solar wind as a single-fluid MHD plasma. We simulate the case in which the IMF is tilted with respect to the incoming solar wind velocity at approximately the Parker spiral angle; this is the first simulation of this particular case which includes all spatial regions of the interaction. A realistic value of beta has also been used.

Our simulations show that a bow shock forms at a height above the ionosphere close to the that deduced from Pioneer Venus Orbiter (PVO) observations. A magnetic barrier beneath the bow shock is found. The bow shock shows an asymmetry in the terminator plane qualitatively similar to results obtained from PVO data analyses. The magnetic field drapes over the planet and forms a two-lobed magnetotail. The magnetic field configuration near the planet is very similar to that recorded by PVO as well.

Our simulations have also produced several interesting results which seem to have not been studied before. In the asymmetric 45° simulation the peak in the

magnetic field buildup is shifted from the subsolar point toward the quasi-perpendicular region of the shock. In contrast, the peaks in thermal pressure and density are shifted toward the quasi-parallel region. In the near-tail region our perpendicular simulation has established the possibility of magnetic reconnection.

These results are published in the article entitled "Three-dimensional MHD simulations of the interaction between Venus and the solar wind" in Journal of Geophysical Research, vol. 100, 21645-21658, 1995.

4. 2-D Numerical simulations of mass loading in the solar wind interaction with Venus

Numerical simulations are performed in the frame work of nonlinear two-dimensional magnetohydrodynamics to investigate the influence of mass loading on the solar wind interaction with Venus. A modified Lax-Wendroff scheme is used to solve the equations in a spherical coordinate system. For these computations the detailed chemistry of the ionosphere is neglected, and the planet is treated as a conducting sphere. Numerical computations have been performed to study the effect of mass loading and the IMF strength on the magnetic barrier and the general configuration of the magnetic tail. The IMF orientation included in this study is parallel to the solar wind flow.

The principal physical features of the interaction of the solar wind with the atmosphere of Venus are presented. The formation of the bow shock, the magnetic barrier, and the magnetotail are some typical features of the interaction. The deceleration of the solar wind due to the mass loading near Venus is an additional feature. The effect of the mass loading is to push the shock farther outward from the planet. The influence of different values of the magnetic field strength on the plasma evolution is considered.

The main results are the following: The mass loading increases the mass density in the overall region, except the terminator and tail where the mass density depletion occurs as a consequence of the nonlinearity action. The mass density depletion is larger for a higher beta. As a consequence of this reduction, the plasma flow, pressure, and temperature are reduced. This scenario depends, however, on the value of the plasma beta. It was found that for beta = 0.1 both the plasma pressure and the temperature are increased at the dayside by the mass loading.

These results were published in the article entitled "Numerical simulations of mass loading in the solar wind interaction with Venus" in Journal of Geophysical Research, Vol. 101, 2547-2560, 1996.

5. 3-D Numerical modeling of the solar wind interaction with Venus

The large scale (global) interaction of atmosphere of Venus with the surrounding medium is numerically simulated in the framework of 3-dimensional magnetohydrodynamics. This study extends the analysis described in Section 4 into the case of the IMF perpendicular to the solar wind flow. The numerical simulations have been carried on for a long time which allow us to believe that the simulation approached a quasi-steady state.

The simulations are performed for the case of the interplanetary magnetic field perpendicular to the solar wind flow. The model reproduces several features of the interaction predicted by earlier theories and observations. The solar wind interaction with Venus is characterized by the mass loading of the solar wind with heavy oxygen ions which are produced by the photoionization of neutrals in the extensive ionosphere. This mass loading slows down the solar wind and ultimately leads to the formation of a magnetic barrier and a magnetotail. The location of the bow shock is barely affected by different values of the magnetic field strength. The numerical results indicate that the presence of mass loading causes the bow shock to move outward from the planet but not so far as observed at Venus during the period of maximum solar activity.

The perpendicular case, although similar in some aspects, differs in a general behavior to the parallel case. In particular, it is found that the plasma dynamics is hardly affected by the strength of the magnetic field which originated from the solar wind. The location of the bow shock is virtually the same for different values of the plasma beta. The IMF lines pile up against the atmospheric plasma and drape over the planet to form a magnetotail with two lobes of opposite magnetic polarity separated by a plasma sheet. The parallel magnetic field causes the plasma dynamics to be highly sensitive to the value of the plasma beta.

These results were published in the article entitled "Numerical modeling of the solar wind interaction with Venus" in Planetary Space Science, Vol. 44, 243-252, 1996.

PUBLICATIONS

Publications and presentations resulting from research supported by this NASA grant are listed below. Copies of the published papers are included in the appendix with this final report.

1. S. Cable and R. S. Steinolfson, MHD simulation of the solar wind interaction with Venus, EOS, Vol. 74, 254, 1993.

2. S. Cable and R. S. Steinolfson, MHD simulation of the Venus bow shock, EOS, Vol. 74, 380, 1993.

3. R. S. Steinolfson and S. Cable, Venus bow shocks at unusually large distances from the planet, Geophysical Research Letter, Vol. 20, 755-758, 1993.

4. S. Cable and R. S. Steinolfson, Three dimensional MHD simulation of the interaction of the solar wind with Venus, EOS, Vol. 75, 272, 1994.

5. S. Cable and R. S. Steinolfson, Three-dimensional MHD simulations of the interaction between Venus and the solar wind, Journal of Geophysical Research, Vol. 100, 21,645 - 21,658, 1995.

6. K. Murawski and R. S. Steinolfson, Numerical simulations of mass loading in the solar wind interaction with Venus, Journal of Geophysical Research, Vol. 101, 2547-2560, 1996.

7. K. Murawski and R. S. Steinolfson, Numerical modeling of the solar wind interactions with Venus, Planet. Space Sci., Vol. 44, 243-252, 1996.

APPENDICES

R. S. Steinolfson and S. Cable, Venus bow shocks at unusually large distances from the planet, Geophysical Research Letter, Vol. 20, 755-758, 1993.

S. Cable and R. S. Steinolfson, Three-dimensional MHD simulations of the interaction between Venus and the solar wind, Journal of Geophysical Research, Vol. 100, 21,645 - 21,658, 1995.

K. Murawski and R. S. Steinolfson, Numerical simulations of mass loading in the solar wind interaction with Venus, Journal of Geophysical Research, VOl. 101, 2547-2560, 1996.

K. Murawski and R. S. Steinolfson, Numerical modeling of the solar wind interactions with Venus, Planet. Space Sci., Vol. 44, 243-252, 1996.

GEOPHYSICAL RESEARCH LETTER, VOL. 20, NO. 8, PAGES 755-758, APRIL 23, 1993

VENUS BOW SHOCKS AT UNUSUALLY LARGE DISTANCES FROM THE PLANET

R. S. Steinolfson and S. Cable

Department of Space Sciences, Southwest Research Institute, San Antonio, Texas

Abstract. Recent analysis of data from the Pioneer Venus Orbiter (PVO) has shown that the bow shock often travels to unusually large distances from the planet when the solar wind magnetosonic Mach number is near unity. We suggest that distant bow shocks can be explained as an integral part of the response of the global solar wind/Venus interaction to the anomalous local solar wind conditions that existed during the time of these observations. The lower than normal plasma beta and magnetosonic Mach number are in a parameter regime for which the usual fast-mode bow shock close to the planet may not provide the necessary compression and deflection of the solar wind. Using MHD simulations we show that, for these conditions, the usual fast shock is replaced by a bow shock consisting of an intermediate shock near the Sun-Venus line and a fast shock at large distances from the Sun-Venus line. This composite bow shock propagates upstream away from the planet at a low speed and appears to be approaching a new equilibrium stand-off location at a large distance from the planet.

Introduction

For typical solar wind conditions the Venus bow shock is located within or near one radii (R_v) of the planet surface along the Sun-Venus line. However, for low magnetosonic Mach numbers during two orbits of PVO the bow shock was observed out to approximately 12 R_v away fron the planet at a 45° angle from the Sun-Venus line for one orbit and at 11 R_v above the terminator for the other [Russell and Zhang, 1992]. These low magnetosonic Mach numbers were due primarily to an enhanced interplanetary magnetic field (about a factor of 3 larger than more typical values) and also to a reduced solar wind density (about a factor of 3 lower than normal). Neither the solar wind speed nor the temperature deviated appreciably from average values; hence, the sound Mach number remained near a typical value. As a result, the plasma beta was lower than normal and most likely became less than or even much less than unity. The plasma beta can be written in terms of the Alfvén Mach number M_A and the sound Mach number M_s as $\beta=2(M_A/M_s)^2/\gamma$. The polytropic index (ratio of specific heats) γ is generally taken as 5/3. In a low-beta environment ($\beta < 1$) the fast-mode magnetosonic Mach number becomes equal to the Alfvén Mach number for parallel propagating shocks.

Russell and Zhang [1992] estimated that the Alfvén and magnetosonic Mach numbers were unity to within their ability to measure them. For a temperature of 10^5 °K and a solar wind speed of 500 km/sec (typical of conditions during their observations), the sound Mach number becomes approximately 9.5. Consequently, the plasma beta is about 0.013. For more usual solar wind conditions near Venus beta would have a value near 1.5.

We suggest that a possible explanation for the above erratic behavior of the bow shock is that the solar wind conditions in the vicinity of Venus become such that the usual fast MHD shock near the planet is no longer a stable solution. The fast MHD shock is replaced by a shock configuration containing an intermediate MHD shock over at least a portion of the shock front, and the resulting configuration propagates upstream.

Paper number 93GL00839
0094-8534/93/93GL-00839$03.00

Formation of Intermediate Shocks in CMEs

We begin by noting the similarity between bow shocks formed in the interaction of the solar wind with Venus and shocks formed ahead of CMEs in the solar corona (illustrated for the formation of fast shocks in the schematic in Figure 1). The analogy is most apparent when the north-south component of the interplanetary magnetic field (IMF) is small as assumed in the figure. The bow shock under normal conditions is approximately stationary in the laboratory frame, while the shock ahead of a CME propagates out through an expanding plasma. The similar behavior for the two examples of shock formation is most apparent in the rest frame of the individual shocks. A spiral component for the IMF (perpendicular to the figure) would not dramatically influence the analogous behavior for the two situations. Clearly, the essential physics should be similar for the two cases even for small north-south or spiral components of the IMF.

For given values of the shock speed and upstream conditions, the MHD shock-jump (Rankine-Hugoniot) equations reduce to a cubic polynomial and formally allow three physically realistic shock solutions with an entropy rise (slow, intermediate and fast shocks). It was long believed that intermediate shocks did not exist in nature and were nonevolutionary or extraneous [e.g., Kantrowitz and Petschek, 1966].

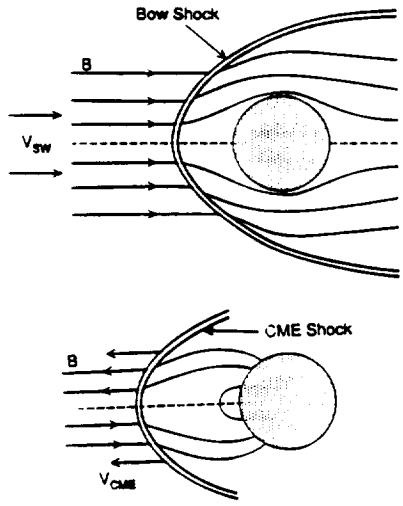

Fig. 1. A schematic illustrating the similarity between (a) the formation of a fast MHD bow shock in the interaction of the solar wind with Venus and (b) the formation of a fast MHD shock ahead of a CME propagating out through the solar corona.

Recent studies, however, lend support to the possibility that they may not be extraneous [e.g., Wu, 1990]. Steinolfson and Hundhausen [1990] show that intermediate shocks are necessary to provide a smooth and continuous transition from fast shocks to slow shocks with decreasing CME speed.

An important difference between the three types of MHD shocks is the effect that the shock has on the component of the magnetic field perpendicular to the shock normal. This component maintains the same direction across both slow and fast shocks. It increases in magnitude across a fast shock and decreases in magnitude across a slow shock. That is, fast shocks bend the magnetic field toward the shock plane, and slow shocks bend the magnetic field away from the shock plane. The perpendicular component of the magnetic field reverses direction across an intermediate shock, and the field magnitude may either increase or decrease.

In order for a particular type of shock to form, the shock speed (or solar wind speed in the case of bow shocks) must exceed the respective linear wave speed upstream of the shock. The wave speeds depend on the angle θ between the shock normal and the upstream magnetic field. For the relatively idealized configurations shown in Figure 1, the relevant wave speeds are close to the values for parallel shock propagation. The slow speed reduces to the sound speed at parallel propagation, and the fast speed becomes the Alfvén speed. The intermediate speed also reduces to the Alfvén speed at parallel propagation when $\beta<1$. Consequently, for the physical conditions we are interested in, intermediate shocks only form when the Alfvén Mach number is larger than 1 ($M_b>1$).

As shown by Steinolfson and Hundhausen [1990], there is also a maximum Alfvén Mach number for which intermediate shocks may form given by $M^2_{b\,crit} = [\gamma(1-\beta)+1]/(\gamma-1)$, where β is the value upstream of the shock. This expression was derived by Kennel and Edmiston [1988] as the maximum value for the formation of switch-on shocks. However, the formation of switch-on shocks and the formation of intermediate shocks are intimately related [Steinolfson and Hundhausen, 1990]. As noted in the introduction, for small values of β ($\approx 10^{-2}$-10^{-1}) the sound Mach number may be large even though the Alfvén Mach number is relatively small (near unity). The maximum value of $M_{b\,crit}$ occurs at $\beta=0$, in which case it has a value of 2 for $\gamma=5/3$, so the shock speed cannot be too high. Intermediate shocks do not exist at all for $\beta>1.2$. The net result is that intermediate shocks form when the CME shock Alfvén Mach number is in the range $1 < M_b < M_{b\,crit}$. By analogy, the solar wind Alfvén Mach number must be in the above range for intermediate shocks to form along a portion of the bow shock. This is exactly the parametric regime of the solar wind parameters for both β and M_b when the distant bow shocks were observed at Venus.

When intermediate shocks do form near the leading edge of CMEs, the shock front has the configuration shown in the schematic in Figure 2 [Steinolfson and Hundhausen, 1990]. The shock is assumed to be propagating vertically along the vertical magnetic field in the figure. The central portion of the shock front that is bowed downward away from the direction of travel (between the two switch-on shocks) contains the intermediate shocks. The shocks at the flanks beyond the switch-on shocks are fast shocks, and a gas dynamic shock exists at the point of parallel propagation at the center of the shock front.

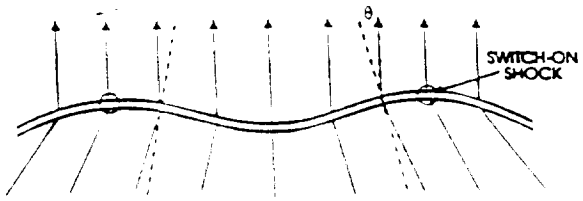

Fig. 2. A schematic illustrating the shape of a CME shock front when an intermediate MHD shock forms along a portion of the shock front. The lines with an arrow at the top indicate magnetic field lines, and the parallel curved lines are the shock front. The shock is travelling vertically along the uniform and parallel magnetic field lines. Note that the component of the magnetic field perpendicular to the shock normal reverses direction across the intermediate shock portion of the shock front located between the two switch-on shocks at parallel propagation.

MHD Simulation of Distant Bow Shocks

The MHD equations without explicit dissipation are used in this study. The equations are solved numerically using the modified Lax-Wendroff scheme given by Rubin and Burstein [1967] with a smoothing term suggested by Lapidus [1967]. In our simulations the planet is replaced by a cylinder aligned along the z-axis in a cylindrical coordinate system. The z-axis is taken to be in the ecliptic plane perpendicular to the Sun-Venus line, and the MHD equations are solved in the r,θ plane. This cylindrical approximation should retain the essential physics for this problem, although more realistic simulations would, of course, use a three-dimensional geometry.

The simulation is carried out for a cross-section of a cylindrical annulus lying between an inner radial boundary at the surface of the planet R_v and an outer radial boundary taken to be at 15 R_v. The θ axis is selected so that $\theta=0°$ is directed toward the Sun along the Sun-Venus line. The solar wind velocity and IMF are chosen such that the physical quantities are either symmetric (for ρ, p, u_r, B_r) or antisymmetric (for u_θ, B_θ) about the $\theta=0°$ and the $\theta=180°$ axes so the computation must be computed only for the numerical box given by $R_v \le r \le 15\ R_v$ and $0° \le \theta \le 180°$. The angular grid spacing is 1.5°, and the radial spacing is 0.15 R_v giving a grid of 122 by 95. The plasma velocity and magnetic field are required to be parallel to the surface of the planet, and zero-order radial extrapolation is used to determine the thermodynamic quantities on the planet surface. The physics and chemistry of the ionosphere should not be significant for the present study and are not included. Solar wind conditions are maintained on the dayside of the outer radial boundary, and zero-order extrapolation along the local flow direction is used to update values on the nightside.

The simulation is initiated without the magnetic field with the solar wind thermodynamic conditions specified throughout the numerical box and the solar wind velocity specified everywhere beyond $r=2R_v$. When this gas dynamic computation reaches a dynamic equilibrium, the initial magnetic field, as given by the potential flow solution for flow over a cylinder, is specified at every grid point. The time-dependent computation is then restarted and follows the solution as far in time as desired.

The results of two separate simulations are shown below. For the first one the solar wind conditions are such that β is near the typical value of 1.5 and is therefore too large for intermediate shocks to form. The magnitude of the IMF is increased for the second computation so that β is in the range for which intermediate shocks may form. All physical values except the IMF magnitude are the same for the two simulations. The solar wind speed is large enough that M_v is in the

appropriate range for intermediate shock formation at the lower value of β. The values that are the same for the two studies are V_{sw}=550 km/sec, n_{sw}=5 cm^{-3}, T_{sw}=10^5 °K, and M_s=10.6. The values for the high β study are B_0=4.8 nT, M_0=11.7, β=1.5, and those for the low β study are B_0=50 nT, M_0=1.1, β=0.014.

The density contours for the low-beta case when an intermediate shock is not formed are given in Figure 3. The solution has been run long enough that the shock, which is now a fast shock, has come to an equilibrium position ahead of the planet. At large distances from the planet the shock becomes very weak.

The solution in Figure 3 is in sharp contrast to that for the lower value of beta shown in Figure 4. This solution is not in dynamic equilibrium (see below) and has evolved for a total of 122 Alfvén times since the magnetic field was introduced into the solution. The Alfvén time is determined from the Alfvén speed computed using the above parametric values and the Venus radius. The bow shock has now taken on an almost planar shape with a depression near the Sun-Venus line that is concave away from the planet. This shape for the shock front is characteristic of one containing an intermediate shock in the concave portion as shown in the schematic in Figure 2.

The density rise at the leading edge of the disturbance near the Sun-Venus line in Figure 4 divides away from the Sun-Venus line into one density increase due to the bow shock and a second that extends downstream. The second rise is just a remnant of the original increase due to the fast shock as in Figure 3. The density distribution behind the planet also changes dramatically as the solution changes from that in Figure 3 with the usual fast shock solution to that in Figure 4 with an upstream propagating shock. The larger density downstream of the planet in Figure 4 is due to material that remains there as the downstream velocity decreases when the shock begins propagating upstream.

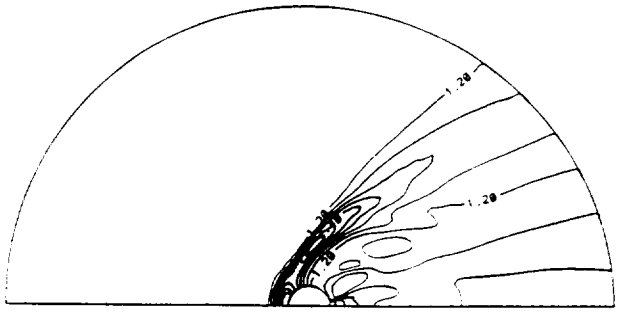

Fig. 3. Density contours for the high beta simulation discussed in the text. The density is normalized to the constant initial value, and the contours are from 0.3 to 3.3 in increments of 0.3.

Fig. 4. Density contours for the low beta simulation discussed in the text (see the caption for Figure 3). The density contours are from 0.5 to 3.9 in increments of 0.2. The dashed box on the density contours locates the boundary used for the plot of magnetic field lines in Figure 5. The small flat portion of the density contours near the Sun-Venus line is indicative of the finite grid spacing.

The magnetic field lines within the dashed box marked on Figure 4 are shown in Figure 5. The plot routine used to make this plot simply fits curves through local values of the magnetic field and arbitrarily begins and ends the curves so these curves should not be interpreted as being actual continuous field lines. The approximate location of the shock front, as determined by the density rise in Figure 4, is sketched on the field lines. Along the dashed portion of the shock front the shock clearly has the effect on the magnetic field lines expected for an intermediate shock (the component parallel to the shock front reverses direction). The shock is a fast shock along the solid part of the indicated shock front, and a switch-on shock separates the intermediate and fast shocks at the approximate location of the solid dot.

As mentioned above, the solution in Figure 4 is not in dynamic equilibrium. The shock front is travelling upstream and is slowly decelerating. For the 24 Alfvén times before the time used for Figure 4, the shock was propagating at an average speed of 20 km/sec, and for 73 Alfvén times prior to that it was propagating at an average speed of 25 km/sec. It is not clear why the shock travels upstream, although it is probably related to the fact that the intermediate shock may not be as capable of reducing the solar wind momentum as a fast shock, and consequently the stand-off distances increases. The numerical box has not been made large enough to allow the shock to reach an equilibrium position, if it indeed eventually will. Such issues are naturally important to fully understand the physics of these solutions, although their study would have more relevance for the case of flow over a sphere than that over a cylinder.

At large distances from the Sun-Venus line in Figure 4, the shock becomes a fast shock and is much weaker than it is closer to the Sun-Venus line where it is an intermediate shock. Such a weak shock at large distances is in general agreement with the weak shock observations reported in Russell and Zhang [1992]. The fast shock primarily deflects the magnetic field and velocity, while the intermediate shock compresses and slows the solar wind.

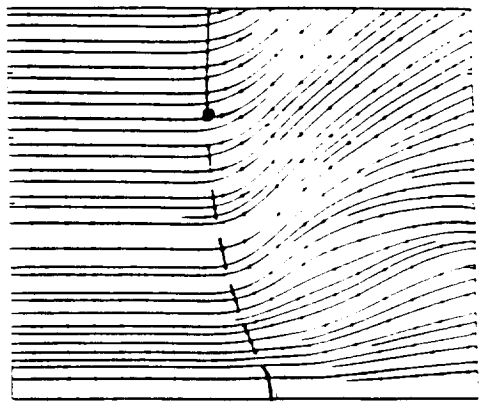

Fig. 5. Representative magnetic field lines within the dashed box on Figure 4. The curve indicates the approximate location of the shock as determined by the leading edge of the density increase.

Discussion

Studies of the formation of MHD shocks near the leading edge of CMEs have indicated that the type of shock formed depends on the plasma beta upstream of the shock and the magnetosonic Mach number of the shock relative to the upstream flow speed [e.g., Steinolfson and Hundhausen, 1990; Steinolfson, 1992]. By analogy, any dependencies on the parametric values found for shocks in CMEs should also exist in the case of bow shocks.

The CME studies suggest that the parametric values (beta and magnetosonic Mach number) during the distant Venus bow shock encounters reported by Russell and Zhang [1992] may be such that the more usual fast MHD bow shock near the planet is not a possible solution. Instead, we hypothesize (subject to two caveats discussed below) that the fast shock should be replaced by a shock front containing an intermediate shock near the Sun-Venus line and a fast shock at large distances from the Sun-Venus line with a switch-on shock separating the intermediate and fast shocks. Furthermore, the shock front should be concave away from the planet over the portion of the front containing the intermediate shock.

Having hypothesized that such a change in the shock types and configuration may occur when the solar wind conditions are similar to those during the observed distant bow shocks, we performed global MHD simulations to investigate this conjecture. As expected, the shock front consisted of the multiple shock types (switch-on, intermediate and fast) with the anticipated concave shape. The composite shock front propagated slowly upstream, and it is because of this movement of the shock front that the distant bow shock observations can be explained. From the simulations performed to date, it is not clear if the shock is simply moving to a new (large) stand-off distance. The shock appears to be decelerating as it travels upstream, and the numerical box may not have been large enough to allow the shock to reach a dynamic equilibrium position. In this parameter regime it is evident that the bow shock location is extremely sensitive to relatively small changes in the solar wind conditions. Additional simulations are needed to examine this sensitivity as well as to better understand the physics governing the upstream propagation and whether an equilibrium stand-off distance is always obtained.

Although the distant shock behavior reported by Russell and Zhang [1992] and that in the present simulations are qualitatively similar, there are at least two distinctions that deserve comment. First, our simulations are two-dimensional while the solar wind interaction with a planet is clearly, in the global sense, a three-dimensional phenomenon. However, the essential physics responsible for the transition from the usual fast shock solution to one with intermediate shocks near the point of parallel propagation is not three-dimensional. It is certainly true that the global ramifications of this shock transition would differ in a three-dimensional simulation from that computed in a two-dimensional such as that used here. The important point, though, is that the necessary physics is included in our simulation.

Second, at least two of the shocks reported by Russell and Zhang were quasi-perpendicular with angles between the shock normal and upstream magnetic field of 61° and 79° (based on the coplanarity assumption), while the upstream propagating bow shock in the simulations is quasi-parallel. As described in the paper, local quasi-parallel propagation is required to make the transition to the traveling shock front containing an intermediate shock. Even in the more realistic case with an azimuthal component of the magnetic field, there would still be some location on the shock envelope where the bow shock is quasi-parallel and all of the logic and results of the present study would apply. The angle between the shock normal and the upstream magnetic field at any location naturally depends on local conditions. It is certainly conceivable that the necessary quasi-parallel propagation exists at one location and that the shocks could still be quasi-perpendicular at the locations reported on by Russell and Zhang. The present work must be viewed as basically a feasibility study, and more extensive simulations including the third dimension are needed to examine the generality and applicability of our results in more realistic global environments.

Acknowledgements. This research was support by the National Aeronautics and Space Administration through research grant NAG2-692.

References

Kantrowitz, A. R., and H. E. Petschek, MHD characteristics and shock waves, *Plasma Physics in Theory and Application*, McGraw-Hill, New York, chap 6, 1966.

Kennel, C. F., and J. P. Edmiston, Switch-on shocks, *J. Geophys. Res.*, *93*, 11,363, 1988.

Lapidus, A., A detached shock calculation by second-order finite differences, *J. Comput. Phys.*, *2*, 154, 1967.

Rubin, E. L., and S. Z. Burstein, Difference methods for the inviscid and viscous equations of a compressible gas, *J. Comput. Phys.*, *2*, 178, 1967.

Russell, C. T., and T. -L. Zhang, Unusually distant bow shock encounters at Venus, *Geophys. Res. Lett.*, *19*, 833, 1992.

Steinolfson, R. S., Coronal shock waves, *Proceedings of the 26th ESLAB Symposium on the Study of the Solar-Terrestrial System, ESA SP-346*, 51, 1992.

Steinolfson, R. S., and A. J. Hundhausen, MHD intermediate shocks in coronal mass ejections, *J. Geophys. Res.*, *95*, 6389, 1990.

Wu, C. C., Formation, structure, and stability of MHD intermediate shocks, *J. Geophys. Res.*, *95*, 8149, 1990.

(Received November 18, 1992;
revised January 26, 1993;
accepted January 26, 1993.)

JOURNAL OF GEOPHYSICAL RESEARCH, VOL. 100, NO. A11, PAGES 21,645–21,658, NOVEMBER 1, 1995

Three-dimensional MHD simulations of the interaction between Venus and the solar wind

S. Cable

Department of Physics, Science University of Tokyo

R.S. Steinolfson

Aurora Science Incorporated, San Antonio, Texas

Abstract. We have developed a three-dimensional, single-fluid, MHD code which has successfully simulated the major qualitative features of the Venus - solar wind interaction. A bow shock forms at a height above the ionosphere close to that deduced from Pioneer Venus Orbiter (PVO) observations. The bow shock shows an asymmetry in the terminator plane qualitatively similar to results obtained from PVO data analyses. The magnetic field drapes over the planet and forms a two-lobed magnetotail. The magnetic field configuration near the planet is very similar to that recorded by PVO as well. We model the Venus obstacle as a hard, conducting sphere. We simulate the case in which the IMF is tilted with respect to the incoming solar wind velocity at approximately the Parker spiral angle; this is the first simulation of this particular case which includes all spatial regions of the interaction.

1. Introduction

The observed features of Venus's interaction with the solar wind have not yet been treated together in a single comprehensive model. Most models of the interaction have treated it as a gasdynamics process and have simplified the structure of the plasma flow in the tail region by attaching an infinite "extension" to the Venus obstacle [*Spreiter and Stahara*, 1980; *Moore et al.*, 1991]. These approaches are a necessary first step in understanding the interaction. However, gasdynamics models have severe limitations. They will never reproduce observed phenomena such as the magnetic barrier behind the bow shock [*Zhang et al.*, 1991] or magnetically produced asymmetries in the terminator plane shock configuration [e.g. *Russell et al.*, 1988]. Also, effectively extending the nightside of the Venus obstacle makes impossible the study of the near-tail region, where we can expect the solar wind flow to be most complex and where magnetic reconnection is most likely to take place.

A model which offers improved understanding of the tail region of Venus (as well as other nonmagnetized bodies impacted by the solar wind) has been developed by Luhmann and Schwingenschuh [*Luhmann and Schwingenschuh*, 1990; *Luhmann*, 1990; *Luhmann et al.*, 1991]. Here the flow outside the tail region is calculated from a gasdynamics model like those referred to above, while the flow inside the tail is calculated by fitting a model of a comet tail inside the obstacle. This model includes effects of mass loading from the Venus ionosphere. It gives good agreement with Phobos measurements of the magnetic field around Mars [*Luhmann et al.*, 1991] at distances outside the solar wind bow shock. However, the above mentioned effects of the magnetic field on the interaction still cannot be studied. Also, a single comprehensive model for the entire interaction is still desirable.

The first three-dimensional MHD simulation of the interaction is that of *Wu* [1992]. Wu simulated the bow shock of a hard, conducting sphere in an MHD fluid. A magnetic barrier was seen to form, and slight asymmetries in the bow shock caused by the interplanetary magnetic field (IMF) were detected. However, the plasma β (i.e., ratio of the thermal pressure to magnetic pressure) in this simulation was unrealistically high ($\beta \approx 8$), the tail region was not simulated, and no account was taken of mass loading.

The first three-dimensional MHD simulation of the Venus-solar wind interaction which treated all spatial regions of the interaction in a single model was *Tanaka*'s [1993] recent simulation. Like *Wu* [1992], Tanaka treats a hard, conducting sphere in an MHD fluid. A magnetic barrier is formed, the magnetic field clearly drapes over the planet, and complex flow in the near-tail region is observed.

In this paper we report the results of simulations we have made with a three-dimensional MHD code. Like *Wu* [1992] and *Tanaka* [1993], we model the Venus ionosphere as a hard, conducting sphere and the solar wind as a single-fluid MHD plasma. Some important physics

Paper number 95JA02174.
0148-0227/95/95JA-02174$05.00

of the problem is neglected in this approximation. We will not see effects from mass loading in the tail [*Brace et al.*, 1987], and the configurations of the shock and magnetic barrier can be reproduced with only limited accuracy without the ionosphere. However, this hard sphere model is an improvement over extending the tail of the obstacle, since it allows study of the near-tail region. In the future this approach can be supplemented with mass loading to give a better approximation of the ionosphere.

Our computational method differs greatly from *Tanaka*'s [1993]. He evolved the MHD equations on an unstructured mesh, while we use irregular spherical coordinates. Our time-stepping schemes are quite different as well. This, in and of itself, gives our code and simulations value: it is desirable to have more than one numerical realization of the same physical phenomenon, since numerical studies are often fraught with hazard and doubt. Further, we have improved the resolution near the surface of the planet at the price of restricting the size of our computational volume. This restriction in volume does not significantly affect the results we obtain, as will be discussed below; the only real sacrifice we have made here is that we are unable to study the far downstream region. We also simulate the Venus-solar wind interaction in the case where the IMF is tilted at an angle of 45° with respect to the incoming solar wind velocity. This case was studied by *Wu* [1992], but, as stated above, the value of $\mathcal{J}$ was unrealistically high and no attempt was made to include the tail region. This is the first time that all spatial regions of this asymmetric case have been simulated and that a realistic value of $\mathcal{J}$ has been used.

2. Numerical Method

2.1. Algorithm

Our simulation code solves the three-dimensional, nonlinear, ideal MHD equations:

$$\frac{\partial \rho}{\partial t} + \nabla \cdot (\rho \mathbf{v}) = 0 \tag{1}$$

$$\frac{\partial (\rho \mathbf{v})}{\partial t} + \nabla \cdot (\rho \mathbf{v}\mathbf{v}) + \nabla p - \frac{1}{4\pi}[\nabla \cdot (\mathbf{B}\mathbf{B}) - \frac{1}{2}\nabla B^2] = 0 \tag{2}$$

$$\frac{\partial \mathbf{B}}{\partial t} - \nabla \times (\mathbf{v} \times \mathbf{B}) = 0 \tag{3}$$

$$\frac{\partial}{\partial t}\left(\frac{\rho v^2}{2} + \frac{p}{\gamma - 1} + \frac{B^2}{8\pi}\right) + \nabla \cdot \left\{\left(\frac{1}{2}\rho v^2 + \frac{\gamma}{\gamma - 1} p\right)\mathbf{v} + \frac{1}{4\pi}[\mathbf{B} \times (\mathbf{v} \times \mathbf{B})]\right\} = 0. \tag{4}$$

where ρ is the mass density, p is the thermal pressure, $\mathbf{v}$ is the fluid velocity, and $\mathbf{B}$ is the magnetic field.

We use the modified Lax-Wendroff scheme developed by *Rubin and Burstein* [1967] to time step these equations. A fourth-order smoother and a smoothing term suggested by *Lapidus* [1967] are added to inhibit numerical instabilities.

We evolve the equations in spherical coordinates with the $\theta = 0$ axis directed toward the Sun. Spherical coordinates allow us to pack grid points more densely near the planet's surface, where the most dramatic changes in the fluid flow occur. Near the planet's surface, the grid spacing is about 0.017 R_V. The grid spacing increases smoothly so that about 30 grid points lie between the planet's surface at 1 R_V and a radius of 1.5 R_V. The θ=0 axis (the Cartesian z axis) points from the center of Venus toward the Sun. The y axis (i.e., $\theta = \pi/2, \phi = \pi/2$) lies in the direction of $\mathbf{v}_\infty \times \mathbf{B}_\infty$, $\mathbf{v}_\infty$ and $\mathbf{B}_\infty$ being the incoming, unperturbed solar wind velocity and magnetic field, respectively. The x axis ($\theta = \pi/2, \phi = 0$) completes the right-handed coordinate system. (An alternative way of stating this is that the x axis is aligned so that $\mathbf{v}_\infty$ and $\mathbf{B}_\infty$ are both contained in the x-z plane, and the y axis completes the right-handed coordinate system.) This coordinate system was by far the most straightforward to code and is certainly the system of choice for giving a clear explanation of our algorithms. Unfortunately, it is not the coordinate system in which most observations of the Venus-solar wind interaction have been expressed in the literature. The results of our computations will be presented therefore in different coordinates, as will be discussed below.

The momentum conservation (2) requires some extra attention. The term

$$\frac{1}{4\pi}\nabla \cdot (\mathbf{B}\mathbf{B})$$

can be written

$$\frac{1}{4\pi}(\mathbf{B} \cdot \nabla \mathbf{B} + \mathbf{B}\nabla \cdot \mathbf{B}).$$

$\mathbf{B}\nabla \cdot \mathbf{B}$ is identically zero in nature. In numerical simulations such as ours, however, $\nabla \cdot \mathbf{B}$ can become large enough to produce sizable, nonphysical forces directed along the magnetic field lines.

We have handled this difficulty by periodically subtracting the part of the magnetic field which contributes to $\nabla \cdot \mathbf{B}$. This is accomplished as follows: the magnetic field can be thought of as composed of two pieces,

$$\mathbf{B} = \mathbf{B}_p + \mathbf{B}_d$$

where $\nabla \times \mathbf{B} = \nabla \times \mathbf{B}_p$ and $\nabla \cdot \mathbf{B} = \nabla \cdot \mathbf{B}_d$. The field $\mathbf{B}_d$ is therefore the gradient of a potential Φ.

$$\nabla^2 \Phi = \nabla \cdot \mathbf{B}_d = \nabla \cdot \mathbf{B}.$$

We solve this equation for Φ, then find $\mathbf{B}_p$ by subtracting $\nabla\Phi$ from $\mathbf{B}$:

$$\mathbf{B} \rightarrow \mathbf{B}_p = \mathbf{B} - \nabla\Phi.$$

The potential Φ is obtained by a successive over-relaxation (SOR) method that we developed by adapt-

ing the SOR method of *Press et al.* [1992] to spherical coordinates with irregular grid spacing.

The values of all quantities at the inflow boundary ($\theta < 90°$) are set by input and held fixed throughout the time of the simulation. Quantities on the outflow boundary ($\theta > 90°$) are determined by first-order interpolation from the interior in such a way that $\partial/\partial z = 0$ for all quantities (z representing the Cartesian axis lying along the $\theta = 0$ line). The outer radius of the simulation box is 3 R_V.

The plane containing the incoming velocity and magnetic field vectors is a plane of reflective symmetry, so we need simulate no more than one hemisphere of the entire spherical volume of the system. Reflective boundary conditions hold therefore at $\phi = 0$ and $\phi = \pi$. When we are simulating flow exactly perpendicular to the IMF, we need simulate only a quarter sphere. In this case, $\phi = 0$ is still a reflective plane. At $\phi = \pi/2$, symmetry boundary conditions hold for the scalar quantities, the velocities, and B_ϕ, while antisymmetry conditions hold for B_θ and B_r.

The Venus obstacle is modeled as a hard, conducting sphere sitting at the radial center of the simulation box. At the Venus surface, $r = 1\ R_V$ and radial velocities and magnetic fields are set equal to zero, while all other quantities are determined by zero-order extrapolation in the radial direction.

Our numerical method, along with most numerical methods, will not work unaided at the coordinates $\theta = 0$ or $\theta = \pi$, since these coordinates are singular. We have found a satisfactory means of dealing with this difficulty. Even though this problem will present itself in almost any effort to model fluid or MHD physics in spherical coordinates, it is not extensively discussed in the literature. We will therefore discuss in some detail our handling of the singular coordinates. We will discuss the $\theta = 0$ coordinate here: the analogy with $\theta = \pi$ can be drawn readily.

Let i, j, and k label nodes in the r, θ, and ϕ directions, respectively. The $j = 1$ coordinate line corresponds to $\theta = 0$. For a given node on the $j = 1$ axis, $(i, 1, k)$, the values of ρ, p, v_r, and B_r are set equal to the averages of these quantities across the surrouding nodes $(i, 2, k)$. That is,

$$\forall k: \begin{Bmatrix} d_{i,1,k} \\ p_{i,1,k} \\ v_{r\,i,1,k} \\ B_{r\,i,1,k} \end{Bmatrix} = \frac{1}{K-2} \sum_{l=2}^{K-1} \begin{Bmatrix} d_{i,2,l} \\ p_{i,2,l} \\ v_{r\,i,1,l} \\ B_{r\,i,1,l} \end{Bmatrix}. \quad (5)$$

The $k = 1$ and $k = K$ grid points are left out of the average, since they are boundary points and lie outside of the proper region of computation. That is to say, we wish to average over one hemisphere (or quarter sphere, in the case of perpendicular flow). The coordinates ϕ_2 and ϕ_{K-1} lie just inside the hemisphere (or quarter sphere), while the coordinates ϕ_1 and ϕ_K lie just outside. To include these outside points in the average would give added and uneven weighting to the values at the ϕ boundaries.

On the axis the magnetic field and velocity lie entirely in the x–z plane which, as discussed above, is a symmetry plane. Therefore, on the $\theta = 0$ axis, there are no components B_y or v_y: $\mathbf{B} = B_x\hat{\mathbf{x}} + B_z\hat{\mathbf{z}}$ and $\mathbf{v} = v_x\hat{\mathbf{x}} + v_z\hat{\mathbf{z}}$. We have already indicated how v_z and B_z are calculated, since $\hat{\mathbf{z}} = \hat{\mathbf{r}}$ on the $\theta = 0$ axis. The $\hat{\mathbf{x}}$ components of these vectors A_x are calculated from the corresponding vectors of the $j = 2$ grid points:

$$\bar{A}_{x\,i,1,k} = \frac{1}{K-2} \sum_{l=2}^{K-1} A_{\theta\,i,2,l}\hat{\theta}_2\cdot\hat{\mathbf{x}} + A_{\phi\,i,2,l}\hat{\phi}_l\cdot\hat{\mathbf{x}}$$

$$= \frac{1}{K-2} \sum_{l=2}^{K-1} A_{\theta\,i,2,l}\cos\theta_2\cos\phi_l - A_{\phi\,i,2,l}\sin\phi_l.$$

Now A_θ and A_ϕ are quite naturally defined on the axis as

$$A_{\theta\,i,1,k} = \bar{A}_x\cos\phi_k \quad (6)$$

$$A_{\phi\,i,1,k} = -\bar{A}_x\sin\phi_k. \quad (7)$$

A factor of $\cos(\theta = 0)$ is implicit in the above formulas. So, on the $\theta = \pi$ axis,

$$A_{\theta\,i,1,k} = -\bar{A}_x\cos\phi_k \quad (8)$$

$$A_{\phi\,i,1,k} = \bar{A}_x\sin\phi_k. \quad (9)$$

since $\cos(\pi) = -1$. With the components of **B** and **v** defined in this manner, **B** and **v** at any location along the axis are unique vectors whose components take on different values depending on the direction from which the axis is approached.

2.2. Initial Conditions

The density and pressure are initially constant throughout the simulation volume. The initial velocity field is the flow of an incompressible fluid over a sphere, directed along the $\theta = 0$ axis:

$$v_r = -v_0\left[1 - \left(\frac{R_V}{r}\right)^3\right]\cos\theta$$

$$v_\theta = v_0\left[1 + \frac{1}{2}\left(\frac{R_V}{r}\right)^3\right]\sin\theta$$

$$v_\phi = 0.$$

The magnetic field is initialized in the same way, except that the field configuration is rotated about the y axis (as defined above) so that the incoming IMF is skewed with respect to the solar wind flow by the desired angle. With the magnetic field initialized in this manner, $\nabla\cdot\mathbf{B}$ is zero everywhere, discounting the effects of the discrete grid. The parameters we have chosen for the solar wind are summarized in Table 1. These parameters are all close to the typical solar wind parameters reported by *Phillips et al.* [1986]. The average solar wind cone angle (i.e., the acute angle between the IMF

Table 1. Simulation Solar Wind Parameters

Parameter	Value
Number density	$20/cm^3$
Thermal pressure	6.06×10^{-2}nPa
Sound speed	55 km/s
Velocity	370 km/s
Sonic mach number	6.73
Dynamic pressure	4.10 nPa
Magnetic field magnitude	10 nT
Plasma beta (β)	1.5

and the solar wind flow direction) is given as 42.2° by Phillips et al.We perform simulations with cone angles of 0°, 45°, and 90°.

3. Results

In this section we report some of the results from our simulations and compare them with published analyses of Pioneer Venus Orbiter (PVO) data. We give particular attention to the configuration of the overall shock structure and to the configuration of the magnetic field. First, though, a few words need to be said regarding nomenclature. We have simulated bow shocks arising in IMF cone angles of 0°, 45°, and 90°. These simulations will be referred to as the parallel, 45°, and perpendicular simulations, respectively. Also, in the following sections, "altitude" refers exclusively to distance measured from the planet's surface, while "radius" denotes distance measured from the center of the planet. Finally, up to this point we have used standard Cartesian and polar coordinates to denote spatial directions. From hereon, however, in order to facilitate comparisons with existing data and data analyses, we will use the B-e coordinate system of *McComas et al.* [1986]: the unperturbed solar wind flows in the $-\hat{\mathbf{x}}$ direction (corresponding to the $-\hat{\mathbf{z}}$ direction in our code), while the cross-flow component of the unperturbed magnetic field lies in the $\hat{\mathbf{y}}$ direction (our code's $-\hat{x}$ direction). The $\hat{\mathbf{z}}$ direction (our code's $-\hat{y}$ direction) completes the right-handed coordinate system.

3.1. Diagnostics

We simulated parallel fast shocks with the three-dimensional (3-D) code, then compared the results with simulations from a well-tested, often used two-dimensional (2-D) spherical geometry code (that is, a code written for spherical geometry and cylindrical symmetry) with identical initial conditions and spatial gridding. The results were virtually identical, as they must be if the 3-D code is working as well as the 2-D code.

The shock jump conditions along the stagnation streamline can be calculated analytically for the parallel and perpendicular shocks. We find that almost all jump conditions are satisfied in both simulations with a relative error of less than 10%. The uncertainty in the jump conditions arises from uncertainty in determining the exact location of the shock and from uncertainty in the applicability of the standard shock jump conditions. Our simulated shocks have finite widths of about 0.05 R_V and smooth, albeit rather sudden, transitions between the upstream and downstream sides. As a result, the values of the physical quantities immediately downstream of the shock are often difficult to determine exactly. The standard shock jump conditions, on the other hand, are derived for shock fronts separating two fluid regions which are in equilibrium, i.e., two regions in which d/dt is zero for all quantitites. In the system we are simulating, d/dt is zero only in the inflow region. Significant pressure and magnetic forces exist behind the shock. So even though we have temporal equilibrium (that is, $\partial/\partial t$ is zero for all quantities), d/dt is certainly not zero in between the shock front and the planet's surface.

As mentioned above, a finite divergence in the magnetic field gives rise to unphysical forces directed along the magnetic field lines. Only if the magnitude of the physical force, $|-\nabla p + \mathbf{B}\cdot\nabla\mathbf{B}/4\pi - \nabla B^2/8\pi|$, is much larger than the magnitude of the purely numerical force, $|\mathbf{B}\nabla\cdot\mathbf{B}/4\pi|$, can we believe the results of our simulations. We have inspected the ratio of these two forces in both the perpendicular and 45° simulations. We find that almost everywhere in the simulation volume the numerical force is less than 1% of the physical force. The exceptions to this rule occur in isolated volumes within the numerical shock front and result from the way our numerical procedure handles discontinuities.

We have examined how the location of the computational outer boundary affects the simulation results by performing simulations of the parallel shock with the outer boundary set at 3 and at 10 R_V. A comparison of pressure contours in the region extending from the surface out to 3 R_V is shown in Figure 1. Figure 1, top, shows the pressure distribution with the outer computational radius set at 3 R_V, and Figure 1, bottom, shows the distribution when the outer computational radius is at 10 R_V. Differences are apparent but small. Likewise, all other quantites show only small differences which are in no way qualitative. On the basis of this study, we have chosen to place the outer radial boundary for all the present simulations at 3 R_V in order to obtain better numerical resolution near the planet's surface.

3.2. Global Behavior

Figure 2 shows field lines from the final configuration of the 45° simulation. The line traces were begun at points on the outer computational boundary, 0.1 R_V above the ecliptic plane. The field lines pile up at the shock front, then slip over the planet. Within the shock they are advected downstream less quickly than outside the shock. By the time they have escaped the vicinity of the planet's surface on the downstream side, they are stretched and bent so that they form a two-lobed magnetotail behind the planet. The magnetic field points largely sunward in one lobe (the top lobe of Figure 2, in this case) and largely antisunward in the other. The two lobes are separated by a distinct current sheet [*McComas et al.*, 1986]. This behavior qualitatively matches the behavior predicted by *Alfvén* [1957] and observed by *McComas et al.* [1986]. Note that in the bow shock the

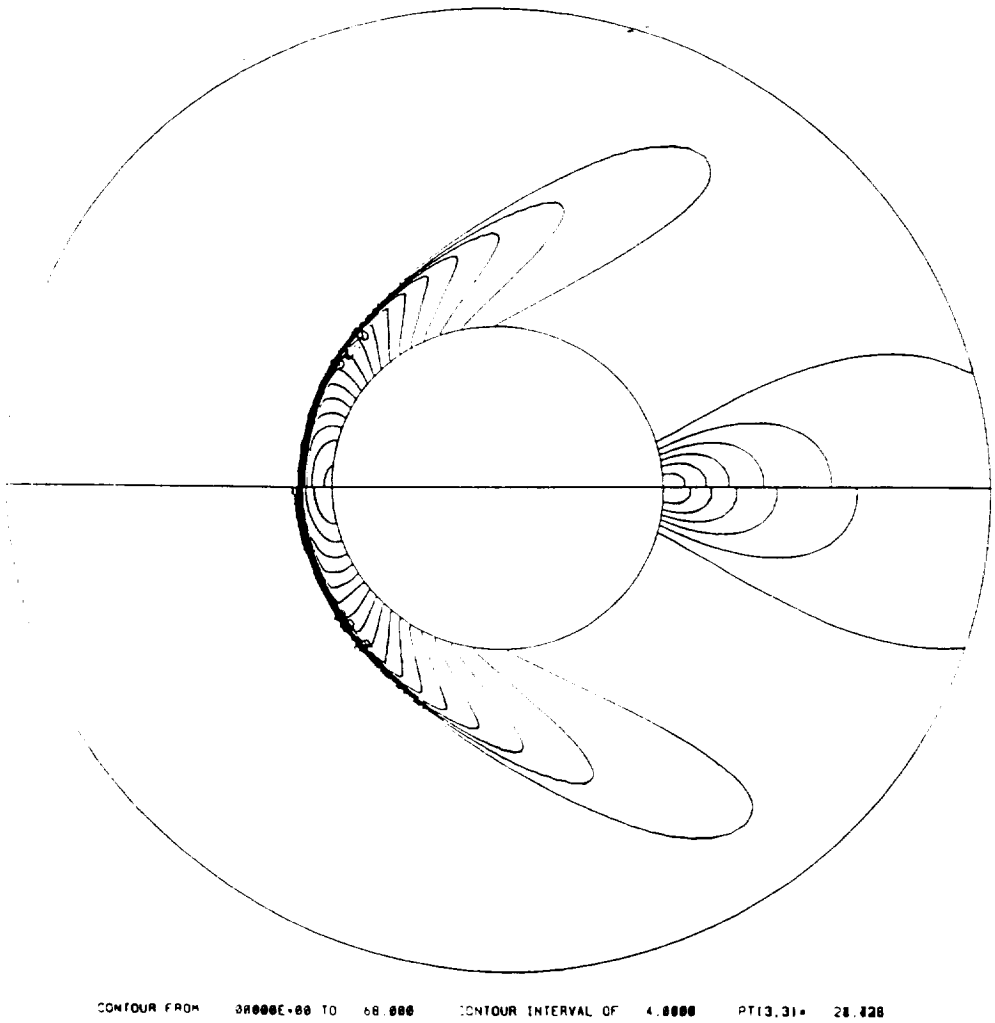

Figure 1. Pressure contours of the solar wind impacting Venus when incoming flow and interplanetary magnetic field (IMF) are aligned along the sunward axis. The top half shows the results of a simulation performed with the outer computational boundary set to 3 R_V; the bottom half shows the results of a simulation with the outer computational boundary at 10 R_V.

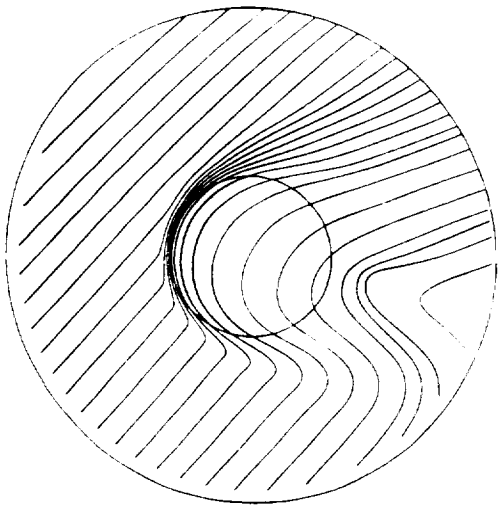

Figure 2. Magnetic field lines of the solar wind plasma impacting Venus. The solar wind flows in from the left and out the right. The incoming magnetic field is tilted at an angle of 45° with respect to the incoming velocity. Note that the stretched magnetic field lines form a two-lobed magnetotail behind the planet.

magnetic field line pileup is greatest where the field is more closely perpendicular to the shock normal. This is expected, since, all other things being equal, as a shock becomes more perpendicular, the increase in the magnitude of the magnetic field becomes larger. The perpendicular simulation shows all of the above global characteristics, but, of course, it is symmetric with respect to the x-z plane (i.e., the x-z plane of the B-V coordinate system). (A note of caution: magnetic field magnitudes cannot be reliably inferred from the field line densities in Figure 2. First, perspective effects make some lines look closer than they actually are. Second, the starting points of the lines, particularly in the tail region, were not chosen to systematically indicate magnetic field magnitude but to clearly show the global behavior of the field lines.)

It can be seen in Figure 2 that the field lines of the unperturbed magnetic field are not perfectly straight. This is because of the intial conditions discussed in the section 3.1. The initial upstream field could not be chosen to be perfectly uniform because we needed to satisfy $\nabla \cdot \mathbf{B} = 0$ in the presence of the conducting

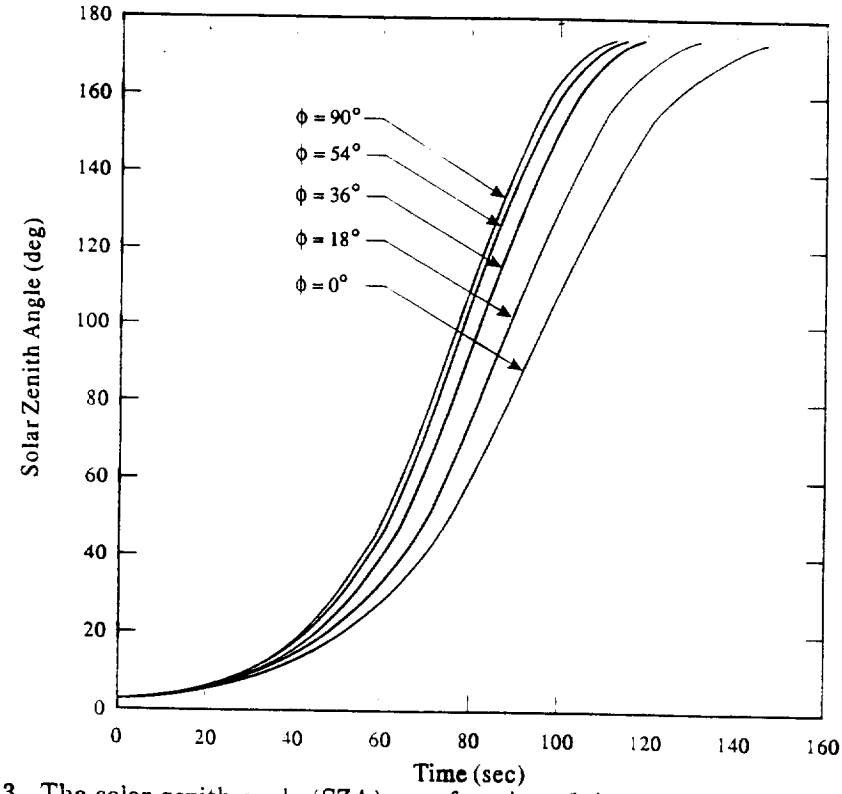

Figure 3. The solar zenith angle (SZA) as a function of time of several fluid elements moving across the surface of the planet. In the simulation that produced these results the IMF was perpendicular to the incoming velocity. Each of the five elements was given an initial SZA of about 5° and initial polar angle positions of 0°, 18°, 36°, 54°, and 90° measured from the ecliptic plane. Magnetic slingshot forces manifest themselves, in that fluid elements moving in the noon-midnight plane ($\phi = 90°$) are accelerated more quickly than fluid elements moving in the ecliptic plane ($\phi = 0$).

planet's surface. Therefore the initial magnetic fields are not exactly parallel to each other. Since the inflow boundary conditions are held fixed throughout the run of the simulation, the incoming upstream magnetic field are slightly curved. Setting the outer computational boundary farther out would ameliorate this effect. The slight departure from uniformity in the upstream magnetic field seems to have no significant effect on the plasma flow.

Magnetic field slingshot forces manifest themselves in the velocity distribution of the plasma near the planet's surface. Figure 3 shows, as a function of time, the solar zenith angle of fluid elements in the perpendicular simulation moving across the surface of the planet. Here the initial positions of the fluid elements were chosen just above the planet's surface, near the subsolar point. The plasma moving across the pole ($\phi = 90°$) is accelerated more quickly and reaches the far side of the planet faster than the plasma moving in the ecliptic plane. This happens because the perpendicular field lines become "hung up" in the bow shock, then slip quickly over the pole, dragging solar wind plasma with them.

3.3. Shock Configuration

We find that the standoff distance at the subsolar point varies with the cone angle, but we do not see a monotonic trend. If we locate the shocks by the outer edges of each shock layer, the standoff distance of the parallel shock is 0.28 R_V, the standoff distance of the 45° shock is 0.22 R_V, and the standoff distance of the perpendicular shock is 0.26 R_V. In absolute terms these numbers translate into 1700, 1340, and 1580 km, respectively. The 45° simulation is the one most representative of the typical solar wind conditions at Venus [*Phillips et al.*, 1986]. *Zhang et al.* [1990] find from PVO data that the subsolar standoff distance varies from 1600 km at solar minimum to 2200 km at solar maximum. The difference between our computed results and the observations can be explained by the lack of a model of Venus's ionosphere in our simulations. If we try to account for the ionosphere by simply adding 300 km to the effective radius of Venus (approximately the altitude found by *Zhang et al.* [1990]), we can expect the computational standoff distances to scale proportionately, since the Venus radius is the only inherent scale length in the system. We then find standoff distances above the ionosphere of 1780, 1400, and 1650 km. To find the altitudes of the shocks above the planet itself, we add in the 300 km thickness of the ionosphere. This gives altitudes of 2080, 1700, and 1950 km. These numbers are now well within the range found by Zhang et al.Including the ionosphere, then, is essential for determining the bow shock location.

Figures 4–8 show distributions of pressure and magnetic field magnitude from the parallel, 45°, and perpendicular simulations. The outer computational boundary was 3 R_V, but here we show only the region contained within 1.5 R_V in order to bring out more details.

The pressure and magnetic field magnitude distributions of the parallel case are shown in Figure 4. Since the parallel configuration is cylindrically symmetric, the distributions shown here represent the distributions in all polar angle planes. The decrease in the magnetic field strength downstream of the shock, around the subsolar line, is the result of MHD physics together with the boundary conditions imposed on the magnetic field. That is, a parallel shock has no increase in magnetic field, so the field strength remains fairly constant through the shock. Also, the field decreases near the planet's surface because the planet is conducting: there can be no radial magnetic field component at the planet's surface, but near the subsolar line, the magnetic field is almost purely radial. Therefore the magnetic field strength drops to zero in this region.

The distributions shown for the 45° (Figures 5 and 6) and perpendicular (Figures 7 and 8) cases represent only the ecliptic and noon-midnight planes. The magnetic field strength rises monotonically to a peak at the planet's surface, while the pressure reaches a maximum just downstream of the shock, then drops to a lower value at the planet's surface. This behavior indicates the formation of a magnetic barrier, which we discuss in more detail below.

The solution for the 45° simulation does not possess reflective symmetry about the $\hat{\mathbf{x}}$ axis (i.e., the axis pointed toward the Sun or the $\theta = 0$ axis in spherical coordinates), a symmetry which the parallel and perpendicular solutions possess by definition. For instance, the part of the shock front where the shock normal is quasi-perpendicular to the magnetic field stands about 6% farther out from the planet's surface than does the part of the front where the shock normal is quasi-parallel. This is to be expected: the magnetosonic speed along the shock normal in the quasi-perpendicular region is higher than the speed in the quasi-parallel region. Consequently, information in the quasi-perpendicular region can propagate farther away from the planet's surface before its progress is impeded by the onrushing solar wind. This is also consistent with *Wu*'s [1992] MHD simulations of a plasma with β=8.

The distributions of the plasma quantities within the bow shock are also asymmetric for the 45° case. The magnetic pressure has a slightly higher buildup in the quasi-perpendicular region than in the quasi-parallel region. This is consistent with the general expectation that perpendicular shocks have a larger buildup

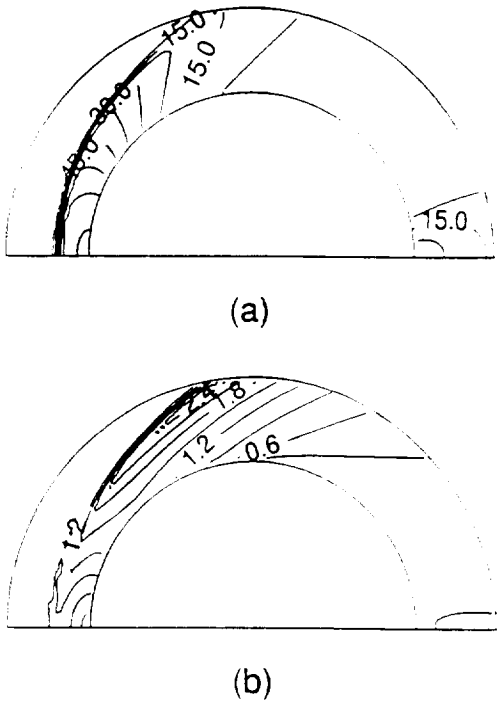

Figure 4. (a) Pressure and (b) magnetic field magnitude distributions of the solar wind. The magnetic field and the incoming velocity are aligned along the sunward axis.

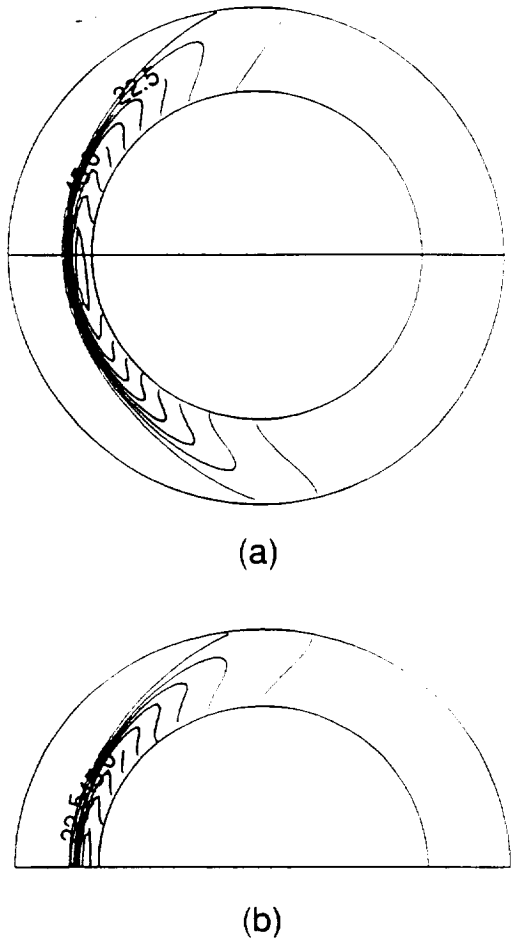

Figure 5. Pressure distributions of the solar wind with (a) the ecliptic plane and (b) the noon-midnight plane shown. The IMF is tilted by 45° with respect to the incoming velocity. The IMF orientation is such that the shock is quasi-perpendicular in the top half and quasi-parallel in the bottom half of Figure 5a.

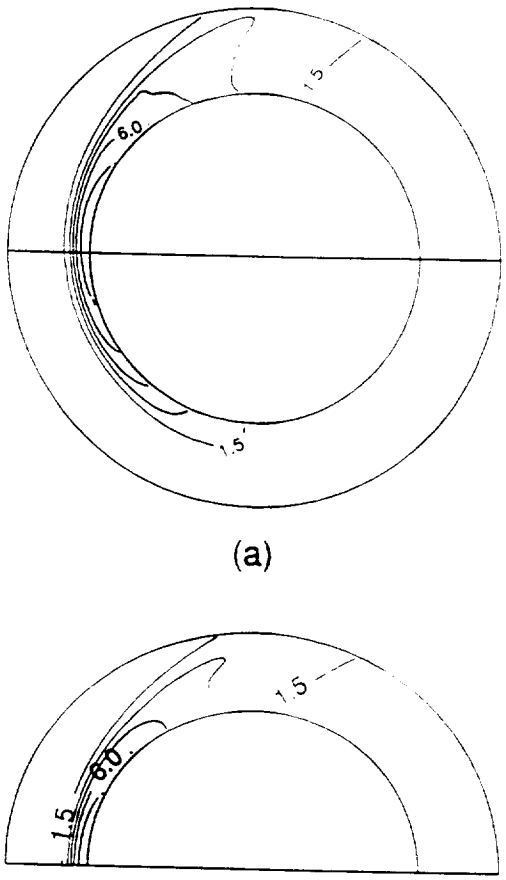

Figure 6. Magnetic field magnitude distributions of the solar wind with (a) the ecliptic plane and (b) the noon-midnight plane shown. The IMF is tilted by 45° with respect to the incoming velocity. The IMF orientation is such that the shock is quasi-perpendicular in the top half and quasi-parallel in the bottom half of Figure 6a.

of magnetic field than parallel shocks. The thermal pressure and density maxima shift away from the subsolar point toward the quasi-parallel side of the shock. The slightly higher buildup of magnetic pressure in the quasi-perpendicular region might explain this, since it would be expected that this pressure would divert some of the plasma flow into the quasi-parallel region.

In the terminator plane we find average distances from the planet center to the bow shock of 1.76, 1.92, and 1.95 R_V, for the parallel, 45°, and perpendicular shocks, respectively. The terminator locations of the 45° and perpendicular shocks are shown in Figure 9. The locations have been determined by the rise in entropy of the shocked solar wind. Regarding the latter two shocks, there is an uncertainty in their positions of the order of 0.1 R_V because, as mentioned above, the simulated shocks are not true discontinuities. The parallel shock, on the other hand, is almost as well defined at the terminator as it is at the nose. *Russell et al.* [1988] find that the average terminator distance varies between 2.14 R_V at solar minimum and 2.40 R_V at solar maximum. The discrepancy here is, again, attributable to the lack of the Venus ionosphere in our simulations.

We find that the average shock altitude at the terminator increases as the cone angle increases. This agrees with *Zhang et al.* [1990], who find that the altitude is typically 1630 km for cone angles less than 45° and 1840 km for cone angles greater than 45°. The relative difference is about 12%. The relative difference between our perpendicular and parallel altitudes is around 25%. This is not necessarily inconsistent with Zhang et al. As they state, if they could have had more data at low cone angles, their relative difference would have been much larger. On the other hand, we have compared the two most extreme cases possible. Comparisons of shock altitudes corresponding to cone angles of 30° and 60° would be more appropriate.

We find that the shock boundary in the terminator plane is asymmetric in a manner qualitatively consistent with the findings of *Russell et al.* [1988]. They find that when the IMF is nearly perpendicular to the solar wind flow, the distance from the planet center to the shock in the noon-midnight plane is about 10% greater than the distance along the equatorial plane. Our perpendicu-

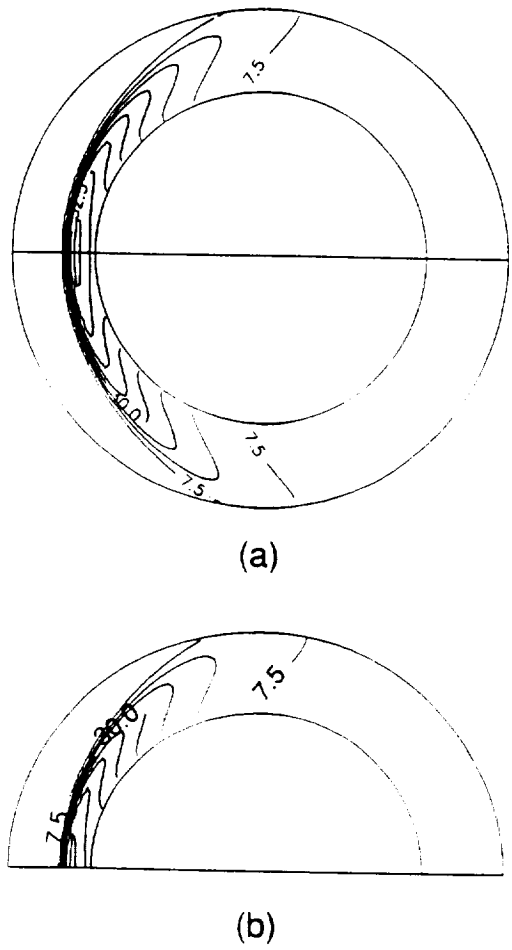

Figure 7. Pressure distributions of the solar wind with (a) the ecliptic plane and (b) the noon-midnight plane shown. The IMF is perpendicular to the incoming solar wind.

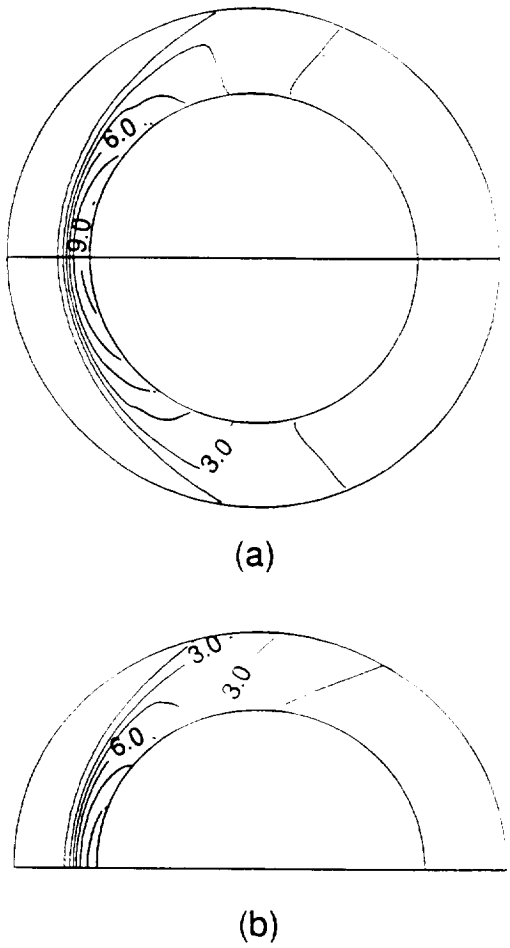

Figure 8. Magnetic field magnitude distributions of the solar wind with (a) the ecliptic plane and (b) the noon-midnight plane shown. The IMF is perpendicular to the incoming solar wind.

lar simulation gives a smaller asymmetry of about 5%, which is consistent with *Tanaka*'s [1993] recent MHD simulation result. This asymmetry can be seen, with some effort, in Figure 9. It has been suggested by Russell et al., among others, that the asymmetry is caused by the difference in the polar and equatorial magnetosonic speeds. Given our code's radial resolution at the terminator shock location ($\Delta r \approx 0.03$), our code should be able to differentiate between a 5% and 10% asymmetry. In light of our agreement with Tanaka and in view of our radial resolution, it seems that the magnetosonic speed accounts for some but not all of the asymmetry. The rest of the asymmetry arises from non-MHD processes, perhaps pole-equator asymmetries in ion pickup, as mentioned by Russell et al.

The ratios of the terminator shock radii to the subsolar or nose radii are given by 1.44, 1.57, and 1.55 for our three simulations. *Zhang et al.* [1990] find a typical value of 1.66.

3.4. Magnetic Fields in the Shock

The most striking feature of the behavior of the magnetic field is the clear draping of the field as it is advected around the planet (as shown in Figure 2 and discussed above). The ecliptic plane magnetic field configuration of the 45° simulation is shown in Figure 10. The solar wind is flowing in from the top. Regarding the magnetotail, the magnetic field of one lobe is fairly uniform in direction and has a magnitude of the order of 10 nT. In the other lobe the magnetic field lines are strongly curved and the magnetic field strength is 0.1-1.0 nT. The results shown in Figure 10 are very similar to the average magnetic field distribution found by *Phillips et al.* [1986]. (See, particularly, *Phillips et al.* [1986, Figure 5d]. Keep in mind that because of the orientation of our simulation magnetic field, our results must be reflected across the x-z plane before a direct comparison can be made with PVO data. This, of course, entails no change in the physics involved here.) Two points deserve particular mention in this regard. First, at low altitudes the field tends to encircle the planet. Second, the separating current sheet is not aligned with the plasma flow. Rather, it is angled toward the lobe of weaker magnetic field. Also regarding the current sheet, we find that it is displaced from the center of the tail by about 0.5 R_V. *McComas et al.* [1986] find a similar displacement 8-12 R_V downstream.

The magnetic field magnitude from the 45° simulation is shown in Figure 11. The half of the ecliptic

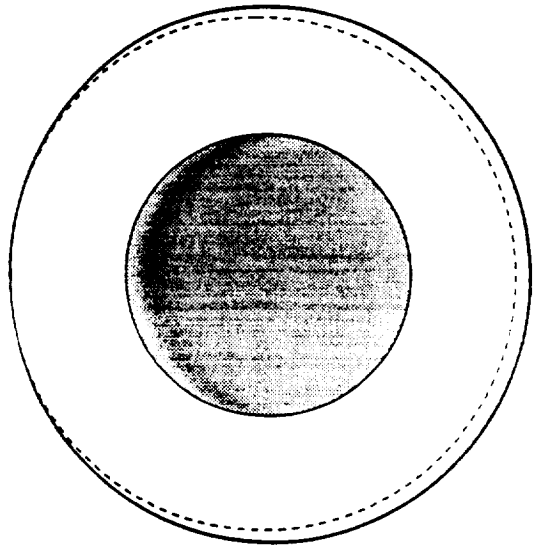

Perpendicular simulation

45°simulation

Figure 9. Cross sections of the shock locations in the terminator plane. The view is from upstream, looking downstream. The solid line is the cross section produced by the simulation where the IMF was perpendicular to the solar wind velocity. Note the slight asymmetry: the distance to the shock is somewhat longer in the noon-midnight plane than in the ecliptic plane. The dashed line is from the simulation where the IMF was tilted at 45° with respect to the velocity: the left side of this cross section is where the shock was most perpendicular.

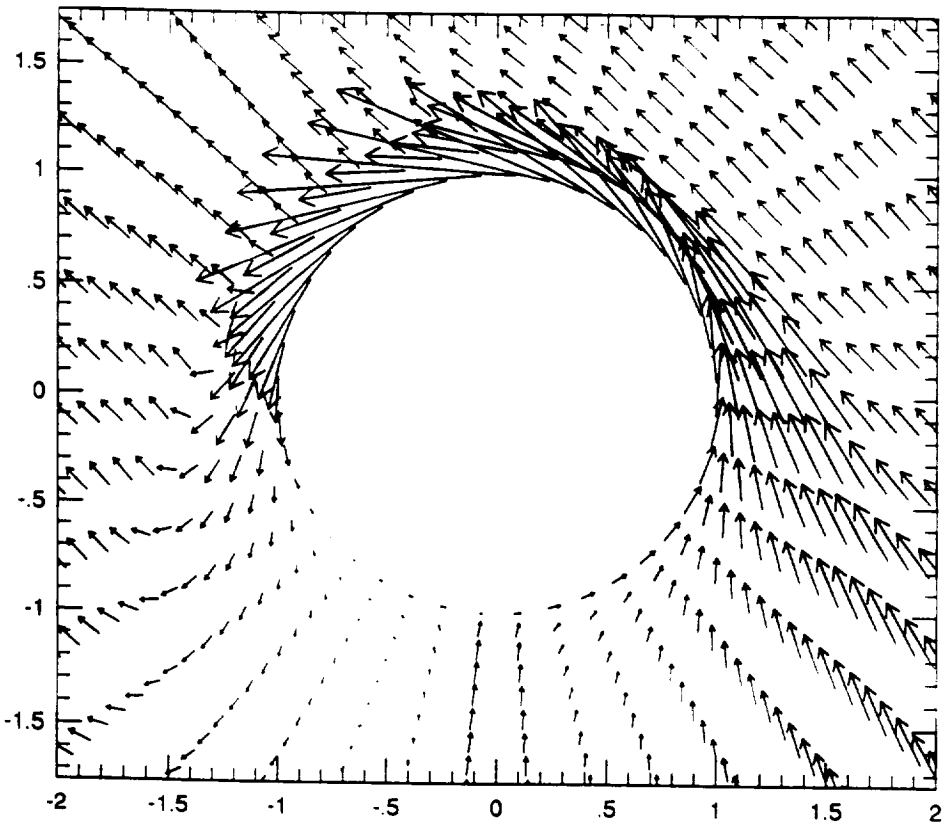

Figure 10. Magnetic field in the ecliptic plane. The IMF is tilted by 45° with respect to the incoming velocity. The solar wind plasma is flowing in from the top. The vectors in the top right corner represent magnitudes of 10 nT.

plane in which the shock is quasi-parallel is shown in Figure 11a, the noon-midnight plane in Figure 11b, and the half of the ecliptic plane where the shock is quasi-perpendicular in Figure 11c. At solar zenith angles surrounding the terminator we find magnetic field magnitudes similar to those found by *Phillips et al.* [1986, Figures 3a and 4a]. Differences near the planet's surface may be caused by the ionopause slowing the flow of the plasma and magnetic field [*McGary*, 1993].

Figure 12 shows the values of the sunward B_x and cross-flow B_y components of the magnetic field of the perpendicular simulation "measured" along a circular orbit of radius 1.4 R_V. The values of the sunward component are very similar in magnitude to those recorded by PVO at similar altitudes and in similar solar wind conditions [*Luhmann et al.*, 1991; *Dubinin et al.*, 1991].

The cross-flow component is another matter, however. At the current sheet in the near-tail region we find that the cross-flow component of the magnetic field is quite small. This is consistent with *Tanaka*'s [1993] MHD simulations. However, this is very different from the results of the analysis of PVO data by *Luhmann et al.* [1991]. Their measurements show that the cross-flow component reaches a sizable maximum ($\approx$ 10 nT) at the current sheet. Although this maximum is not always a clear feature in observations reported by other authors, the cross-flow magnetic field in this region is, in fact, consistently higher than our result [*Luhmann et al.*, 1991; *Brace et al.*, 1987; *Dubinin et al.*, 1991]. It would appear that processes apart from MHD phenomena are at work maintaining the cross-flow field strength in this region. For instance, this could be an indication of the importance of mass loading in the tail region.

Inspection of Figure 12 will show not only that the cross-flow component of the magnetic field becomes small, but also that it actually changes sign as well. This sign change indicates field reversal in the cross-tail component. This is consistent with magnetic reconnection. In fact, the field line traces of Figure 13 show that a region of reconnected magnetic field lies directly behind the planet. The field lines shown in Figure 13 were traced from 20 starting points lying in the tail region of the noon-midnight plane about 0.1 R_V above the ecliptic plane. The reconnected fields are stretched out into the tail in a roughly conical volume with a height of about 1 R_V and a base radius of about 0.3 R_V. It would not be possible to produce a coherent figure that gave a representative sample of all the reconnected field lines in the simulation. However, we have found that reconnected field lines cover the surface of the planet, and that they cover the the nightside much more densely than the dayside.

The lower third of the reconnection region is within the altitude of the nightside ionosphere. So, if this re-

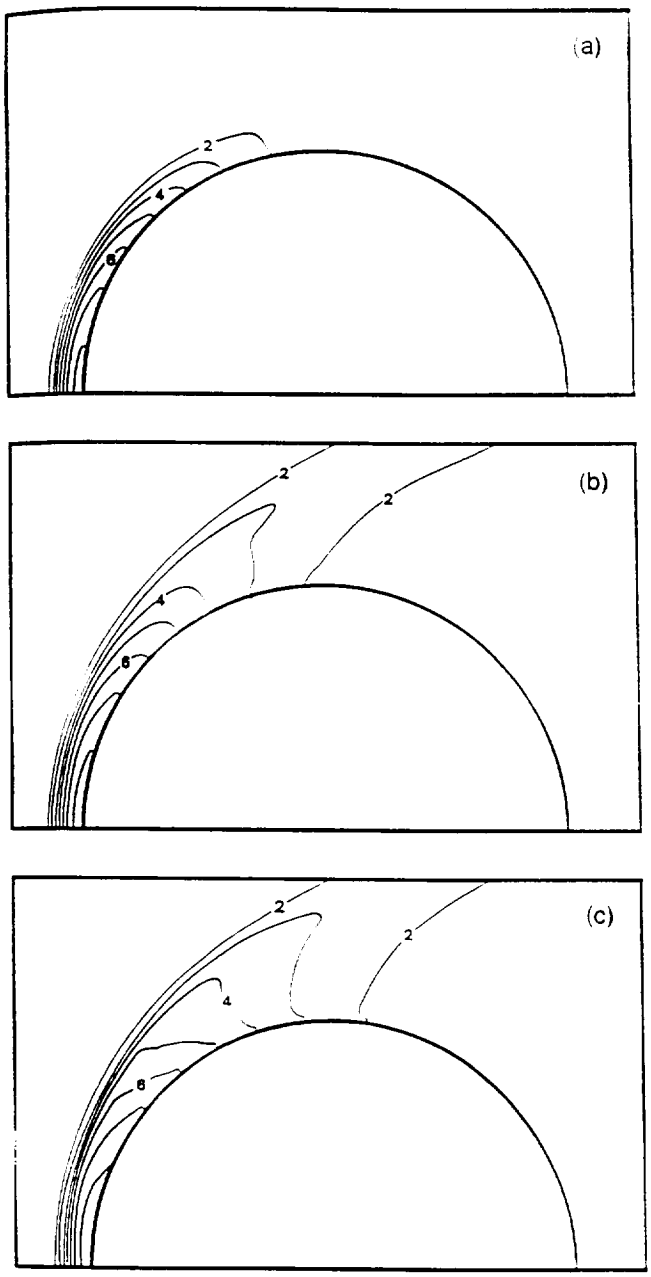

Figure 11. Contours of magnetic field magnitude showing (a) the half of the ecliptic plane where the shock is quasi-parallel, (b) the noon-midnight plane, and (c) the half of the ecliptic plane where the shock is quasi-perpendicular. Labels show magnitude of the local magnetic field relative to the magnitude of the IMF. The IMF magnitude is 10 nT. The IMF is tilted at 45° with respect to the incoming flow velocity.

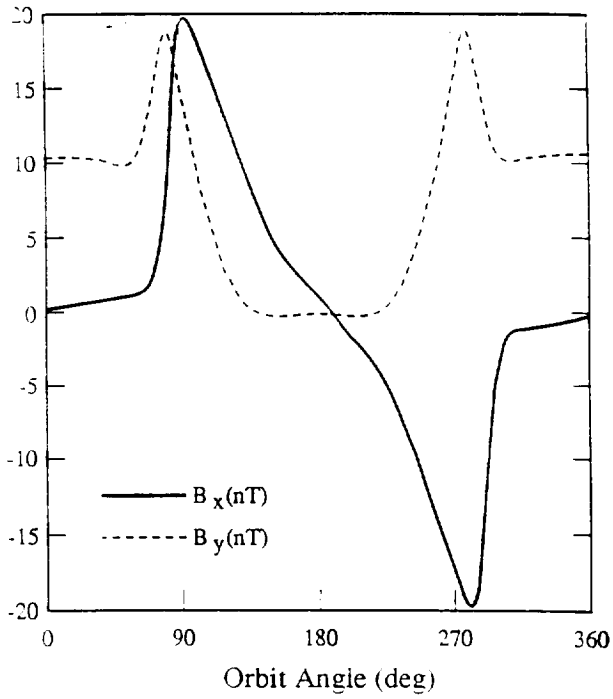

Figure 12. Sunward or $\hat{x}$ component (solid line) and cross-flow or $\hat{y}$ component (dashed line) of magnetic field in a circular orbit in the ecliptic plane 0.4 R_V above the Venus surface. The cross-flow component becomes slightly negative in the tail region (orbit angle$\approx$ 180°), indicating field reversal and magnetic reconnection. The IMF is perpendicular to the flow velocity.

gion does indeed exist in the near tail of Venus, it is certainly located at a higher altitude than we have found here and is probably much more complex in its configuration. Nevertheless, our finding that reconnection takes place over a very limited region of the magnetotail is consistent with *McComas et al.*'s [1986] result that 8 – 12 R_V downstream the cross-flow field is reversed only about 5% of the time. The resistivity producing our reconnection originates in numerical dissipation and is not a part of our algorithm. We have found reconnection only in the perpendicular simulation. If there is reconnection in the 45° simulation, it is occuring only in

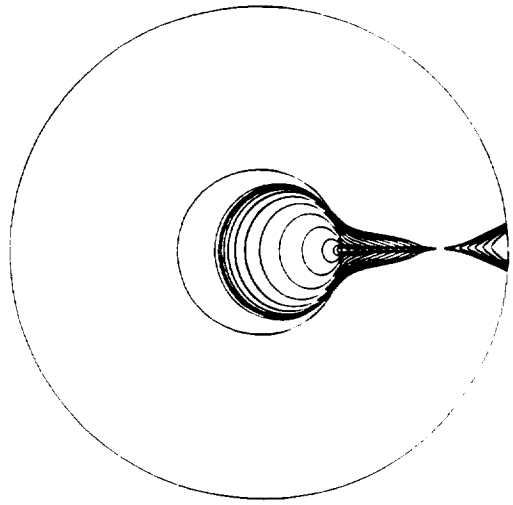

Figure 13. Reconnected field lines in the tail region. The IMF is perpendicular to the incoming flow velocity. The reconnected lines are pulled away from the planet into a roughly conical volume of height 1 R_V and base radius of 0.3 R_V.

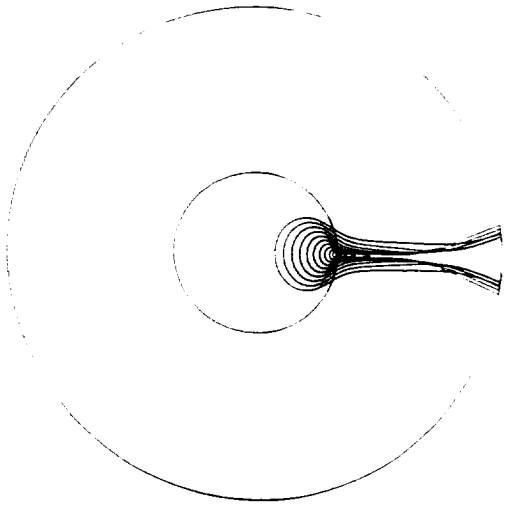

Figure 14. Field lines showing spiraling behavior in the tail region. These lines pass through the noon-midnight plane at very low altitudes above the planet on the nightside. The IMF is perpendicular to the incoming flow velocity. Some reconnected field lines are shown as well.

a region small enough to have escaped our determined searching.

We find complex behavior in the magnetic field lines behind the planet in both the 45° and perpendicular cases. The most sunward (and antisunward) directed lines spiral around one another as they head out from the planet. Some of these field lines from the perpendicular simulation are shown in Figure 14 along with some reconnected field lines. It should be noted that since our simulation box extends to only 3 R_V, these lines are not "anchored" in the solar wind plasma outside the shock. Therefore extending the outer boundary of the simulation may alter this behavior.

Looking at the nose of the shock, we see the formation of a definite magnetic barrier at the subsolar point in both the 45° and perpendicular simulations. Figure shows the values of the magnetic and thermal pressure relative to the solar wind thermal pressure, along the subsolar line in both simulations. No magnetic barrier is formed in the parallel simulation, as is consistent with MHD magnetic flux conservation and our boundary conditions. See the discussion of Figure 4.1 The thermal pressure of the 45° simulation peaks at about 0.08 R_V above the planet's surface, reaching a value of about 4.12 nPa. The magnetic field rises monotonically to a peak value of only 2.85 nPa. In the perpendicular simulation the pressure peaks at about 0.1 R_V, reaching a value of about 3.76 nPa. At the planet's surface the pressure drops to about 3.12 nPa. The magnetic pressure, on the other hand, rises monotonically to a value of 3.88 nPa at the surface. The magnetic pressure in the perpendicular case makes up a much larger percentage of the total pressure than in the 45° case. As indicated in Table 1, the solar wind dynamic pressure is 4.10 nPa.

Measuring the thickness of the magnetic barrier is imprecise not only because our shocks have finite widths, but also because the definition of the magnetic barrier is somewhat arbitrary. If we define the magnetic barrier location by *Zhang et al.*'s [1991] criterion as the point where the magnetic pressure is equal to half of

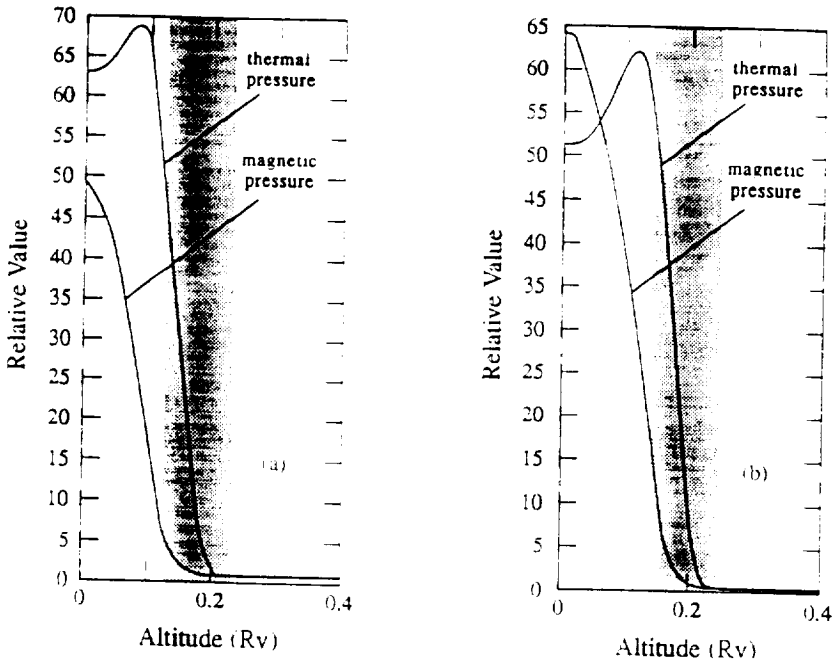

Figure 15. Thermal and magnetic pressures plotted along the subsolar line for the (a) 45° simulation and (b) perpendicular simulation. The shaded regions indicate the shock boundary layers in each case. In both simulations, the solar wind dynamic pressure, when scaled by the unperturbed thermal pressure, has a value of 0.7.

the upstream dynamic pressure, we get thicknesses of 0.05 and 0.1 R_V. These numbers translate into 300 and 600 km. *Zhang et al.*, [1991] find that the magnetic barrier has a median altitude of about 1000 km when the upstream dynamic pressure is around 4.6 nPa (our present dynamic pressure). Recalling the value of 300 km given by *Zhang et al.* [1990] for the typical ionosphere thickness, this gives an observed magnetic barrier thickness of 700 km. If we try to account for the ionosphere here in the same way as we did when discussing the bow shock location in section 2.2, we find magnetic barrier thicknesses of 330 and 630 km from the 45° and perpendicular simulations, respectively. These numbers fall short of *Zhang et al.*'s [1991] value. However, it must be remembered that the ionosphere is not a perfect sphere but is a rather oblate obstacle: its radius of curvature at the subsolar point is significantly larger than 1 R_V. Could we account for the shape of the ionosphere in a simple manner, the thicknesses of our simulated magnetic barriers would increase even more, perhaps agreeing very well with Zhang et al.'s value.

4. Discussion

Our three-dimensional MHD code has successfully simulated the observed major qualitative features of the interaction between Venus and the solar wind. Our simulations show a bow shock at slightly lower altitude than observed by PVO, a magnetic barrier beneath the bow shock, asymmetry in the terminator cross section of the shock, and a two-lobed magnetotail formed by draping of the field lines over the planet's surface. All quantities given by the simulations (except the near-tail magnetic field) are similar in magnitude to those determined from PVO data.

We have also shown some limits of single-fluid MHD as a model of the Venus-solar wind interaction. Most obviously, the lack of an ionosphere changes the scale of many of the results such as the bow shock standoff distance and the magnetic barrier thickness. Including the ionosphere "by hand," i.e., adding 300 km to the effective radius of Venus, brings the standoff distances into the range of observations. However, the magnetic barrier thickness remains too small. The 10% asymmetry of the shock in the terminator plane is only partially accounted for by single-fluid MHD. Some other process must be found to explain a missing 5%. Finally, single-fluid MHD does not give correct results for the qualitative behavior of the cross-flow magnetic field component in the near-tail region. In this region we find cross-flow magnetic fields which are much smaller than those typically observed.

Our simulations have produced several results which seem to have not been studied in depth heretofore. In the asymmetric 45°simulation the peak in the magnetic field buildup is shifted from the subsolar point toward the quasi-perpendicular region of the shock. In contrast, the peaks in thermal pressure and density are shifted toward the quasi-parallel region. This is to be expected, since quasi-perpendicular shocks have higher buildup of magnetic field, and such a buildup can be expected to divert plasma flow toward the quasi-parallel region. In the near-tail region our perpendicular simulation has established the possibility of magnetic reconnection, although the magnetic field configuration in the actual near-tail region of Venus is certain to be more complex than what we have seen in our simulations. Lastly, in the perpendicular and 45° simulations we have seen a new class of field lines which exhibit a spiraling behavior as they are traced away from the planet's surface. This spiraling behavior seems to be intermediate in some sense to reconnection on the one hand and to smooth motion of the field lines along with the plasma flow on the other.

In future research we will model the ionopause and add mass loading terms to the MHD evolution equations. On the basis of the outcomes of our present simulations, we have good reason to hope that future results will show improved quantitative agreement with the PVO data.

Acknowledgments. This work was performed at division 15 of the Southwest Research Institute in San Antonio, Texas, and supported by the National Aeronautics and Space Administration.

The Editor thanks A.F. Nagy and another referee for their assistance in evaluating this paper.

References

Alfvén, H., On the theory of comet tails, *Tellus*, *9*, 92, 1957.

Brace, L.H., W.T. Kasprzak, H.A. Taylor, R.F. Thies, C.T. Russell, A. Barnes, J.D. Mihalov, and D.M. Hunten, The ionotail of Venus: Its configuration and evidence for ion escape, *J. Geophys. Res.*, *92*, 15, 1987.

Dubinin, E., R. Lundin, W. Riedler, K. Schwingenschuh, J.G. Luhmann, C.T. Russell, and L.H. Brace, Comparison of observed plasma and magnetic field structures in the wakes of Mars and Venus, *J. Geophys. Res.*, *96*, 11,189, 1991.

Lapidus, A., A detached shock calculation by second-order finite differences, *J. Comput. Phys.*, *2*, 154, 1967.

Luhmann, J.G., A model of the ion wake of Mars, *Geophys. Res. Lett.*, *17*, 869, 1990.

Luhmann, J.G. and Schwingenschuh K., A model of the energetic ion environment of Mars, *J. Geophys. Res.*, *95*, 939, 1990.

Luhmann, J.G., C.T. Russell, K. Schwingenschuh, and Ye. Yeroshenko, A comparison of induced magnetotails of planetary bodies: Venus, Mars, and Titan, *J. Geophys. Res.*, *96*, 11,199, 1991.

McComas, D.J., H.E. Spence, C.T. Russell, and M.A. Saunders, The average magnetic field draping and consistent plasma properties of the Venus magnetotail, *J. Geophys. Res.*, *91*, 7937, 1986.

McGary J.E., Gasdynamic simulations of the solar wind interaction with Venus: Boundary layer formation, *Planet. Space Sci.*, *41*, 395, 1993.

Moore, K.J., D.J. McComas, C.T. Russell, S.S. Stahara, and J.R. Spreiter, Gasdynamic modeling of the Venus magnetotail, *J. Geophys. Res.*, *96*, 5667, 1991.

Phillips, J.L., J.G. Luhmann, and C.T. Russell, Magnetic configuration of the Venus magnetosheath, *J. Geophys. Res.*, *91*, 7931, 1986.

Press, W.H., S.A. Teukolsky, W.T. Vetterling, and B.P. Flannery, *Numerical Recipies*, Cambridge Univ. Press, New York, 1992.

Rubin, E.L., and S.Z. Burstein, Difference methods for the inviscid and viscous equations of a compressible gas, *J. Comput. Phys.*, *2*, 154, 1967.

Russell, C.T., E. Chou, and J.G. Luhmann, Solar and interplanetary control of the location of the Venus bow shock, *J. Geophys. Res.*, *93*, 5461, 1988.

Spreiter, J.R., and S.S. Stahara, Solar wind flow past Venus: Theory and comparisons, *J. Geophys. Res.*, *85*, 7715, 1980.

Tanaka, T., Configurations of the solar wind flow and magnetic field around the planets with no magnetic field: Calculation by a new MHD scheme, *J. Geophys. Res.*, *98*, 17,251, 1993.

Wu, C.C., MHD flow past an obstacle: Large-scale flow in the magnetosheath, *Geophys. Res. Lett.*, *19*, 87, 1992.

Zhang, T.-L., J.G. Luhmann, and C.T. Russell, The solar cycle dependence of the location and shape of the Venus bow shock, *J. Geophys. Res.*, *95*, 14,961, 1990.

Zhang, T.-L., J.G. Luhmann, and C.T. Russell, The magnetic barrier at Venus, *J. Geophys. Res.*, *96*, 11,145, 1991.

S. Cable, Dept. of Physics, Science University of Tokyo, 1-3 Kagurazaka, Shinjuku-ku, Tokyo 162, Japan. (e-mail:cable@astro1.yy.kagu.sut.ac.jp)

R.S. Steinolfson, Aurora Science, Inc., 4502 Centerview Dr., San Antonio, TX 78228.

(Received June 15, 1995; accepted July 12, 1995.)

JOURNAL OF GEOPHYSICAL RESEARCH, VOL. 101, NO. A2, PAGES 2547-2560, FEBRUARY 1, 1996

Numerical simulations of mass loading in the solar wind interaction with Venus

K. Murawski[1] and R. S. Steinolfson

Department of Space Science, Southwest Research Institute, San Antonio, Texas

Abstract. Numerical simulations are performed in the framework of nonlinear two - dimensional magnetohydrodynamics to investigate the influence of mass loading on the solar wind interaction with Venus. The principal physical features of the interaction of the solar wind with the atmosphere of Venus are presented. The formation of the bow shock, the magnetic barrier, and the magnetotail are some typical features of the interaction. The deceleration of the solar wind due to the mass loading near Venus is an additional feature. The effect of the mass loading is to push the shock farther outward from the planet. The influence of different values of the magnetic field strength on plasma evolution is considered.

Introduction

Data from the Pioneer Venus Orbiter (PVO), as well as data from Venera 9 and 10 and other sources, have contributed to a growing understanding of the interaction of the solar wind with an unmagnetized planet such as Venus. The general picture derived from the available data is that, for typical solar wind conditions, an electrically conducting ionosphere deflects the supersonic and superalfvénic solar wind around the planet. A bow shock forms upstream of the ionosphere and serves to slow and also assists in deflecting the solar wind. The size of the bow shock depends on the sonic and alfvénic Mach numbers and on the shape and the size of the effective obstacle, whereas asymmetries in the shock shape are determined by the direction of the interplanetary magnetic field (IMF) [*Khurana and Kivelson*, 1994]. *Zhang et al.* [1990] have proven that at Venus the effective obstacle undergoes a systematic size change of 0.13 R_v (where R_v is the radius of Venus) during a solar cycle. The boundary separating the shocked and magnetized solar wind plasma from the thermal ionosphere plasma is referred to as the ionopause, and the region between the bow shock and the ionosphere is referred to as the magnetosheath. The inner portion of the magnetosheath contains a region of enhanced magnetic pressure referred to as the magnetic barrier [e.g., *Luhmann*, 1986]. There are physical processes involved in these relatively large-scale interaction regions as well as in the magnetic tail that the present work has application to.

Zhang et al. [1991] have used PVO data to show that the convected field gasdynamic model of *Spreiter et al.* [1966] predicts the correct bow shock location if the magnetic barrier is taken as the obstacle around which the plasma is deflected. They also found that the magnetic barrier is strongest and thinnest (about 200 km thick) at the subsolar point and becomes weaker and thicker at the terminator. The magnetic barrier is responsible for transferring most of the solar wind dynamic pressure to the ionosphere through the enhanced magnetic pressure.

Observations at Venus have revealed that a magnetic tail forms as a consequence of the solar wind interaction with the Venusian ionosphere. The portions of IMF lines passing near the surface of Venus are slowed due to the interaction with newly ionized atmospheric neutrals. The two ends of the magnetic ropes continue to be pulled downstream by the solar wind [e.g., *Spreiter and Stahara*, 1980]. *Slavin et al.* [1989] have estimated that the magnetotail extends to between 50 to 150 R_v from the center of the planet for a typical solar wind flow with the Alfvén speed V_A = 60 km/s and the Alfvén Mach number M_A = 7.2.

A study by *Nagy et al.* [1981] showed that Venus has a dayside neutral exosphere dominated by oxygen at altitudes above ~ 400 km calculated from the planetary surface. The exospheric oxygen together with other particles present can be ionized by solar radiation and charge exchange. Newly ionized particles are electromagnetically coupled to the shocked solar plasma of the magnetosheath. As a consequence, near the ionopause the plasma becomes mass loaded due to interactions with ions, particularly O^+ [e.g., *Luhmann et al.*, 1991]. Model computations by *Gombosi et al.*, [1980] using input from PVO ionosheath and neutral atmosphere profiles indicate that approximately 10 % by number of the solar wind protons may undergo charge exchange with neutrals at ionopause altitudes. As a result of the mass loading (ML), the plasma is slowed and compressed. When the plasma then flows around the planet into the

[1] Also at Faculty of Mechanics, Politechnic of Lublin, Lublin, Poland.

Paper number 95JA002433.
0148-0227/96/95JA-02433$05.00

magnetosheath, momentum conservation requires an increase in flow speed into the magnetotail.

It has been noted by *Luhmann* [1986] that the above general behavior tends to prevail providing the thermal pressure in the upper ionosphere is sufficiently larger than the solar wind pressure and the pressure balance occurs where the ionospheric plasma is collisionless. As the solar wind pressure increases, relative to that of the ionospheric plasma, the magnetic barrier eventually breaks down and the height of the dayside ionosphere decreases. When the ionopause is too close to the planet, the transterminator transport of ionospheric plasma ceases, thereby leading to a nightside phenomenon known as the disappearing of the ionosphere [*Cravens et al.*, 1982].

Cloutier et al. [1987] have noted that ML processes at Venus should be asymmetric since the solar wind electric field depends on the relative directions of the flow velocity and the IMF. *Phillips et al.* [1987] have claimed that the flow and field configuration of the magnetosheath plasma, together with the large gyroradius of the pickup ions, cause ML to occur preferentially on one side of the magnetosheath. More efficient pickup of newly created ions should occur over the hemisphere that produces an electric field directed outward, away from the ionosphere. *Luhmann et al.* [1991] and *Phillips et al.* [1986] have presented observations indicating an increase in the magnetic field intensity and current over the hemisphere where the electric field is directed outward. The enhanced solar UV during solar maximum increases the ionization rate of neutrals, which moves the bow shock out from the planet both in the equatorial plane and at the terminator [*Zhang et al.*, 1990]. Similarly, *Alexander and Russell* [1985] have shown that the position of the bow shock at the terminator depends on solar activity. This dependence may be indirect evidence of ML since, when the solar EUV is high, more mass may be added to the shocked solar wind, thereby forcing the bow shock to recede from the planet. *Linker et al.* [1989] have revealed that ML can increase or decrease the plasma temperature, depending on the value of the sonic Mach number M_S. When $\gamma = 5/3$, $M_S > \sqrt{9/5}$ is required for heating to occur. Numerical simulations performed show that the effects of ML on plasma temperature and velocity are most pronounced in a wake region. However, this theory was developed for the case of Io's atmosphere, which is described by MHD equations with the source terms in the mass continuity, Euler, and energy equations. In the case of Io, the magnetic field lines are in the north-south direction and are perpendicular to the horizontal flow.

Recent computer simulations of the three-dimensional global interaction between the solar wind and unmagnetized bodies have proven to be extremely useful for improving our understanding of the associated large-scale processes [e.g., *Wu*, 1992; *Tanaka*, 1993; *Cable and Steinolfson*, 1995; *Gombosi et al.* 1994; *McGary and Pontius*, 1994]. Venus is of particular interest since the planet does not have a significant intrinsic magnetic field, and the interaction of the solar wind with the Venusian ionosphere involves fundamentally different physical processes than occur at magnetized Earth. In addition, a large quantity of relevant observations are now available for Venus. When interpreted in association with the simulated results, this data set provides a test of the physical processes included in the model.

Single-fluid MHD simulations of the global interaction of the solar wind with Venus without consideration of the ionosphere have been performed by several investigators. *Wu* [1992] limited his study to the dayside. *Tanaka* [1993] included the nightside as well but only considered magnetic field orientations parallel and perpendicular to the solar wind flow and was in a parameter regime not directly applicable to average solar-wind conditions at Venus. *Cable and Steinolfson* [1995] carried out simulations for typical observed solar wind conditions at Venus and for an IMF orientation near the Parker spiral. *McGary and Pontius* [1994] studied the effects of ML, but they considered only the dayside. Moreover, they discussed the case of a cylinder with $\partial/\partial z = 0$ and $\mathbf{B}$ along the cylinder axis (z - axis) and the perpendicular flow, namely, $\mathbf{V} \perp \mathbf{B}$.

Our purpose is to extend the model of McGary and Pontius to study the nightside and to discuss various strengths of the magnetic field. We also considered a more realistic spherical model.

The paper is organized as follows. The physical model used in the present study is described in the next section. Section 3 describes the numerical model which is used in the present studies. We present and discuss our detailed results in section 4. The paper concludes with a short summary.

Physical Model

We solve the following form of the compressible MHD equations as an initial value problem:

$$\frac{\partial \rho}{\partial t} + \nabla \cdot (\rho \mathbf{V}) = q_0 \exp[-(h - h_0)/H_0], \tag{1}$$

$$\frac{\partial (\rho \mathbf{V})}{\partial t} + \nabla \cdot [(\rho \mathbf{V})\mathbf{V}] = -\nabla p + \frac{1}{4\pi}(\nabla \times \mathbf{B}) \times \mathbf{B}, \tag{2}$$

$$\frac{\partial \mathbf{B}}{\partial t} = \nabla \times (\mathbf{V} \times \mathbf{B}), \tag{3}$$

$$\frac{\partial}{\partial t}\left(\frac{\rho V^2}{2} + \frac{p}{\gamma - 1} + \frac{B^2}{8\pi}\right) + \nabla \cdot \left\{\left(\frac{\rho V^2}{2} - \frac{\gamma}{\gamma - 1} p\right)\mathbf{V} + \frac{1}{4\pi}[\mathbf{B} \times (\mathbf{V} \times \mathbf{B})]\right\} = 0, \tag{4}$$

$$\nabla \cdot \mathbf{B} = 0. \tag{5}$$

Here ρ is the plasma density. $\mathbf{V}$ is the velocity. $\mathbf{B}$ is the magnetic field. p is the plasma pressure, and q_0 is the production rate at a reference altitude h_0. H_0 is the scale height of the hot neutral oxygen population, and the ratio of specific heats is $\gamma = 5/3$.

In the present first-order approximation, the newly created photoions are considered as cold ($T = 0$) and motionless ($\mathbf{V} = 0$) particles. A more rigorous approach would be to add corresponding source terms to the Euler (2) and energy (4) equations [e.g., *Gombosi et al.*, 1994]. However, it was shown by *Biermann et al.* [1967] that the major effect is that associated with the mass continuity equation and that contributions to the momentum and energy density are small. Therefore in these preliminary calculations source terms in the momentum and energy equations are neglected. The ML term is given by the right-hand side of the mass continuity equation (1). Oxygen photoionization is considered to be the only mass source with an altitude distribution described by the exponential function. This production rate is based on PVO observations for solar maximum, where the hot neutral oxygen atmosphere had a scale height $H_0 = 400$ km in the subsolar region and a reference production rate of $q_0 = 3 \times 10^5$ cm^{-3}s^{-1} at altitude $h_0 = 400$ km [*Belotserkovskii et al.*, 1987]. As numerical simulations, which were made for various mass addition rates, revealed that the boundary layer develops when oxygen ion production rate is $q_0 = 3 \times 10^5$ cm^{-3}s^{-1} [*McGary*, 1993; *McGary and Pontius*, 1994], we carried on our simulations for this value of q_0.

Numerical Model

These numerical calculations were performed with HEMIS3D, a three - dimensional ideal MHD code. The code utilizes the modified Lax-Wendroff scheme developed by *Rubin and Burstein* [1967], which yields stable solutions by adding numerical diffusion to the scheme. The dissipative terms (kept as small as possible) are included to help damp out short-wavelength ripples generated by numerical dispersion and numerically induced reflections from the simulation boundaries, while leaving the longer-wavelength phenomena minimally affected. The equations are solved in all three spatial dimensions of a spherical (r, θ, ϕ) coordinate system in which the $\theta = 0$ axis is directed toward the Sun or into the solar wind flow. The generally small deviations of the solar wind flow from the radial direction (with respect to the Sun) are neglected so the solar wind flow impacting the Venusian ionosphere can be assumed parallel to the Sun-Venus line ($\theta = 0$). The spherical coordinate system is centered on the planet so $r = R_v$ represents the planetary surface.

Although a grid defined in spherical coordinates introduces some computational complexity, it has a number of advantages for studying flow past planetary obstacles such as Venus. One obvious advantage is that the boundary at the planetary surface occurs at a fixed value of the radial coordinate, which avoids the complications of interpolating in a Cartesian coordinate system. Another distinct advantage is that as the center of Venus is located at the center of the spherical coordinate system, high resolution near Venus is obtained without the expense of high resolution everywhere in the simulation. The code is constructed in such a manner that it can be applied to a single r, θ plane when the phenomenon being studied is cylindrically symmetric about the poles at $\theta = 0$ and $\theta = 180°$, as is the case when the magnetic field is parallel to the solar wind

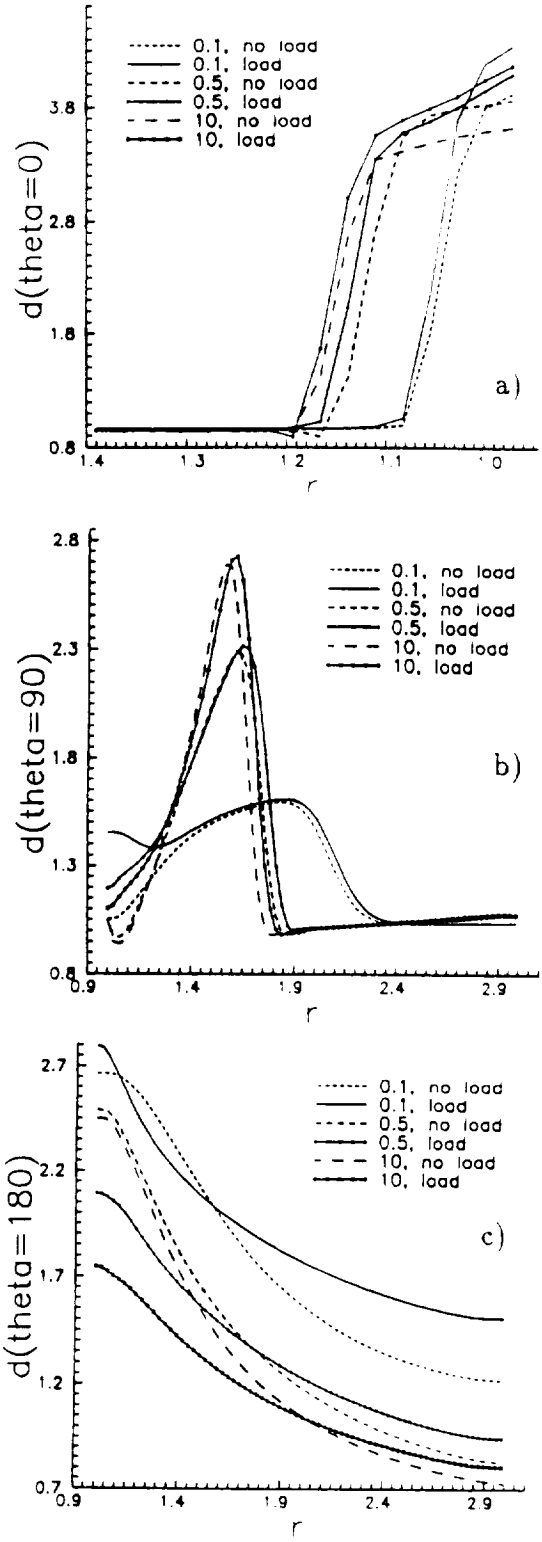

Figure 1. Plots of the normalized mass density profiles along θ = *const* lines for $\beta = 0.1$, $\beta = 0.5$, $\beta = 10$ and for the NL and ML simulations. (a) the Sun-Venus ($\theta = 0$) line, (b) the terminator ($\theta = 90°$) line, and (c) the $\theta = 180°$ line. Mass loading shifts the bow shock farther away from Venus.

flow. In this case, the simulation code uses a 73×74 grid (r, θ grid dimensions), which corresponds to $\Delta\theta = 2.5$, with a radial extent of the simulations of $3R_V$. The largest $\Delta r = 0.083R_V$. We have checked that the results for larger extend of the numerical boundaries were very close to those presented in this paper. For the corresponding discussion, see also *Cable and Steinolfson* [1995].

The time step limit for methods using explicit temporal differencing for advective problems is the well-known

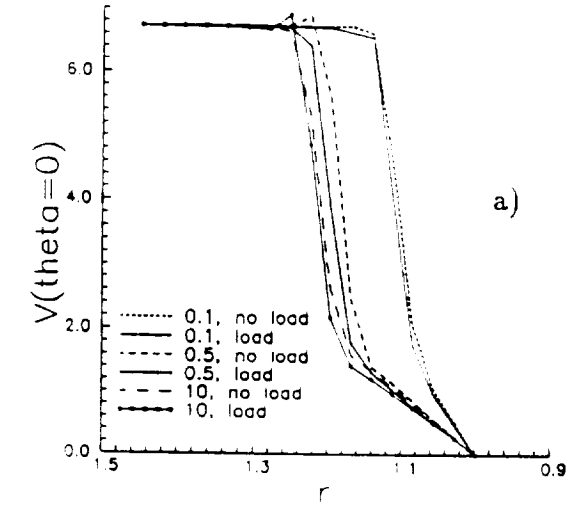

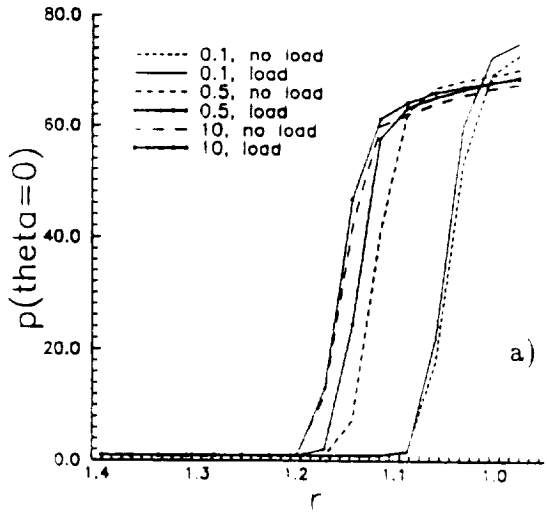

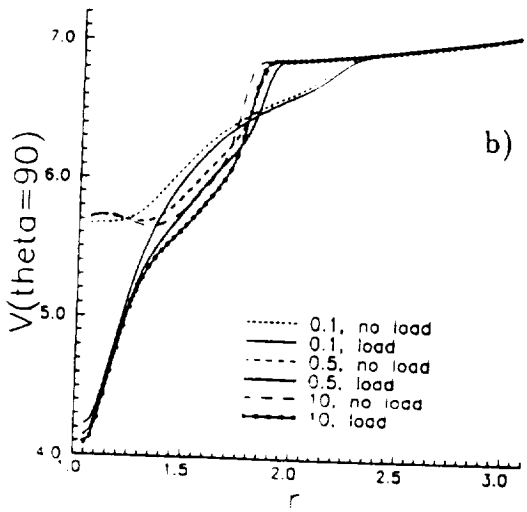

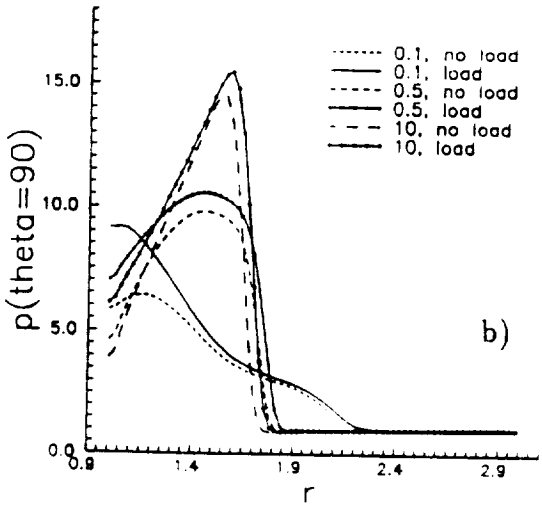

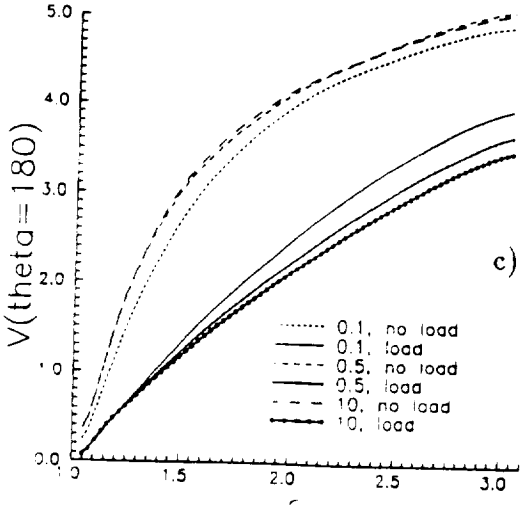

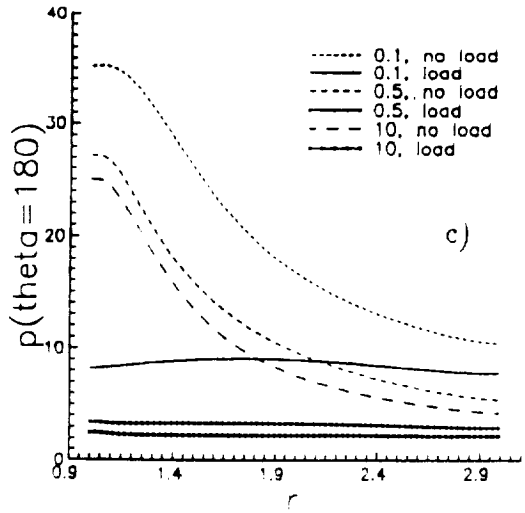

Figure 2. As in Figure 1 but for the normalized velocity profiles.

Figure 3. As in Figure 1 but for the normalized pressure profiles.

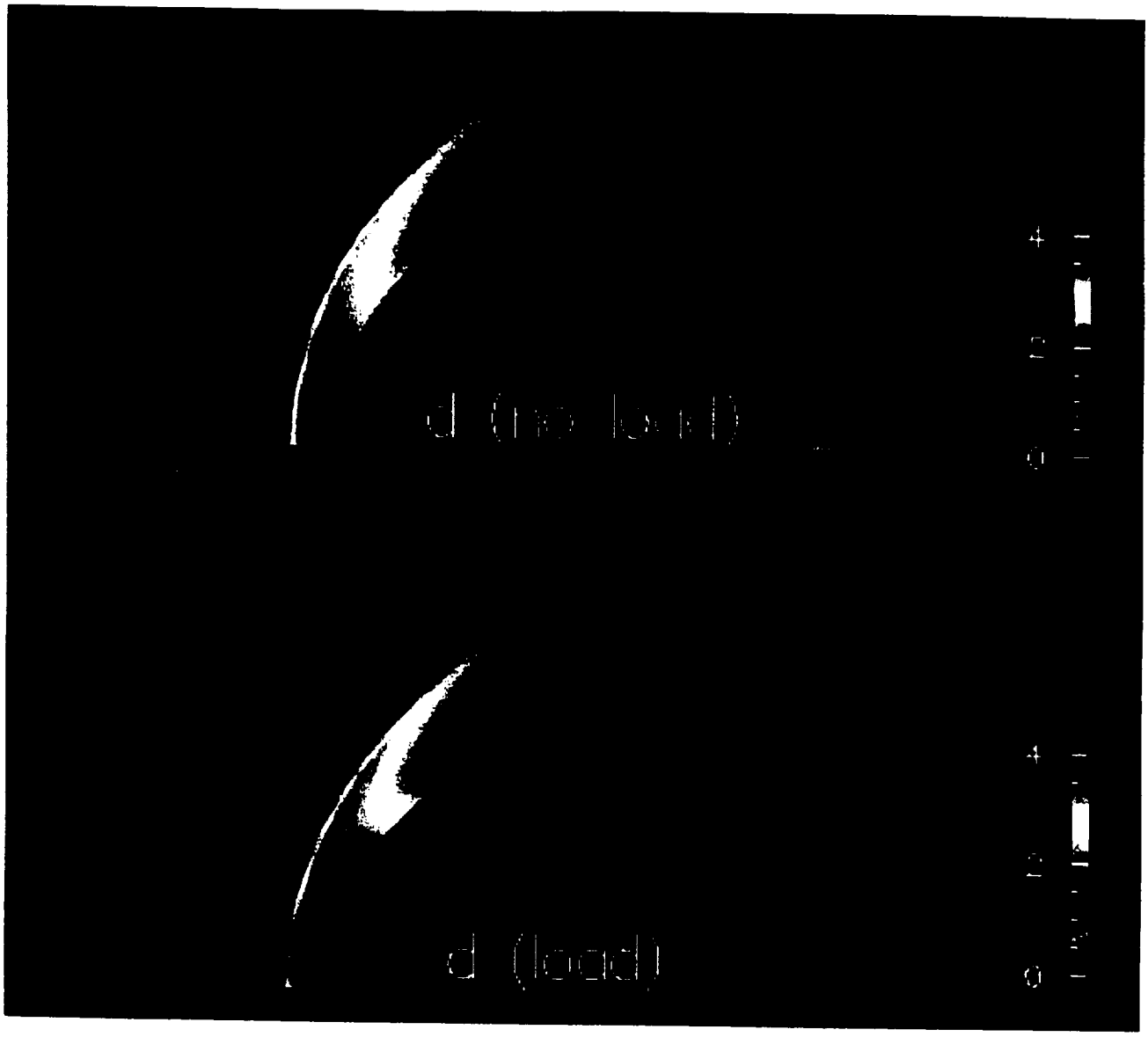

Plate 1. Normalized mass densities (ρ/ρ_∞) for the MHD non loaded (top) and mass loaded (bottom) simulations for the case of a parallel ($\mathbf{B}||\mathbf{V}$) magnetic field and the plasma $\beta = 0.5$. Here, ρ_∞ is the density of the solar wind. The effect of mass loading (ML) is to increase the mass density in the overall region, except the tail region in which the mass density is reduced. ρ_∞ denotes the solar wind mass density.

CFL condition, $\Delta t \leq \Delta l/|V|$, where the cell size is Δl and V is the fastest physical speed in the system. The resulting computer code [*Cable and Steinolfson*, 1995] is second-order accurate in space and time.

Defining a spherical boundary for the problem is easily accomplished. However, solving the equations of magnetohydrodynamics in spherical coordinates requires some modification of the usual Lax-Wendroff scheme. In particular, the singular points at $\theta = 0$ and $\theta = 180°$ are handled through application of L'Hospital's rule to extrapolate values from grid points next to the singular points. Since the value of each variable at the singular points may vary depending on the angle ϕ at which the singular points are approached, a flux-weighted average of the values at all angles is used for the final updated value. This procedure is described in more detail by *Cable and Steinolfson* [1995].

We used a simple model for the boundary conditions that is physically motivated and performs adequately well. Venus is modeled as a hard, highly electrically conducting sphere. The inner boundary is taken at the planetary surface (1 R_v) where the radial components of both the magnetic field and velocity are set to zero. All other physical variables are computed by extrapolation of values along a radial line. At the dayside of the outer radial boundary, all quantities are set to the solar wind values. The values at the nightside of the outer radial boundary are determined by extrapolation along the local flow direction. Moreover, we have never encountered transient conditions where the flow was coming in from the outer radial boundary. A typical computation begins with the introduction of the desired solar

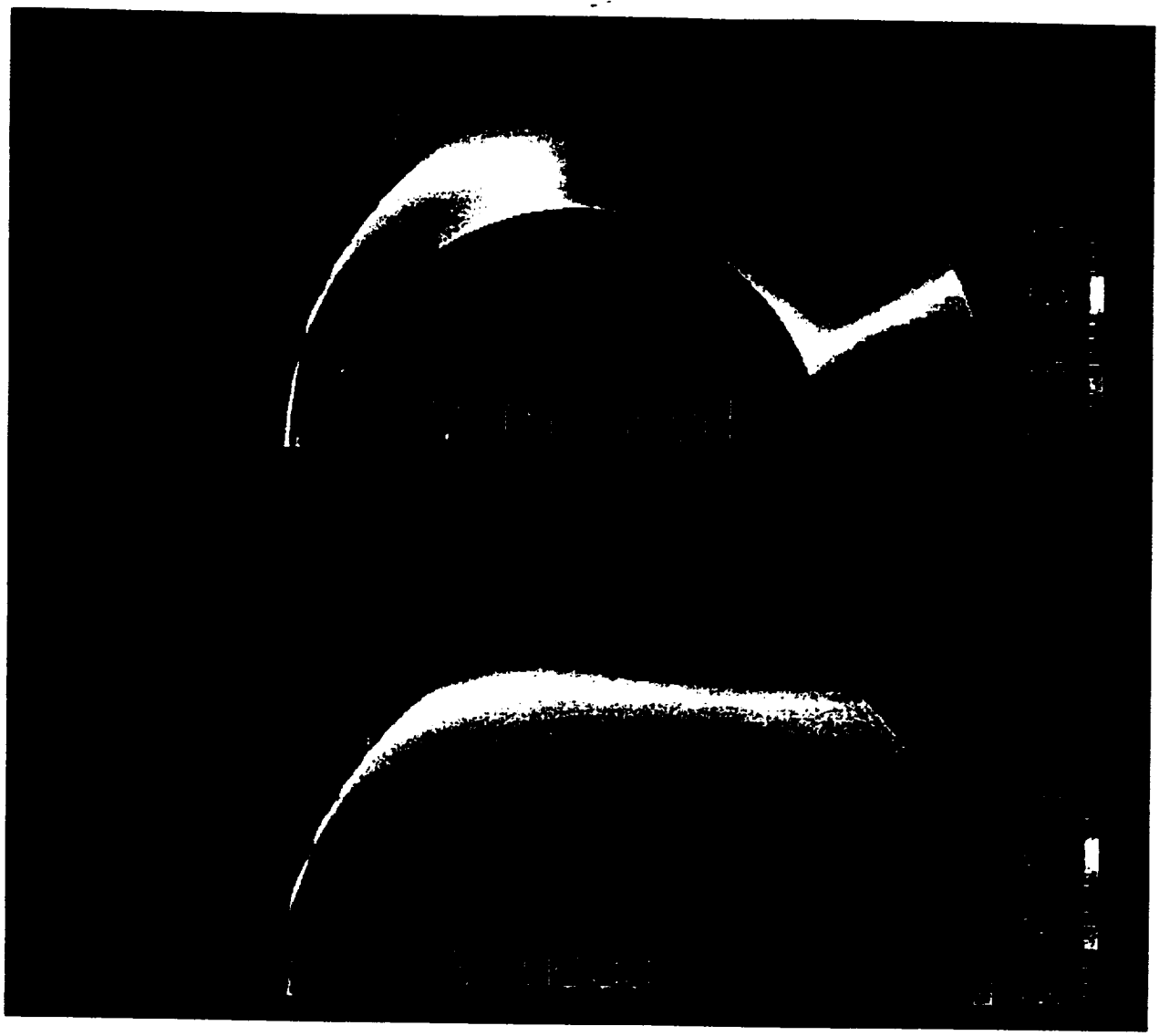

Plate 2. Normalized plasma flows (V/a_∞) for the MHD non loaded (top) and mass loaded (bottom) simulations for the case of a parallel ($\mathbf{B}||\mathbf{V}$) magnetic field and the plasma $\beta = 0.5$. Here, a_∞ is the sound speed of the solar wind. The effect of ML is to decrease the plasma flow.

wind values in the dayside within the numerical box. The initial IMF is taken from the potential solution for flow over a sphere so that $\nabla \cdot \mathbf{B} = 0$ in the initial state. The continued satisfaction of $\nabla \cdot \mathbf{B} = 0$ is assured by solving a Poisson equation and updating the magnetic field. The numerical solution then continues until the interaction achieves an approximate steady state.

The density and pressure are initially constant throughout the simulation region. The initial velocity field is the flow of an incompressible fluid over a sphere, directed along the $\theta = 0$ line:

$$V_r(r,\theta,\phi,t=0) = -V_0[1-(\frac{R_o}{r})^3]\cos\theta, \quad (6)$$

$$V_\theta(r,\theta,\phi,t=0) = V_0[1+\frac{1}{2}(\frac{R_o}{r})^3]\sin\theta, \quad (7)$$

$$V_\phi(r,\theta,\phi,t=0) = 0, \quad (8)$$

where V_0 is the solar wind speed. The magnetic field is initialized in a similar way, except that $\mathbf{B}$ is skewed with respect to the solar wind flow by the desired angle. In the present paper, this angle is 0°. This is clearly not a frequently occurring case [*Phillips et al.*, 1986], but it is a reasonable first-order approximation which will serve as a reference for comparison with results for cone angles of 45° and 90°. These processes will be realistically modeled in future calculations.

Results and Discussion

We present all numerical results for the oxygen ion production rate $q_0 = 3 \times 10^5$ cm^{-3}s^{-1} [*McGary and Pontius*, 1994] and discuss several values of the plasma $\beta = 8\pi p_0/B_0^2$, namely $\beta = 0.1$, $\beta = 0.5$, $\beta = 10$, and a typical value of $\beta = 1.5$. The case of $\beta = 0.1$ ($\beta = 10$) corresponds to the strong (weak) magnetic field case. The physical solar wind values used are: electron density $n_e = 20$ cm^{-3}, temperature $T = 10^5$ °K, sound

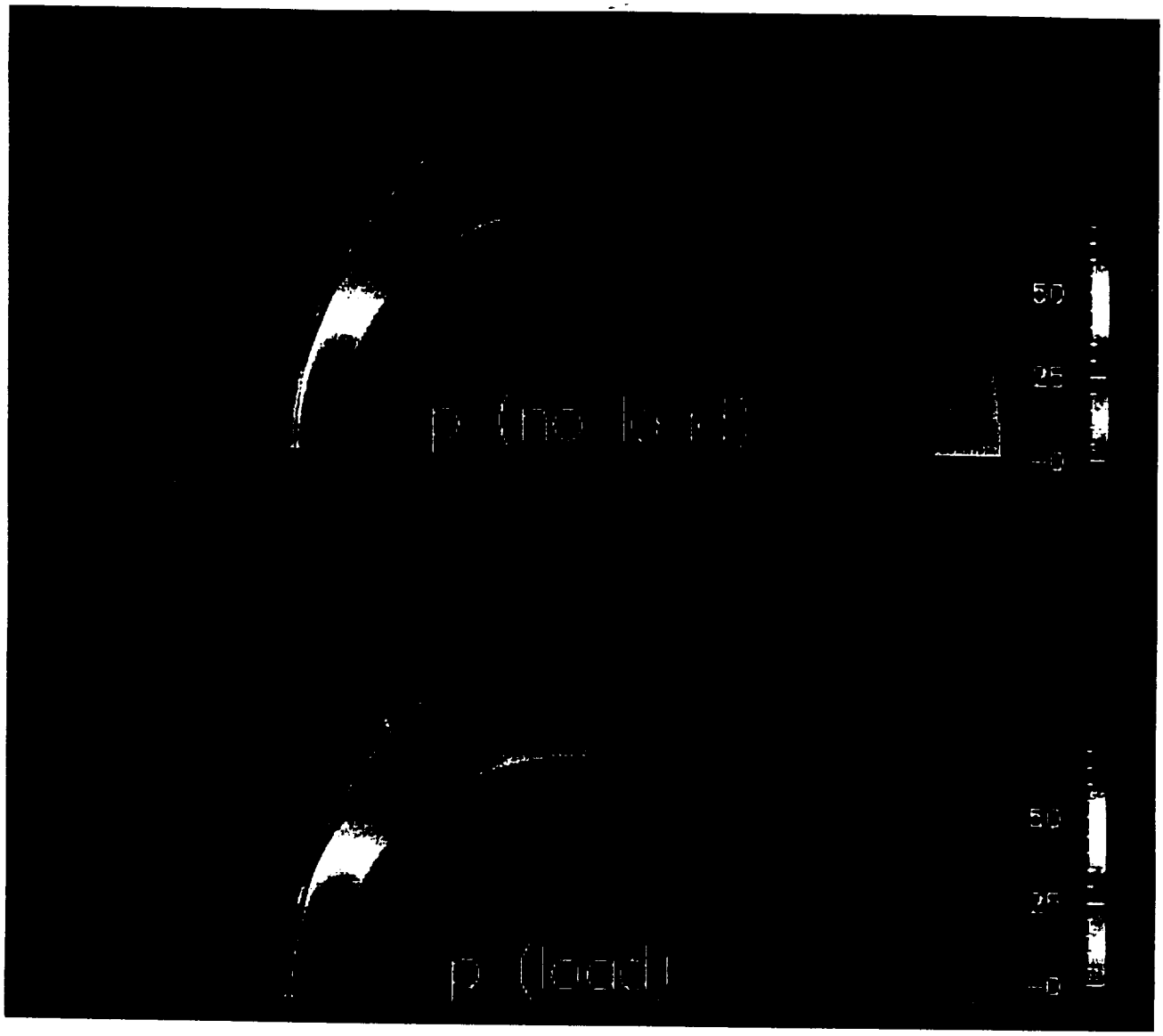

Plate 3. Normalized plasma pressure ($p/(\rho_\infty a_\infty^2)$) for the MHD non loaded (top) and mass loaded (bottom) simulations for the case of a parallel ($\mathbf{B}||\mathbf{V}$) magnetic field and the plasma $\beta = 0.5$. The effect of ML is to decrease the plasma pressure.

speed 55 km/s, flow velocity 370 km/s, sonic Mach number 6.73, and thermal pressure $6.06 \cdot 10^{-10}$ dyn/cm^2. Other physical parameters are chosen the same as in the work by *Cable and Steinolfson* [1995].

As a first step to apply the methodology to the problem of ML in the atmosphere of Venus, we consider an axisymmetric case with the magnetic field lines parallel to the solar wind flow. Consequently, **B** is parallel to the Sun-Venus line and the entire solution is rotationally symmetric around this line, $\partial/\partial\phi = 0$. We used the numerical technique described in the previous section to obtain a solution of the set of (1)-(5). The flow is from left to right and all physical quantities are either symmetric or antisymmetric about the lower boundary.

As shown in Plate 1, the mass density is increased in the case of mass loaded (ML) solutions. This finding is consistent with a simple analysis of mass continuity equation (1) and with previously published results [e.g., *Linker et al.*, 1989; *McGary and Pontius*, 1994]. However, a more detailed close-up reveals that in the tail and terminator regions the mass density is reduced by the ML effects (Figure 1). Similar reduction is observed in the case of $\beta = 0.5$ along the Sun-Venus line, at $r \simeq 1.07\ R_\varphi$ (Figure 1a). The density reduction does not occur at the terminator for $\beta = 0.1$, while this effect takes place for $\beta = 0.5$ and $\beta = 10$ (Figure 1b). The density depletion is stronger for a higher value of β. Just at the planetary surface, at $r < 1.3\ R_\varphi$, the mass density increase is observed (Figure 1b). In the magnetotail, the plasma density reduction occurs at the planetary surface for all values of the plasma β. Again, the rate of density depletion is proportional to β. The case of $\beta = 0.1$ differs from the other cases just as at the planetary surface ρ is increased, but farther on there is a region of mass depletion which is followed by a region of mass enhancement (Figure 1c). To our

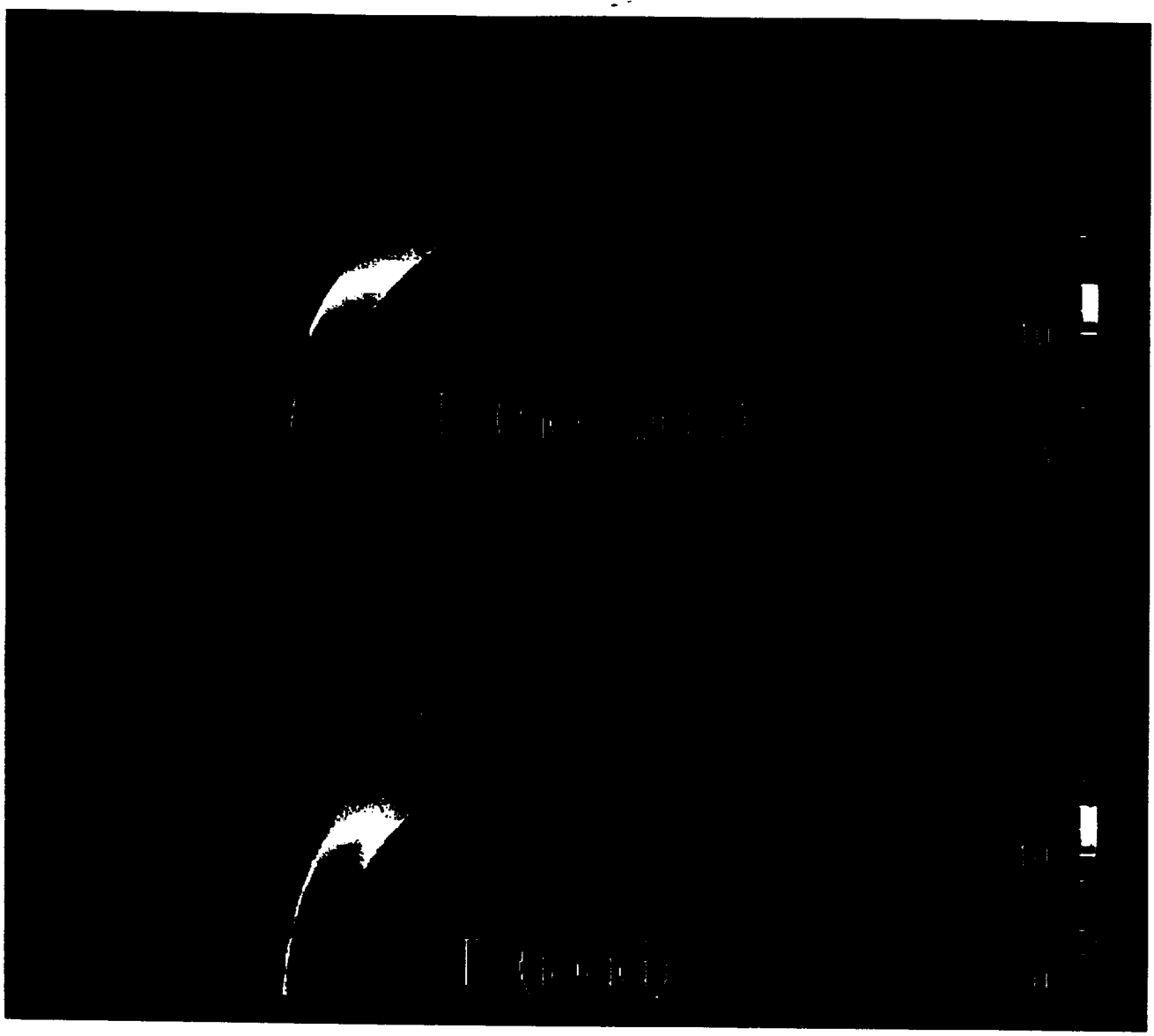

Plate 4. Normalized plasma temperature (T/T_∞) for the MHD non loaded (top) and mass loaded (bottom) simulations for the case of a parallel ($\mathbf{B}||\mathbf{V}$) magnetic field and the plasma $\beta = 0.5$. The effect of ML is to decrease the plasma temperature.

knowledge, this is the first report of mass depletion due to the ML. The density depletion is a consequence of the nonlinear term $\nabla \cdot (\rho \mathbf{V})$, which is smaller due to the plasma flow reduction by the ML effects. Indeed, the largest density (velocity) increase (decrease) occurs in the magentotail at $r = 3\ R_v$ for $\beta = 0.1$. The normalized density jumps from $\rho_{NL} \simeq 1.25$ to $\rho_{ML} \simeq 1.5$ (Figure 1c), while the magnitude of plasma flow is reduced from $V_{NL} \simeq 4.9$ to $V_{ML} \simeq 4$ (Figure 3c). Consequently, $\rho_{NL} V_{NL} = 6.125 > \rho_{ML} V_{ML} = 6$. Therefore the effect associated with this nonlinear term overcomes the density increasing effect exerted by the exponential term $q_0 \exp[-(h - h_0)/H_0]$. The density reduction in the tail may also be due to the changed shape of the bow shock. A different bow shock shape may result in less mass being carried into the tail, regardless of other factors.

It follows from Euler equation (2) that we can expect the reduction of a velocity magnitude because conservation of momentum and energy requires that the plasma flow is decelerated as a consequence of the mass density reduction. Plate 2 presents results both for the ML and no loading (NL) simulations. By examining the two solutions, one can see a fundamental difference between them. The effect of ML is to decrease the flow. A decreasing rate is highest in the tail region where slow flows in the case of NL are much more reduced by ML. The decreasing rate is larger for a smaller value of β at the terminator and in the tail region. The plasma starts decelerating because of ML well ahead of the shock. In the subsolar region, this rate is largest for $\beta = 0.5$. A large flow deceleration occurs also at the terminator, close to the planetary surface where the plasma flow drops from $V_{NL} \simeq 5.7$ to $V_{ML} \simeq 4.2$ (Figure 2b). Inspection of Plate 2 reveals the global structure of the shock and the stagnation region behind it. The flow

decelerates at the shock as approaching solar wind absorbs an increasing number of ions. At the planetary surface, $r = R_\odot$, there is no perpendicular flow as a consequence of the boundary conditions imposed. Velocity shears in the radial direction are present at the bow shock region both for the ML and NL flows, which is consistent with PVO observations [Mihalov *et al.*, 1982] and the gasdynamic results by *McGary* [1993].

From (4) we can derive an equation which governs the evolution of the NL plasma pressure p

$$\frac{\partial p}{\partial t} + \nabla \cdot (p\mathbf{V}) = (1 - \gamma) p \nabla \cdot \mathbf{V}. \tag{9}$$

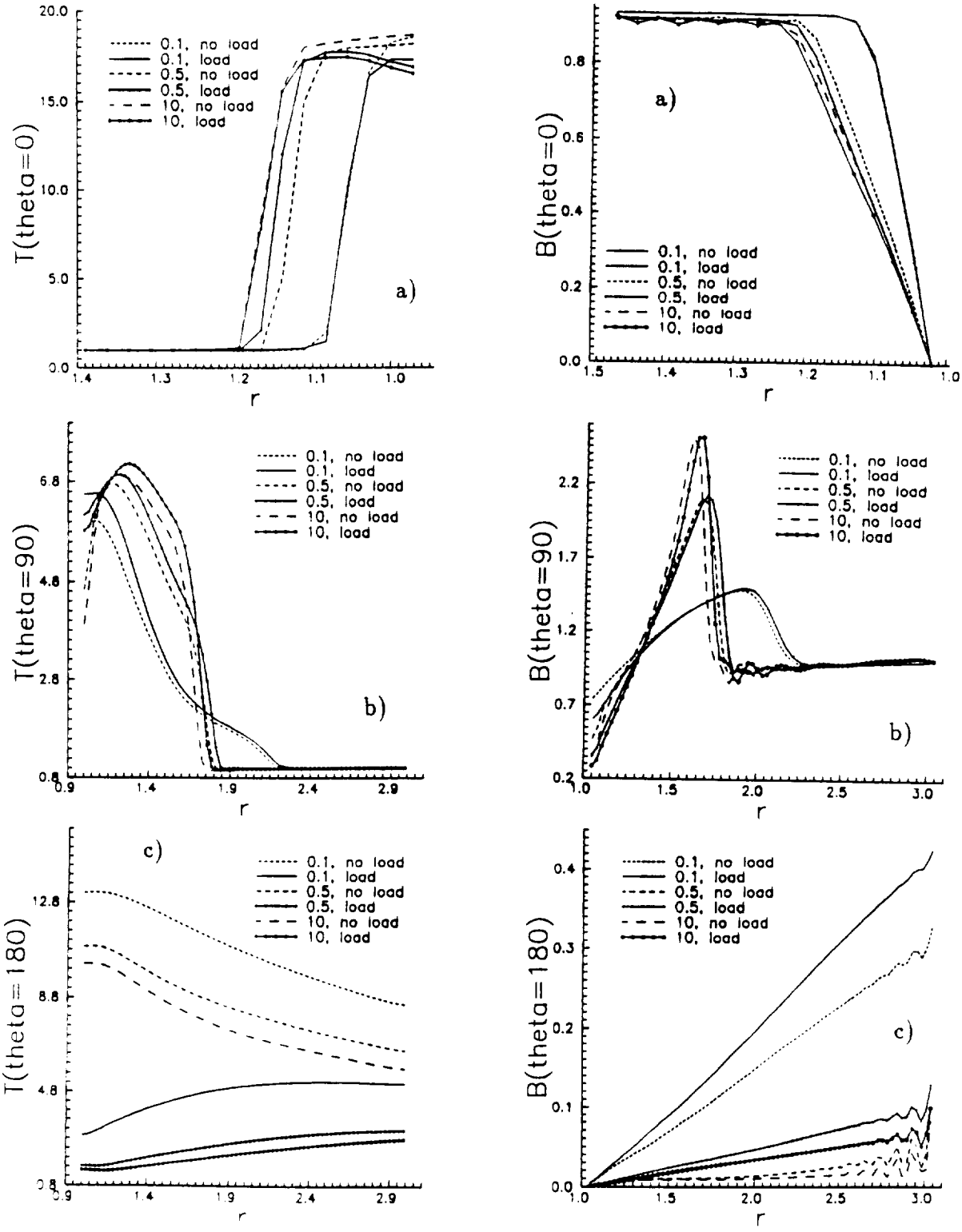

Figure 4. As in Figure 1 but for the normalized temperature profiles.

Figure 5. As in Figure 1 but for the normalized magnitude of the magnetic field profiles.

As the plasma flow velocity V is decreased by the ML effects we can expect a pressure reduction. The simulation results shown in Plate 3 are qualitatively consistent with our expectations. However, Plate 3 shows that the plasma pressure is increased near the terminator region, in the region $\theta < 90°$. This increase is caused by a nonlinear interaction which is described by the $\nabla \cdot (p\mathbf{V})$ and $p\nabla \cdot \mathbf{V}$ terms. Our results differ from the conclusion made by *McGary and Pontius* [1994], who claimed that the dynamics of the plasma flow are not significantly affected by ML. A reason for the difference between the present results and those of McGary and Pontius has to do with the different models applied; McGary and Pontius performed gasdynamic (with $\mathbf{B} = 0$) simulations for the cylinder flow, whereas our model concerns MHD and a plasma sphere.

The above scenario may differ for different values of β. It occurs in the case of a sufficiently small value of β that the magnetic field is so strong that the fast shock becomes an intermediate one [*Steinolfson and Hundhausen*, 1990]. For example, the ML increases the gas pressure along the whole Sun-Venus line in the case of $\beta = 0.1$ and $\beta = 10$ (Figure 3a) but reduces it in the case of $\beta = 0.5$, $\beta = 1$, and $\beta = 1.5$ at the planetary surface. In the bow shock region, an enhancement of p due to the ML is observed for all values of β. The strongest enhancement seems to occur for $\beta = 0.5$. At the terminator (Figure 3b), the gas pressure is increased by ML. The rate of decrease is highest at the planetary surface for $\beta = 0.1$, while at larger distances the influence of ML on p is negligible. The pressure reduction at the planetary surface is caused by the right-hand side term of (9) which becomes small at the surface because of the flow reduction. The bow shock is closer to the planetary surface for a higher value of β, in accordance with our expectations. At the magnetotail the pressure is reduced (Figure 3c). The reduction rate is highest at the planetary surface for the smallest value of β and is a monotonic function of β.

The next point of comparison between the ML and NL results is the temperature distribution around Venus. As for the ideal gas the plasma temperature T is proportional to p/ρ so both p and ρ play a major role in determining its behavior. We already learned that for $\beta = 0.5$ ρ (p) is increased (decreased) by the ML effects everywhere except in the terminator and tail (nose) regions. Therefore, we may expect the general behavior of T would be to decrease its magnitude by the ML effects. Indeed, Plate 4 indicates that the ML significantly cools the flow relative to the NL case. The cooling occurs as zero-temperature oxygen ions are introduced into the flow and thermalized [*McGary and Pontius*, 1994]. The behavior of T is interesting to discuss in more detail as a function of the radial direction r at different locations of θ. In the case of $\theta = 0$, for $\beta = 0.1$ and $\beta = 10$ the temperature is decreased by ML both at the planetary surface and at the sunward side of the bow shock (Figure 4a), while in the shock the effect of ML is negligible. The curves which correspond to the ML possess maxima in the magnetosheath, while no maxima exist for the NL case. A similar maximum occurs also in the

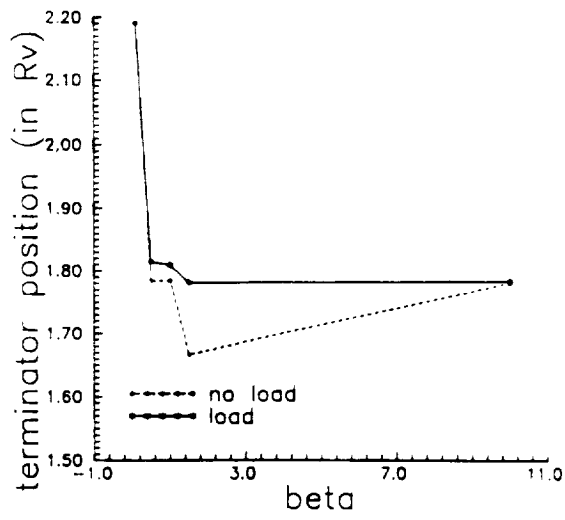

Figure 6. Terminator positions for different values of the plasma β and for the non loaded and mass loaded simulations. The bow shock at the terminator is shifter farther away farther away from the surface of Venus.

case of $\beta = 0.5$ for the ML curve. Now, however, ML cools the plasma at the planetary surface but warms it in the bow shock region. The temperature increase at the bow shock was observed recently by *Gombosi et al.* [1994] in their simulations of the interaction of an expanding cometary atmosphere with the solar wind. At the terminator, the plasma is warmed by ML (Figure 4b). The warming is more significant at the planetary surface and is higher for a higher value of β. The cooling occurs at the magnetotail (Figure 4c). The cooling rate is higher at the surface of Venus and for a smaller value of β. This is a consequence of the pressure decrease at the planetary surface (Figure 3c). The mass density is increased for $\beta = 0.1$ and decreased for $\beta = 0.5$ and $\beta = 10$, but the decreasing rate is smaller than the pressure decreasing rate (Figure 1c). Consequently, $T \sim p/\rho$ is much decreased at the surface of Venus. The cooling rate is much more significant than the warming effect. The bow shock position is closest to the planetary surface for the smallest presented values of β. The bow shock distance from Venus grows with β.

Plate 5 shows the magnitude of the magnetic field. In the subsolar region there is no jump in the magnitude of the magnetic field across the bow shock. At the flanks, however, the magnetic field increases through the bow shock. The magnetic tail is a region of reduced magnetic field. It can be seen that the ML exerts some influence on the magnetic field strength. Small differences occur at the sunward side of the shock where the magnetic field is decreased by the ML effects (Figure 5a). This effect is small for $\beta = 0.1$ and grows with β. The decrease in the magnetic field strength nearest the planet along the stagnation streamline, is the result of the boundary conditions ($B_r(r = R_V, \theta, t) = 0$) imposed together with the fact that the parallel shock does not change a value of the magnetic field across the shock. As the planet is conducting there can be no radial magnetic field component at the surface of

Venus. But near the subsolar line, the solar wind magnetic field is purely radial. Consequently, the magnetic field strength has to drop to zero in this region. This behavior counter to the common picture of **B** piling up in the stagnation region in the case of $\mathbf{B} \perp \mathbf{V}$ [*Cable and Steinolfson*, 1995; *Murawski and Steinolfson*, 1995] and would only occur for the magnetic field nearly parallel to **V**. At the terminator, the ML enhances the magnitude of **B** at the bow shock. Therefore at the planetary surface B is reduced. A decreasing rate is hardly dependent on β. The largest differences occur in the magnetotail where the magnetic field is enhanced by ML. The strongest enhancement occurs for $\beta = 0.1$. This behavior contradicts our expectations, which follow a simple analysis of (3) wherein as a consequence of V decrease we expect the magnetic field reduction by the ML effects. However, **V** couples nonlinearly with the magnetic field. The coupling occurs through the term $\nabla \times (\mathbf{V} \times \mathbf{B})$, which determines the overall behavior of the magnetic field rather than the plasma flow **V** only.

Inspection of Plates 1-5 reveals that a bow shock is formed upstream of Venus. The principal effects are that the bow shock is displaced farther from Venus in the case of the ML plasma [*Belotserkovskii et al.*, 1987; *Breus et al.*, 1989; *McGary and Pontius*, 1994]. For precise investigation of the bow shock structure, Figures 1-5 exhibit the plasma mass density, velocity, gas pressure, temperature, and magnetic field distribution along the Sun-Venus ($\theta = 0°$), terminator ($\theta = 90°$), and $\theta = 180°$ line. Inspection of these figures reveals that the pressure at the planetary surface is larger for a smaller value of β. The ML effects also shifts the shock at the terminator farther away from the planetary surface (Figure 6). This shift is largest for intermediate values of the plasma β. These results show the bow shock at the terminator is in about the position of the PVO observations [*Tatrallyay et al.*, 1984; *Russell et al.*, 1990]. Average subsolar and terminator distances of the bow shock are about 1.15 R_v and 2 R_v (from the center of the planet), respectively. To match the observed locations (at the nose) of the bow shock, the MHD model requires that the mass loading be greatly enhanced.

Russell and Zhang [1992] in their analysis of PVO data found that during periods when the solar wind magnetosonic Mach number is near unity and the plasma beta is low, the bow shock may travel to distances greater than 10 R_v away from the planet. On the basis of previous work on the formation of MHD shocks in coronal mass ejections [*Steinolfson and Hundhausen*, 1990], it was felt that the solar wind conditions had become (during the far bow shock excursions) such that the usual fast MHD shock is no longer a stable solution. The lower than normal plasma beta and magnetosonic Mach number are in a parameter regime for which the usual fast-mode bow shock close to the planet may not provide the necessary compression and deflection of the solar wind. Using MHD simulations, it was shown [*Steinolfson and Cable*, 1993] that, for these conditions, the usual fast shock is replaced by a bow shock

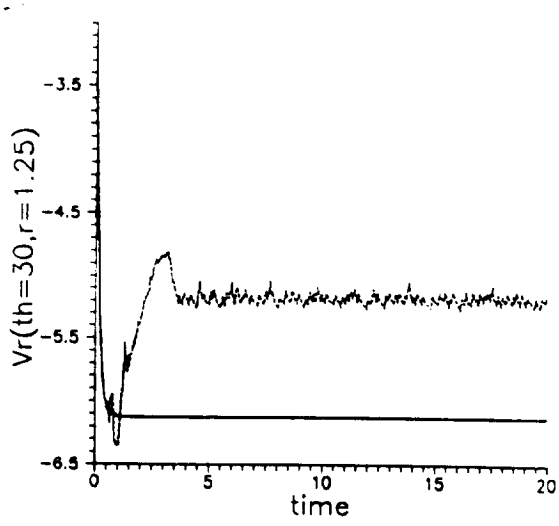

Figure 7. Time history of the radial velocity component (V_r) at the spatial position very close to the bow shock for the non loaded simulations. The upper (lower) curve corresponds to β 10 ($\beta = 0.1$). Not the stabilizing effect of the stronger magnetic field.

configuration containing an intermediate shock near the Sun-Venus line and a fast shock at large distances from the Sun-Venus line. The resulting configuration propagates upstream away from the planet at a low speed and appears to be approaching a new equilibrium stand-off location at a large distance from the planet.

Plates 1-5 exhibit waves which propagate along the bow shock boundaries. We have checked that these waves are not numerical artifacts as they do not disappear for a finer numerical grid and are persistent in time (not shown). These waves are generated by the solar wind impact, which is exerted by the solar wind on the plasma surrounding the planet. The first impact shifts the plasma towards the surface of Venus, while later in time the magnetic field recovers and the plasma is displaced farther away from the planet. Moreover, the bow shock first builds closer to the planet and then its altitudes at the equator ($\theta = 0°$) and at the terminator ($\theta = 90°$) grow in time. As a consequence, the nose of the bow shock oscillates in time. The Alfvén and slow oscillations, which are guided by the magnetic field lines [e.g., *Murawski et al.*, 1995], are fed by the Kelvin-Helmholtz (KH) instabilities [e.g., *Rankin et al.*, 1993], which are more apparent in the case of a weak magnetic field case. Figure 7 presents the radial component of the plasma flow as a function of time and for $\beta = 0.1$ and $\beta = 10$. This component is calculated at a spatial position which is very close to the bow shock. As expected, the stronger magnetic field makes the flow less unstable as the amplitude of oscillations is smaller in the case of $\beta = 0.1$ than in the case of $\beta = 10$. The KH instabilities criterion [e.g., *Rankin et al.*, 1993]

$$\omega^2 = \frac{\rho_1 \rho_2}{(\rho_1 + \rho_2)^2}[\mathbf{k}\cdot(\mathbf{V}_2 - \mathbf{V}_1)]^2 - \frac{(\mathbf{B}_1 \cdot \mathbf{k})^2 + (\mathbf{B}_2 \cdot \mathbf{k})^2}{4\pi(\rho_1 + \rho_2)} \tag{10}$$

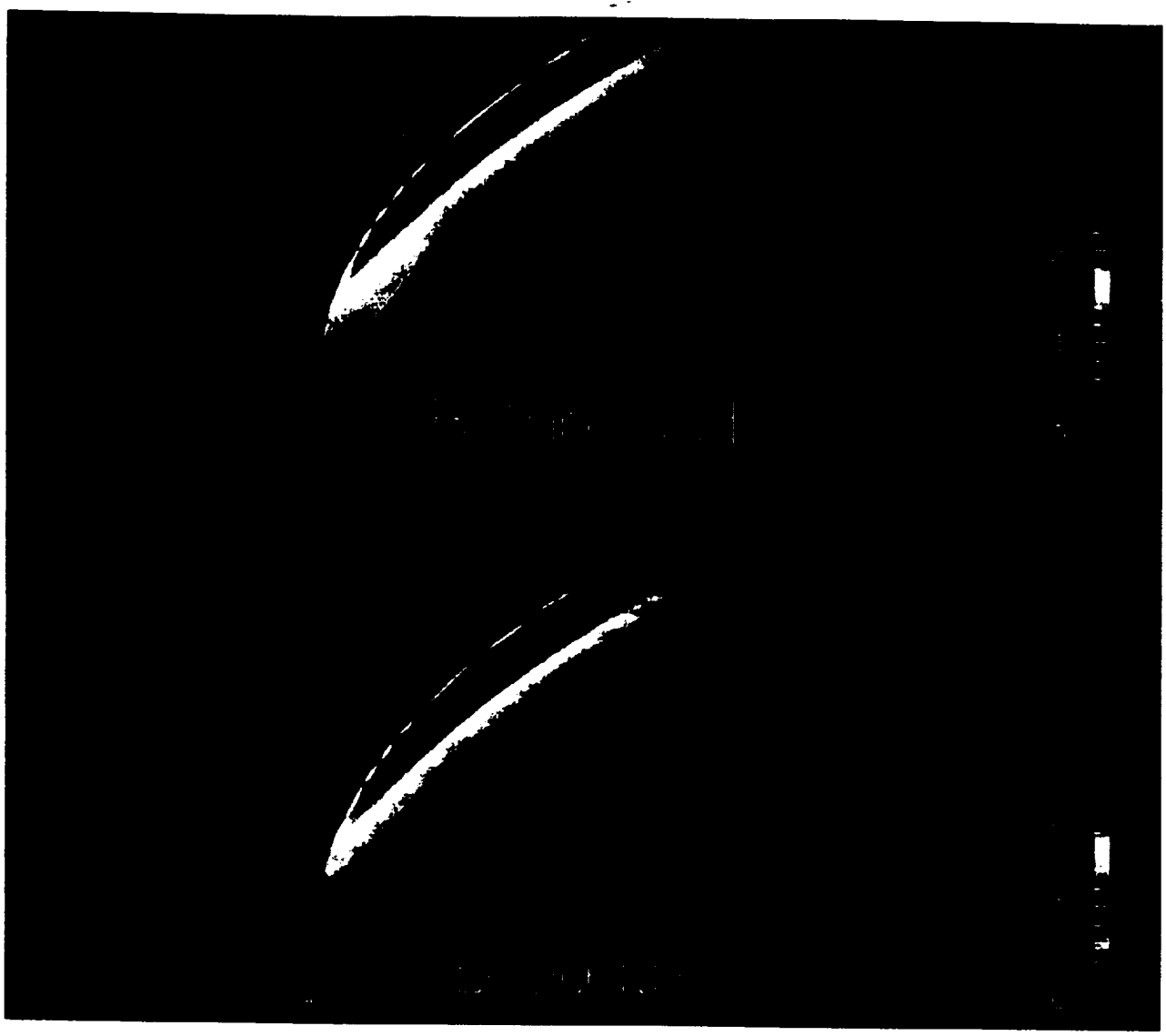

Plate 5. Normalized magnitude of the magnetic field ($B/\sqrt{\mu_0 \rho_\infty a_\infty^2}$) for the MHD non loaded (top) and mass loaded (bottom) simulations for the case of a parallel ($\mathbf{B}||\mathbf{V}$) magnetic field and the plasma $\beta = 0.5$. The effect of ML is to increase the magnitude of B in the terminator region.

is satisfied easier for a less magnetized flow. In this formula indices 1 and 2 correspond to variables on different sides of the bow shock, while ω_i denotes the growth rate of the KH instabilities. It is easy to find out that the flow is unstable ($\omega_i^2 > 0$) for a non-magnetic plasma ($\mathbf{B_1} = \mathbf{B_2} = 0$). On the other hand, strong magnetic fields can make the flow stable ($\omega_i^2 < 0$). Intermediate values of the magnetic fields stabilize the flow and in particular the flow can be marginally stable ($\omega_i^2 = 0$). These instabilities occur in the region where the flow has a large gradient such as at the bow shock. Assuming that the wave propagation $\mathbf{k}$ is parallel to the flow $\mathbf{V}$ and magnetic field $\mathbf{B}$, it follows from (10) that

$$(\rho_1+\rho_2)^2\frac{\omega_i^2}{k^2}/V_A^2 = \rho_1\rho_2(V_2-V_1)^2-(\rho_1+\rho_2)(B_1^2+B_2^2), \quad (11)$$

where now the plasma parameters are normalized by the units of the solar wind. V_A is the Alfvén speed of the solar wind. At the surface of Venus, $V_2 = B_2 = 0$. Upstream of the bow shock, the mass density ρ_1 and the plasma flow V_1 are hardly dependent on the plasma β. Therefore we can put $\rho_1 \simeq 0.95$ and $V_1 \simeq 6.7$ in normalized units. For $\beta = 0.1$ ($\beta = 10$) we have $\rho_2 \simeq 3.9$ ($\rho_2 \simeq 3.7$) and $B_1 \simeq 0.93$ ($B_1 \simeq 0.91$). It is easy to check that the right-hand side of (11) is positive, indicating that the flow is KH unstable for both $\beta = 0.1$ and $\beta = 10$.

Summary

The interaction of the solar wind with Venus is studied using numerical solutions of the time-dependent ideal two - dimensional MHD equations. A modified Lax-Wendroff scheme [*Cable and Steinolfson*, 1995] is used to solve the equations in a spherical coordinate

system. For these computations the detailed chemistry of the ionosphere is neglected, and the planet is treated as a conducting sphere. Numerical computations have been perfomed to study the effect of ML and the IMF strength on the magnetic barrier and the general configuration of the magnetic tail. The IMF orientation included in this study is parallel to the solar wind flow direction.

The main results are the following: The ML increases the mass density in the overall region, except the terminator and tail where the mass density depletion occurs as a consequence of the nonlinearity action. The mass density depletion is larger for a higher β. As a conseqence of this reduction, the plasma flow, pressure, and temperature are reduced. This scenario depends, however, on a value of the plasma β. It was found that for $\beta = 0.1$ both the plasma pressure and the temperature are increased at the dayside by the ML.

Acknowledgments. The authors thank the referees and Jim Burch for their helpful comments on the earlier version of this paper. K. M. is grateful for Sam Cable's assistance on several numerical issues. This work was financially supported by NASA grant NAGW-4054 and by the Internal Research and Development Program at Southwest Research Institute.

The Editor thanks D. L. de Zeeuw and J. L. Phillips for their assistance in evaluating this paper.

References

Alexander, C. J., and C. T. Russell, Solar cycle dependence on the location of the Venus bow shock, *Geophys. Res. Lett.,12*, 369, 1985.

Belotserkovskii, O. M., T. K. Breus, A. M. Krymskii, V. Y. Mitnitskii, A. F. Nagy, and T. I. Gombosi, The effect of the hot oxygen corona on the interaction of the solar wind with Venus, *J. Geophys. Res. Lett., 14*, 503, 1987.

Biermann, L., B. Brosowski, and H. M. Schmitt, The interaction of the solar wind with a comet, *Solar Phys.,1*, 254, 1967.

Breus, T. K., S. J. Bauer, A. M. Krymskii, and V. Y. Mitnitskii, Mass loading in the solar wind interaction with Venus and Mars, *J. Geophys. Res.,94*, 2375, 1989.

Cable, S., and R. S. Steinolfson, Three dimensional MHD simulations of the interaction between Venus and the solar wind, *J. Geophys. Res., 100*, 21,645, 1995.

Cloutier, P. A., H. A. Taylor Jr., and J. E. McGary, Steady state flow/field model of solar wind interaction with Venus: Global implication of local effects, *Planet. Space Sci.,22*, 967, 1987.

Cravens, T. E., et. al., Disappearing ionospheres on the nightside of Venus, *Icarus,51*, 271, 1982.

Gombosi, T. I., T. E. Cravens, A. F. Nagy, R. C. Elphic, and C. T. Russell, Solar wind absorption by Venus, *J. Geophys. Res.,85*, 7747, 1980.

Gombosi, T. I., K. G. Powell, and D. L. De Zeeuw, Axisymmetric modelling of cometary mass loading on an adaptively refined grid: MHD results, *J. Geophys. Res.,99*, 21,525, 1994.

Khurana, K. K., and M. G. Kivelson, A variable cross-section model of the bow shock of Venus, *J. Geophys. Res., 99*, 8505, 1994.

Linker, J. A., M. G. Kivelson, and R. J. Walker, The effect of mass loading on the temperature of a flowing plasma, *Geophys. Res. Lett.,16*, 763, 1989.

Luhmann, J. G., The solar wind interaction with Venus, *Space Sci. Rev.,44*, 241, 1986.

Luhmann, J. G., C. T. Russell, K. Schwingenschuh, and Y. Yeroshenko, A comparison of induced magnetotails of planetary bodies: Venus, Mars, and Titan, *J. Geophys. Res.,96*, 11,199, 1991.

McGary, J. E., Gasdynamic simulations of the solar wind interaction with Venus: boundary layer formation, *Planet. Space Sci.,41*, 395, 1993.

McGary, J. E., and D. H. Pontius Jr., MHD simulations of boundary layer formation along the dayside Venus ionopause due to mass loading, *J. Geophys. Res.,99*, 2289, 1994.

Mihalov, J. D., J. R. Spreiter, and S. S. Stahara, Comparison of gasdynamic model with steady solar wind flow around Venus, *J. Geophys. Res.,87*, 10,363, 1982.

Murawski, K., R. C. DeVore, S. Parhi, and M. Goossens, Numerical simulations of MHD wave excitation in bounded plasma slabs, *Planet. Space Sci.*, in press, 1995.

Murawski, K., and R. S. Steinolfson, Numerical modelling of the solar wind interaction with Venus, *Planet. Space Sci.*, in press, 1995.

Nagy, A. F., T. E. Cravens, J. H. Yee, and A. I. F. Stewart, Hot oxygen atoms in the upper atmosphere of Venus, *Geophys. Res. Lett.,8*, 629, 1981.

Phillips, J. L., J. G. Luhmann, and C. T. Russell, Magnetic configuration of the Venus magnetosheath, *J. Geophys. Res.,91*, 7931, 1986.

Phillips, J. L., J. G. Luhmann, C. T. Russell, and K. R. Moore, Finite Larmor radius effect on ion pickup at Venus, *J. Geophys. Res.,92*, 9920, 1987.

Rankin, R., B. G. Harrold, J. C. Samson, and P. Frycz, The nonlinear evolution of field line resonances in the Earth's magnetosphere, *J. Geophys. Res.,98*, 5839, 1993.

Rubin, E. L., and S. Z. Burstein, Difference methods for the inviscid and viscous equations of a compressible gas, *J. Comput. Phys.,2*, 178, 1967.

Russell, C. T., E. Chou, J. G. Luhmann, and L. H. Brace, Solar cycle variations in the neutral exosphere inferred from the location of the Venus bow shock, *Adv. Space Res.,10*, (5), 3, 1990.

Russell, C. T., and T. -L. Zhang, Unusually distant bow shock encounters at Venus, *Geophys. Res. Lett.,19*, 833, 1992.

Slavin, J. A., D. S. Intriligator, and E. J. Smith, Pioneer Venus Orbiter magnetic field and plasma observations in the Venus magnetotail, *J. Geophys. Res.,94*, 2383, 1989.

Spreiter, J. R., and S. S. Stahara, Solar wind flow past Venus: Theory and comparison, *J. Geophys. Res.,85*, 7715, 1980.

Spreiter, J. R., A. L. Summers, and A. Y. Alksne, Hydromagnetic flow around the magnetosphere, *Planet. Space Sci.,14*, 223, 1966.

Steinolfson, R. S., and S. Cable, Venus bow shocks at unusually large distances from the planet, *J. Geophys. Res. Lett., 20*, 755, 1993.

Steinolfson, R. S., and A. J. Hundhausen, MHD intermediate shocks in coronal mass ejections, *J. Geophys. Res.,95*, 6389, 1990.

Tanaka, T., Configurations of the solar wind flow and magnetic field around the planets with no magnetic field: Calculation by a new MHD simulation scheme, *J. Geophys. Res.,98*, 17,251, 1993.

Tatrallyay, M., C. T. Russell, J. G. Luhmann, A. Barnes,

and J. D. Mihalov, On the proper Mach number and ratio of specific heats for modelling the Venus bow shock, *J. Geophys. Res.*, *89*, 7381, 1984.

Wu, C. C., MHD flow past an obstacle: Large-scale flow in the magnetosheath, *Geophys. Res. Lett.*, *19*, 87, 1992.

Zhang, T. L., J. G. Luhmann, and C. T. Russell, The solar cycle dependence on the location and shape of the Venus bow shock, *J. Geophys. Res.*, *95*, 14,961, 1990.

Zhang, T. L., J. G. Luhmann, and C. T. Russell, The magnetic barrier at Venus, *J. Geophys. Res.*, *96*, 11,145, 1991.

K. Murawski and R. S. Steinolfson, Department of Space Science, Southwest Research Institute, San Antonio, TX 78228-0510 (e-mail: KMurawski@solar.stanford.edu; richs@txdirect.net)

(Received March 16, 1995; revised August 3, 1995; accepted August 3, 1995.)

Pergamon

Planet. Space Sci., Vol. 44, No. 3, pp. 243–252, 1996

0032–0633/96 $15.00 + 0.00

0032–0633(95)00108–5

Numerical modeling of the solar wind interaction with Venus

K. Murawski and R. S. Steinolfson

Department of Space Science, Southwest Research Institute, San Antonio, TX 78228-0510, U.S.A.

Received 27 March 1995; revised 8 June 1995; accepted 20 June 1995

Abstract. The large-scale (global) interaction of the atmosphere of Venus with the surrounding medium is numerically simulated in the framework of 3-dimensional magnetohydrodynamics. The simulations are performed for the case of the interplanetary magnetic field perpendicular to the solar wind flow. The model reproduces several features of the interaction predicted by earlier theories and observations. The solar wind interaction with Venus is characterized by the mass loading of the solar wind with heavy oxygen ions which are produced by the photoionization of neutrals in the extensive ionosphere. This mass loading slows down the solar wind and ultimately leads to the formation of a magnetic barrier and a magnetotail. The location of the bow shock is barely affected by different values of the magnetic field strength.

1. Introduction

The solar wind is an almost collisionless plasma consisting mainly of protons and electrons which flow outward from the Sun, eventually exerting an impact on planets. Although the solar wind carries with it the interplanetary magnetic field (IMF), Venus has virtually no intrinsic magnetic field (e.g. Luhmann, 1986). Direct observations (by the *Mariner*, *Venera*, and *Pioneer Venus* missions) at Venus have demonstrated that the planet's atmosphere consists of a magnetosheath bounded by a bow shock on the outward side and ionopause on the lower side. The bow shock is a thin region across which the plasma parameters change drastically. The bow shock exists because the solar wind is supersonic and super-Alfvénic and must become subsonic in order to flow around the obstacle. The ionospheric plasma which tries to exclude the solar wind plasma with its associated IMF is a very good electrical conductor. Hence, the ionosphere forms a nearly impenetrable obstacle which can serve to divert the solar wind around it. The shocked solar wind slows down as it approaches the planet, and as a consequence, the magnetic field strength builds up, resulting in the formation of a magnetic barrier located outside the dayside ionopause. The ionopause is usually coincident with the bottom of the magnetic barrier. It is one of the major aims of space plasma physics to measure the plasma properties throughout the whole atmosphere and to develop computer models for its representation. Evaluation of a computer model must depend ultimately on how well the results match observations, but valuable insight can also be gained by comparison of the results that were obtained by different numerical techniques and by analytical estimation if available.

Application of magnetohydrodynamics to the solar wind interaction with Venus was initiated by Spreiter *et al.* (1970). At that time the gasdynamic equations were solved for the density, velocity, and pressure, while the magnetic field was evaluated in a subsequent step by solving the induction equation using values for the density provided by the gasdynamic solution. This approach concerns the scenario in which the magnetic field lines are convected with the local flow of the plasma.

Mass loading (ML) effects have been implemented by Belotserkovskii *et al.* (1987), Cloutier *et al.* (1987), Phillips *et al.* (1987), Stahara *et al.* (1987), Breus *et al.* (1989), and Sauer *et al.* (1994). A comparison of the results of Stahara *et al.* with those of Belotserkovskii *et al.* reveals several major differences. The results of Belotserkovskii *et al.* indicate that the ML has a large effect on the location of the bow shock, moving it to a position slightly beyond that observed by PVO, while Stahara *et al.* claim that the location of the bow shock is barely affected by the ML of the flow.

It has been shown by Murawski and Steinolfson (1995) that in the case where the IMF is parallel to the solar wind flow, the ML increases the mass density in the overall region, except the terminator and tail where the mass density depletion occurs because of the nonlinearity action. As a consequence of this reduction the plasma flow, pressure, and temperature are reduced. This scenario

Correspondence: K. Murawski

depends, however, on a value of the plasma β. It was found that for $\beta = 0.1$ both the plasma pressure and the temperature are increased at the dayside by the ML.

It is the purpose of this paper to test the conclusions of Stahara *et al.* and Belotserkovskii *et al.*, and extend the analysis of Murawski and Steinolfson into the case of the IMF perpendicular to the solar wind flow.

The paper is organized as follows. Mathematical and numerical models of the dynamics of a Venusian plasma are shown in Section 2. Numerically obtained results are presented in a later section of this paper. The paper closes with a brief summary of presented results and general remarks.

2. Simulation model

The interaction between a solar wind and the atmosphere of Venus is assumed to be governed by ideal MHD equations which represent coupling of the fluid dynamic equations with Maxwell's equations of electrodynamics by neglecting electrostatic force, displacement current, heat transfer, and damping effects. We solve the following form of the compressible MHD equations as an initial value problem:

$$\frac{\partial \rho}{\partial t} + \nabla \cdot (\rho \mathbf{V}) = M \tag{1}$$

$$\frac{\partial (\rho \mathbf{V})}{\partial t} + \nabla \cdot [(\rho \mathbf{V})\mathbf{V}] = -\nabla p + \frac{1}{\mu}(\nabla \times \mathbf{B}) \times \mathbf{B} \tag{2}$$

$$\frac{\partial}{\partial t}\left(\frac{\rho V^2}{2} + \frac{p}{\gamma - 1} + \frac{B^2}{2\mu}\right) + \nabla \cdot \left\{\left(\frac{\rho V^2}{2} + \frac{\gamma}{\gamma - 1} p\right)\mathbf{V} + \frac{1}{\mu}[\mathbf{B} \times (\mathbf{V} \times \mathbf{B})]\right\} = 0 \tag{3}$$

$$\frac{\partial \mathbf{B}}{\partial t} = \nabla \times (\mathbf{V} \times \mathbf{B}). \tag{4}$$

Here ρ is the gas density, $\mathbf{V}$ the velocity, $\mathbf{B}$ the divergence free ($\nabla \cdot \mathbf{B} = 0$) magnetic field, p the gas pressure, and the ratio of specific heats is $\gamma = 5/3$.

We assume that the only important source of ion pickup is due to the photoionization of the hot oxygen corona. The newly created ions move so slowly that essentially their flow does not contribute to momentum and energy equations. Moreover, we consider the case that the ion production rate is proportional to neutral atmosphere oxygen density. In the present first-order approximation, the newly created photoions are considered as cold ($T = 0$) and motionless ($\mathbf{V} = 0$) particles. A more rigorous way would be to add corresponding source terms to Euler (2) and energy (3) equations (e.g. Gombosi *et al.*, 1994). However, it was shown by Biermann *et al.* (1967) that the major effect is that associated with the mass continuity equation and contributions to the momentum, magnetic field, and energy density are small. Therefore, in these preliminary calculations source terms in the momentum, magnetic field, and energy equations are neglected. The mass loading term M can thus be represented as (McGary and Pontius, 1994)

$$M = M_0 \exp[-(h - h_0)/H_0] \tag{5}$$

where M_0 is proportional to the product of the number density of the neutral hot oxygen molecules at the planet's nose and their mass, divided by the characteristic time for photoionization. The magnitude of the intensity of ion pickup at Venus appears to vary significantly over the solar cycle (Russell *et al.*, 1990).

The ion production rate is based on *Pioneer Venus* observations for solar maximum, where the hot neutral oxygen atmosphere had a scale height $H_0 = 400$ km in the subsolar region and a reference production rate of $M_0 = 3 \times 10^5$ cm^{-3} s^{-1} at altitude $h_0 = 400$ km (Belotserkovskii *et al.*, 1987). As numerical simulations made for various mass addition rates revealed that the boundary layer develops when the oxygen ion production rate is $M_0 = 3 \times 10^5$ cm^{-3} s^{-1} (McGary, 1993; McGary and Pontius, 1994), we carried on our simulations for this value of M_0.

The MHD equations are solved numerically using the modified Lax–Wendroff algorithm (Rubin and Burstein, 1967). In our 3-dimensional simulations the equations are solved in a spherical (r, θ, ϕ) coordinate system in which the $\theta = 0$ axis is directed toward the Sun and $\phi = 0$ corresponds to the equatorial plane. This coordinate system is centered on the planet which is modeled as a hard, highly electrically conducting sphere. Consequently, the plasma velocity and magnetic field are required to be parallel to the surface of the planet, and zero-order radial extrapolation is used to determine the other quantities on the planet surface. The values at the nightside of the outer radial boundary are determined by extrapolation along the local flow direction. To carry out numerical simulations, solar wind conditions are maintained on the dayside of the outer radial boundary. The simulation code used a $73 \times 74 \times 41$ grid (r, θ, ϕ grid dimensions). This corresponds to the angular grid spacings, $\Delta\theta = 2.5$ and $\Delta\phi = 4.75$, with a radial extent of the simulations of $3R_V$. The largest radial spacing is $\Delta r = 0.083R_V$. The resulting computer code (Cable and Steinolfson, 1995) is second-order accurate in space and time.

The denisty and pressure are initially constant throughout the simulation region. The initial velocity field is the flow of an incompressible fluid over a sphere, directed along the $\theta = 0$ line:

$$V_r(r, \theta, \phi, t = 0) = V_0\left[\left(\frac{R_V}{r}\right)^3 - 1\right]\cos\theta \tag{6}$$

$$V_\theta(r, \theta, \phi, t = 0) = V_0\left[1 + \frac{1}{2}\left(\frac{R_V}{r}\right)^3\right]\sin\theta \tag{7}$$

$$V_\phi(r, \theta, \phi, t = 0) = 0. \tag{8}$$

The magnetic field is initialized in a similar way, except that $\mathbf{B}$ is skewed with respect to the solar wind flow by the desired angle. The initial IMF is taken from the potential solution for flow over a sphere so that $\nabla \cdot \mathbf{B} = 0$ in the initial state. The continued satisfaction of $\nabla \cdot \mathbf{B} = 0$ is assured by solving a Poisson equation and updating the

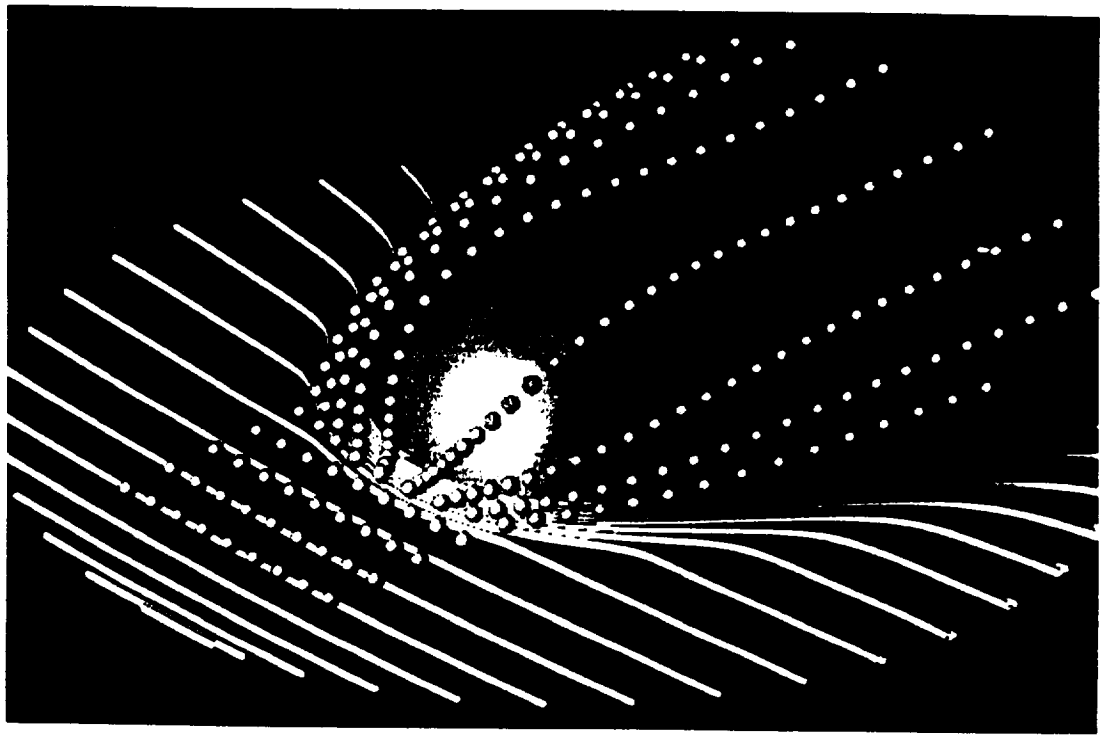

Fig. 1. Overall behavior of the solar wind–Venus interaction for the case of the perpendicular magnetic field. The initial locations of the blue fluid elements were equally spaced along a line located well ahead of the shock front, perpendicular to the solar wind flow. Their positions are shown in the figure at time increments of 5 s. Note that the fluid elements are slowed as they entered the shock front, then accelerated again when they passed over the planet surface. The magnetic field lines, in yellow, piled up at the planet surface

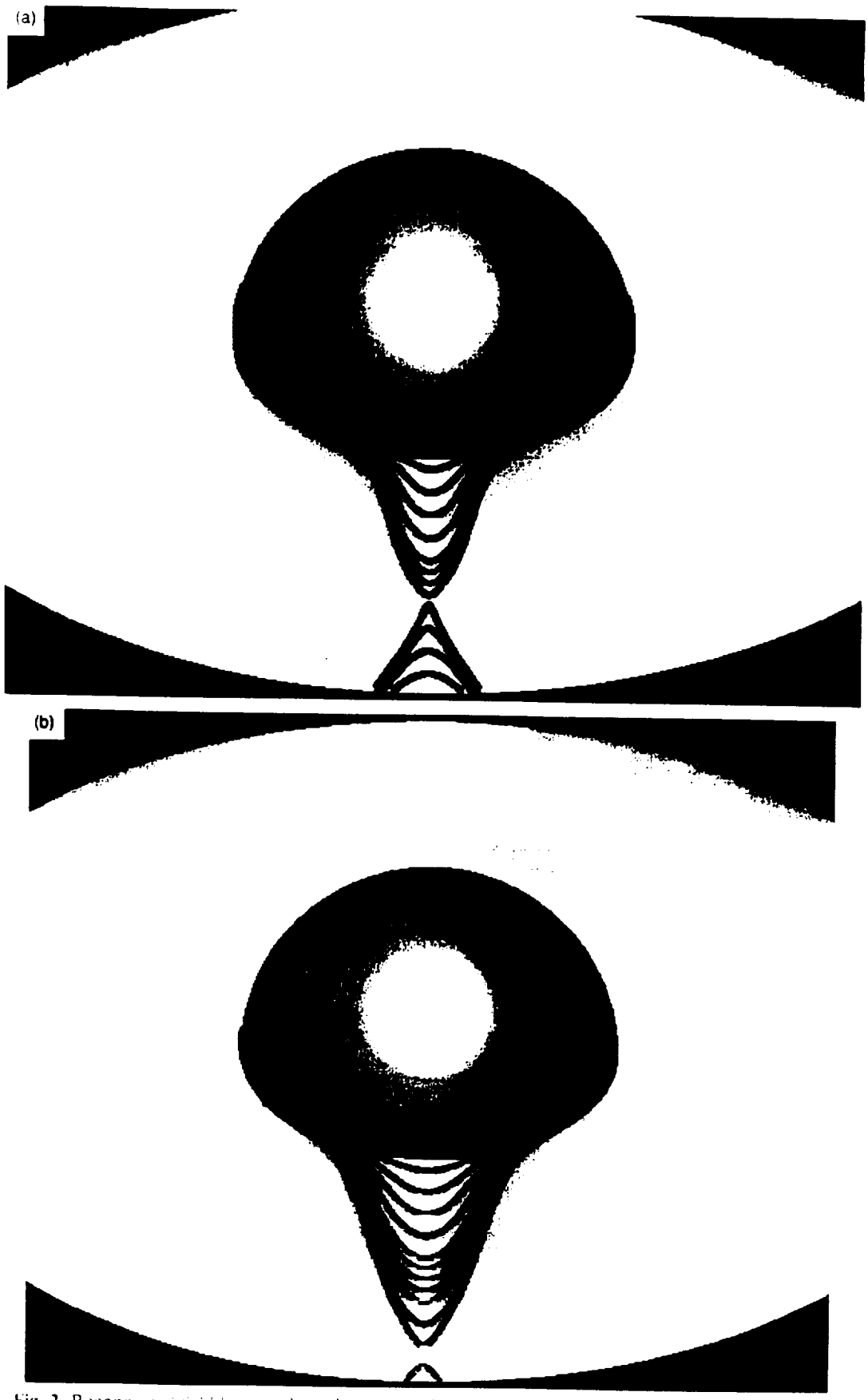

Fig. 2. Reconnected field lines in the tail region in the case of the magnetic field perpendicular to the solar wind flow (a) the NL case; (b) the ML case. Note that as a consequence of the plasma flow reduction, the reconnected lines are pulled away from the planet by the ML effects

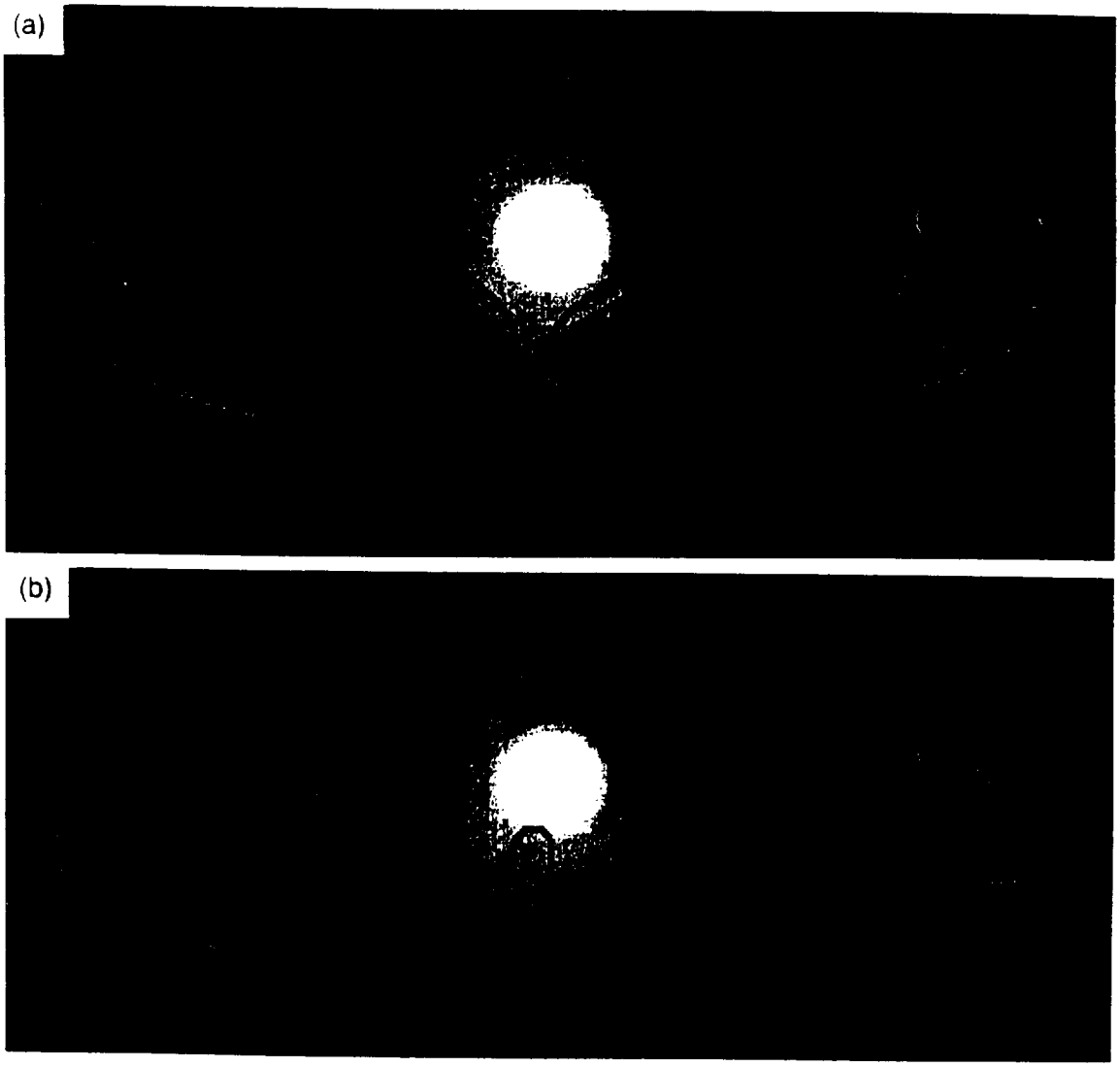

Fig. 3. A summary of the field line behaviors in the NL (a) and ML (b) cases. The view is from the tail looking at the nightside of the planet

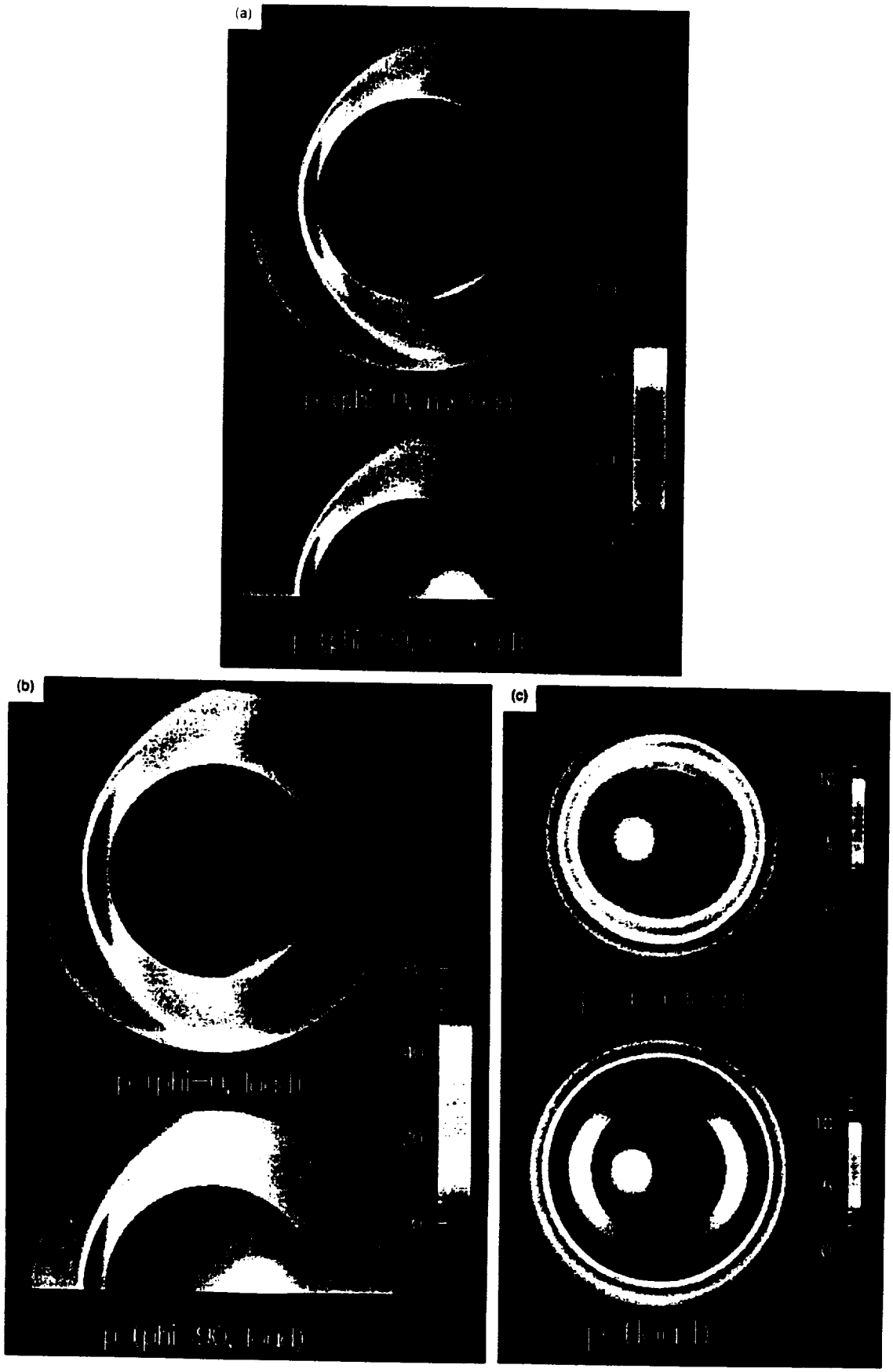

Fig. 5. The pressure distributions of the solar wind: (a) the ecliptic and noon–midnight planes for the NL simulations; (b) the ecliptic and noon–midnight planes for the ML simulations; (c) the terminator plane for the NL and ML simulations

magnetic field. The numerical solution then continues until the interaction achieves an approximate steady state. A typical computation begins with the introduction of the desired solar wind values in the dayside within the numerical box.

3. Numerical results

We present all numerical results for the oxygen ion production rate $M_{ni} = 3 \times 10^{7}$ cm $^{-3}$ s $^{-1}$ (McGary and Pontius, 1994) and perform computations with a cone angle of 90° (the perpendicular case), while the average solar wind cone angle is reported as 42.2° (Phillips *et al.*, 1986). The computations with the cone angle of 0° (the parallel case) have been reported previously by Murawski and Steinolfson (1995). The physical solar wind values used are: electron density $n_e = 20$ cm $^{-3}$, temperature $T = 10^5$ K, sound speed 55 km s $^{-1}$, flow velocity 370 km s $^{-1}$, sonic Mach number 6.73, and thermal pressure 6.06×10^{-10} dyn cm $^{-2}$. Other physical parameters are chosen the same as in Cable and Steinolfson (1995).

Figure 1 shows the global configuration of the magnetic field lines and fluid elements traces from the final configuration of the numerical simulation. The solar wind flows in from the left-hand side towards the planet. Yellow lines indicate magnetic field lines which pile up at the shock front, and then slip over the planet, forming magnetotail. The blue dots represent the instantaneous positions of nine fluid elements moving from left to right in the plate. Successive positions for each fluid element are separated from one another by a time increment of 5 s. The fluid elements that enter the bow shock center are significantly slowed in their courses, then accelerated again as they pass over the surface of the planet. In the dayside part of the planet, flow velocities become small, and a stagnation point is formed ahead of the planet. This scenario is hardly affected by the ML effects and is similar for different values of the solar wind magnetic field strength.

Figure 2 shows the reconnected magnetic field lines in the magnetotail of Venus. These lines are stretched out into the tail in a roughly conical volume with a base radius which depends on the strength of ML. As the ML effects reduce a plasma flow in the tail region, the reconnected region is shifted farther out from the planet surface for non-zero ML effects. The ionosphere of Venus captures field lines which drape over the planet to form an antiparallel magnetic field configuration in the magnetotail. Converging flows in the magnetic lobes squeeze the antiparallel magnetic lines to form a thin plasma sheet. Eventually, magnetic reconnection occurs in this region. The resistivity producing the reconnection originates in numerical diffusion which inherently builds up in a numerical scheme. This scenario resembles reconnection events in the magnetotail of comets (Ogino *et al.*, 1986). Our findings of the magnetic reconnection in the tail region are consistent with McComas *et al.*'s (1986) result, that 8–12 R_V downstream, the crossflow field is reversed only about 2% of the time. The present results suggest also that a higher value of the ML rate is needed to shift the reconnection region farther out from the surface of Venus.

Figure 3 summarizes the various field lines we have observed in the case of no loading (NL) and ML simulations. The field line passing around the opposite side of Venus has flowed downstream with the impacting solar wind and has become caught on the dayside of the planet. The uppermost field line slips over the planet's surface and bends into a U-shaped form, with the U-opening in the downstream direction. Spiraling field lines which exhibit reconnection can be seen toward the bottom. The ML affects mostly the magnetic field lines at the magnetotail (Fig. 3b) where two lines already underwent the reconnection, and the third one, in a U-shaped form, is close to a reconnection state. A plasma flow in the equatorial plane brings the two magnetic field lines into the U-shaped form. These lines may undergo reconnection if the flow in the $\phi = 0°$ plane is small enough not to reduce the curvature of magnetic field lines. As ML decreases, the flow in the tail region of the reconnection occurs farther out from the planet surface.

Figure 4 shows the influence of the ML effects on the radial (or B_r) and tangential (or B_θ) components of the magnetic field. These components are measured along the circular orbit of $r = 1.4R_V$ in the equatorial ($\phi = 0°$) plane. The values of the radial component are increased by the ML effects and are very similar in magnitude to those recorded by PVO (Luhmann *et al.*, 1991; Dubinin *et al.*, 1991). Although the ML enhances the tangential component of the magnetic field, its value is still too small at the current sheet which is located at $\theta = 180°$. Luhmann *et al.* (1991) show that this component reaches a value of ~10 nT at the current sheet. This disagreement indicates that the rate of the ML effects is too small or other processes apart from MHD phenomena are at work maintaining the cross-flow field strength in this region.

Figure 5 exhibits the spatial distributions of the gas

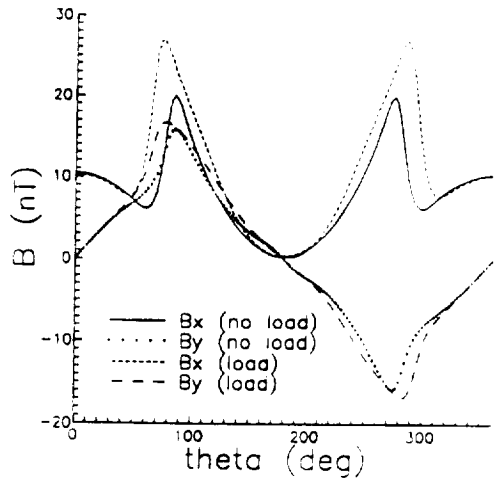

Fig. 4. Radial or r and θ or x components of the magnetic field in a circular orbit in the ecliptic plane of $r = 1.4R_V$. Note that the ML effects increase the magnitude of B in the overall region of θ. The B_r component is increased by the ML effects everywhere except $\theta \simeq 0°$ (sunward) direction. Note that in the numerical simulations $0 \leq \theta \leq 180°$. To draw this figure the symmetry boundary conditions were applied for $180° < \theta < 360°$

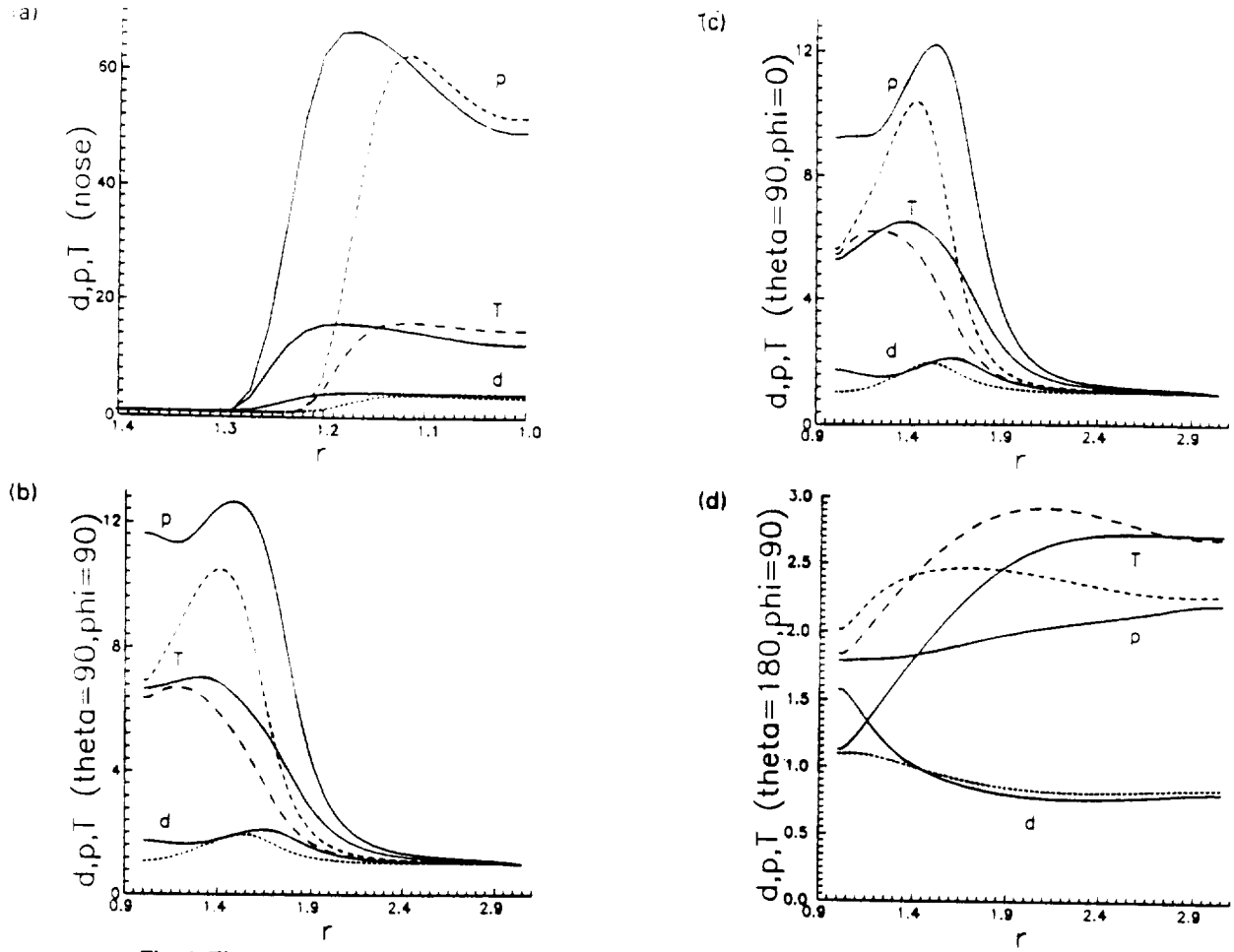

Fig. 6. The plasma (p, T, ρ) profiles in the case of the perpendicular magnetic field for the NL (broken lines) and ML (solid lines) simulations. Profiles are made along: (a) the Sun–Venus line; (b) $\theta = 90°$, $\phi = 90°$ line; (c) $\theta = 90°$, $\phi = 0°$ line; (d) $\theta = 180°$ line. The grid points were denoted by stars in the profile of the ML plasma pressure p (a). The mass density ρ is denoted here by d

pressure from the perpendicular simulations. As stated above, the outer computational boundary was $3R_V$, but here we show only the region contained within $1.75R_V$ in order to bring more details. Figure 4a (4b) shows the ecliptic and noon–midnight planes for the case of NL (ML) simulations. Formation of the bow shock can be seen in front of Venus. The distance between the shock and Venus is larger in the case of ML. This is in agreement with observations by PVO. When the solar activity was near its maximum these observations indicated that the bow shock receded significantly from the surface of Venus (e.g. Slavin *et al.*, 1983). As the time progressed toward solar minimum, the shock approached the planet's surface, and the process eventually repeated following a trend similar to that of the previous solar cycle (Tatrallyay *et al.*, 1984).

Note that the pressure maximum occurs downstream of the shock, then drops to a lower value at the planet's surface (Fig. 6a). See also Tanaka (1993), and Cable and Steinolfson (1995). In the parallel case the pressure maximum occurs at the planet surface (Cable and Steinolfson, 1995; Murawski and Steinolfson, 1995). The effect of ML is to increase (decrease) the pressure upstream (downstream) of the NL bow shock. This behavior is independent of the magnetic field strength. In the parallel case a similar gas pressure reduction due to the ML occurs for $\beta = 0.5$. For $\beta = 0.1$ and 10, the gas pressure is enhanced by the ML (Murawski and Steinolfson, 1995). Similar behavior occurs for the plasma temperature which is higher at the subsolar side of the NL bow shock. Such plasma warming is observed also in the case of the parallel simulations for $\beta = 0.5$. However, the cases of $\beta = 0.1$ and 10 differ from this behavior (Murawski and Steinolfson, 1995). The mass density is increased at the nose region (Fig. 6a), as in the case of the parallel simulations (Murawski and Steinolfson, 1995).

Figure 5c shows the pressure distribution in the terminator plane ($\theta = 90°$). Again, the pressure is increased (together with T and ρ increase), and the bow shock distance from the planet's surface is increased when the ML is applied (Fig. 6b). The increase of p occurs mainly in the magnetosheath. Note also that the bow shock is thicker in the case of ML. There are two small depletions of p which occur for the ML solutions at both the equatorial and day–night planes (Figs 5 and 6b,c).

It appears with some effort on Figs 5c and 6b,c that the bow shock is flattened at the terminator plane. The flattening occurs in the equatorial plane as the shock distance from the planet surface is larger in the $\phi = 0$ plane than in the $\phi = 90°$ plane. Although this is in agreement

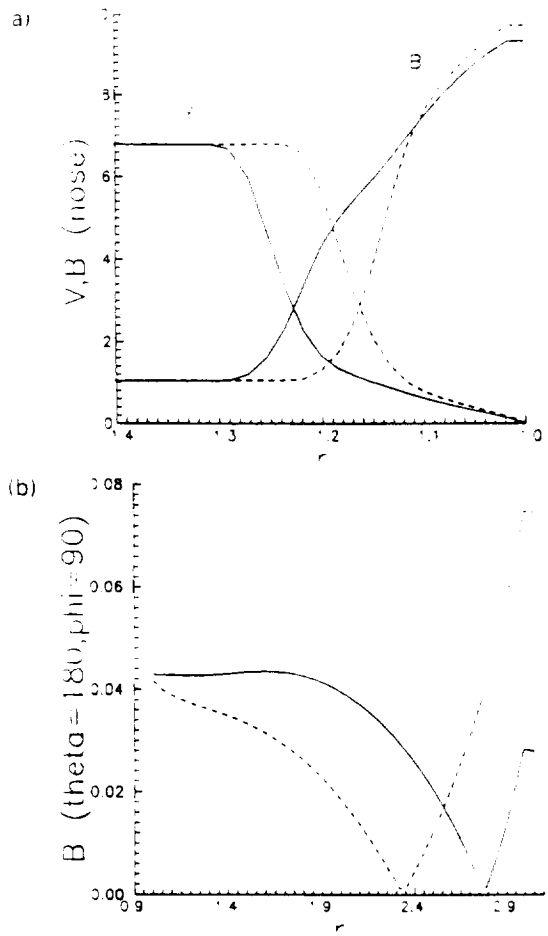

Fig. 7. As for Fig. 2 but for B and V. Profiles are along the Sun–Venus line (a) and along the $\theta = 180°$ line (b)

with the results by Russell *et al.* (1990), it is rather unlikely that the degree of flattening of the Venus bow shock could be accounted for in this way to match the observations. These results are also in agreement with the conclusion drawn by Russell *et al.* (1988) who showed that the cross section of the bow shock in the terminator plane was almost perfectly circular when the IMF was aligned with the solar wind flow but departed from circularity by about 10% when the IMF was perpendicular to the solar wind direction. For the asymmetric case the smaller diameter was found to be aligned with the IMF.

In the magnetotail region the mass density is enhanced at the planet surface due to the ML. At farther distances, the ML reduces ρ (Fig. 6d). This behavior differs from the parallel case for which ρ is reduced at the planet and enhanced in the tail, at larger distances. In the parallel case ρ is enhanced for $\beta = 0.1$ but, depletion regions exist for $\beta = 0.5$ and 1.0 (Murawski and Steinolfson, 1995). The gas pressure and temperature increase due to the ML (Fig. 6d).

The magnetic field strength rises monotonically to a peak at the planet's surface indicating the formation of a magnetic barrier (Cable and Steinolfson, 1995). A detailed investigation of the magnetic field along the Sun–Venus line shows that B is enhanced (reduced) by ML upstream (downstream) of the non-loaded bow shock (Fig. 7a). At the terminator ($\theta = 90°$) B is increased by the ML effects while in the parallel case, B is enhanced at distances farther (closer) to the planet's surface (Murawski and Steinolfson, 1995). The departure of the bow shock from the planet's surface as a consequence of the ML applied is also discernible on the spatial distribution of the magnetic field. In the magnetotail, ML enhances B at the planet surface ($r < 2.5R_V$) and reduces it at longer distances (Fig. 7b). Note also two minima which correspond to reconnection regions. ML shifts the reconnection region from $r \simeq 2.35R_V$ to $2.8R_V$.

4. Summary

The interaction of the solar wind with Venus is studied using numerical solutions of the time-dependent ideal 3-dimensional MHD equations. A modified Lax–Wendroff scheme (Cable and Steinolfson, 1995) is used to solve the equations in a spherical coordinate system. For these computations the detailed chemistry of the ionosphere is neglected, and the planet is treated as a conducting sphere. Numerical computations have been performed to study the effect of ML, the IMF orientation and strength on the magnetic barrier, draping of the magnetic field over the planet, the slippage of the field around Venus, and the general configuration of the magnetic tail. The IMF orientation included in this study is perpendicular to the solar wind flow direction. The numerical computations have been carried on for a long time which allow us to believe that we approached a quasi-steady state.

The perpendicular case, although similar in some aspects, differs in a general behavior to the parallel case. In particular, it has been found that the plasma dynamics is hardly affected by the strength of the magnetic field which originated from the solar wind. The location of the bow shock is virtually the same for different values of the plasma β. The IMF lines pile up against the atmospheric plasma and drape over the planet to form a magnetotail with two lobes of opposite magnetic polarity separated by a plasma sheet. The parallel magnetic field causes the plasma dynamics to be highly sensitive to a value of the plasma β (Murawski and Steinolfson, 1995).

The numerical results indicate that the presence of ML causes the bow shock to move outward from the planet but not so far as observed at Venus during the period of maximum solar activity. Some part of the outward displacement of the bow shock from that indicated for flows without ML thus appears to be accounted for, but additional considerations are required to achieve a good quantitative agreement with the observational data set. Whether the main source of these differences arises from shortcomings in the model itself or in the interpretation of observational data remains uncertain, and is the subject of continuing study.

It should be recalled in this regard that the mass loading model presented in this work concerns only the ions pickup due to photoionization. The neglect of other ions production processes such as proton–neutral charge exchange and impact ionization could result in underestimations of the ion production rate. As a consequence, the inclusion of such additional processes would undoubt-

ually indicate the bow shock recedes farther from the planet's surface.

Acknowledgements. K.M. is grateful for Sam Cable's assistance on several numerical issues and for Dianne LeBlanc for reading this manuscript. This work was financially supported by NASA grant NAGW-4054. Finally, we wish to thank an anonymous referee for his/her many helpful criticisms and constructive comments on an earlier version of this paper.

References

Belotserkovskii, O. M., Breus, T. K., Krymskii, A. M., Mitnitskii, V. Ya., Nagy, A. F. and Gombosi, T. I., The effect of the hot oxygen corona on the interaction of the solar wind with Venus. *J. geophys. Res.* **14**, 503, 1987.

Biermann, L., Brosowski, B. and Schmitt, H. M., The interaction of the solar wind with a comet. *Solar Phys.* **1**, 254, 1967.

Breus, T. K., Bauer, S. J., Krymskii, A. M. and Mitnitskii, V. Ya., Mass loading in the solar wind interaction with Venus and Mars. *J. geophys. Res.* **94**, 2375, 1989.

Cable, S. and Steinolfson, R. S., Three dimensional MHD simulations of the interaction between Venus and the solar wind. *Astron. Astrophys.*, submitted, 1995.

Cloutier, P. A., Taylor Jr, H. A. and McGary, J. E., Steady state flow/field model of solar wind interaction with Venus: global implication of local effects. *Planet. Space Sci.* **22**, 967, 1987.

Dubinin, E., Lundin, R., Riedler, W., Schwingenschuh, K., Luhmann, J. G., Russell, C. T. and Brace, L. H., Comparison of observed plasma and magnetic field structures in the wakes of Mars and Venus. *J. geophys. Res.* **96**, 11,189, 1991.

Gombosi, T. I., Powell, K. G. and De Zeeuw, D. L., Axisymmetric modelling of cometary mass loading on an adaptively refined grid: MHD results. *J. geophys. Res.* **99**, 21,525, 1994.

Luhmann, J. G., The solar wind interaction with Venus. *Space Sci. Rev.* **44**, 241, 1986.

Luhmann, J. G., Russell, C. T., Schwingenschuh, K. and Yeroshenko, Ye., A comparison of induced magnetotails of planetary bodies: Venus, Mars, and Titan. *J. geophys. Res.* **96**, 11,199, 1991.

McComas, D. J., Spence, H. E., Russell, C. T. and Saunders, M. A., The average magnetic field draping and consistent plasma properties of the Venus magnetotail. *J. geophys. Res.* **91**, 7939, 1986.

McGary, J. E., Gasdynamic simulations of the solar wind interaction with Venus: boundary layer formation. *Planet. Space Sci.* **41**, 395, 1993.

McGary, J. E. and Pontius Jr, D. H., MHD simulations of boundary layer formation along the dayside Venus ionopause due to mass loading. *J. geophys. Res.* **99**, 2289, 1994.

Murawski, K. and Steinolfson, R. S., Numerical simulations of mass loading in the solar wind interaction with Venus. *J. geophys. Res.*, in press, 1995.

Ogino, T., Walker, R. J. and Ashour-Abdalla, M., An MHD simulation of the interaction of the solar wind with the outflowing plasma from a comet. *J. geophys. Res.* **13**, 929, 1986.

Phillips, J. L., Luhmann, J. G. and Russell, C. T., Magnetic configuration of the Venus magnetosheath. *J. geophys. Res.* **91**, 7931, 1986.

Phillips, J. L., Luhmann, J. G., Russell, C. T. and Moore, K. R., Finite Larmor radius effect on ion pickup at Venus. *J. geophys. Res.* **92**, 9920, 1987.

Rubin, E. L. and Burstein, S. Z., Difference methods for the inviscid and viscous equations of a compressible gas. *J. Comp. Phys.* **2**, 178, 1967.

Russell, C. T., Chou, E., Luhmann, J. G., Gazis, P., Brace, L. H. and Hogey, W. R., Solar and interplanetary control of the location of the Venus bow shock. *J. geophys. Res.* **93**, 5461, 1988.

Russell, C. T., Chou, E., Luhmann, J. G. and Brace, L. H., Solar cycle variations in the neutral exosphere inferred from the location of the Venus bow shock. *Adv. Space Res.* **10**(5), 1990.

Sauer, K., Bogdanov, A. and Baumgartel, K., Evidence of an ion composition boundary (protonopause) in bi-ion fluid simulations of solar wind mass loading. *Geophys. Res. Lett.* **21**, 2255, 1994.

Slavin, J. A., Holzer, R. E., Spreiter, J. R., Stahara, S. S. and Chaussee, D. S., Solar wind flow about the terrestial planets 2. Comparison with gasdynamic theory and implications for solar–planetary interaction. *J. geophys. Res.* **88**, 1983.

Spreiter, J. R., Summers, A. L. and Rizzi, A. W., Solar wind flow past non-magnetic planets—Venus and Mars. *Planet. Space Sci.* **18**, 1281, 1970.

Stahara, S. S., Molvik, G. A. and Spreiter, J. R., A new computational model for the prediction of mass loading phenomena for solar wind interactions with cometary and planetary ionospheres. *AIAA* **87**, 1410, 1987.

Tanaka, T., Configurations of the solar wind flow and magnetic field around the planets with no magnetic field: calculation by a new MHD simulation scheme. *J. geophys. Res.* **98**, 17,251, 1993.

Tatrallyay, M., Russell, C. T., Luhmann, J. G., Barnes, A. and Mihalov, J. D., On the proper Mach number and ratio of specific heats for modelling the Venus bow shock. *J. geophys. Res.* **89**, 7381, 1984.